Institute of Bioorganic Chemistry, Polish Academy of Sciences

Department of Plant Functional Metabolomics

DOCTORAL THESIS

Nicolas Jedrzejczak-Rey

Characterization of specialized metabolism pathways involved in immune responses of the model grass *Brachypodium distachyon*

Supervisor:
Dr hab. Paweł Bednarek, prof. IBCh PAS

Poznań 2019

I would like to thank my supervisor,
Dr hab. Paweł Bednarek
for his help and guidance during these years,
and by accepting me in his team in the first place,
a decision that changed the course of my life.

I also would like to thank
Prof. dr hab. Maciej Stobiecki
for his warm welcome
and his help to make me feel a little less alone when I arrived in Poznań.

This project would never have been completed without the support
of all my co-workers.
Danuta Ciesołka, who was always here to save the day,
Mariola Piślewska-Bednarek, who was the best co-bench-worker,
and the best listening ear,
Anna Piasecka, who tremendously helped to complete this project,
Marta Pastorczyk, who always had a word of (nonsensical) wisdom,
Paweł Czerniawski, who always said « yes » to help, even when he shouldn't,
Karolina Krystkowiak, who always had good advice, except when she (rarely) didn't,
and all the people who crossed my path in the team during these years,
Karolina Kułak, **Małgorzata Zielińska**, **Kamila Karoń**…

Our neighbors were also of great help,
and I will never thank enough
all the people of the **Department of Plant Molecular Physiology**.
They were always available to reply to my numerous questions with a smile.
Special thanks to **Michał Jasiński** for our French conversations
which often took unpredictable turns.

To finish, I want to acknowledge the people
who unknowingly supported me during these years.
Dr Laura Collard, who cannot be a closest friend, despite the 1168 km between us.
My parents and sisters, who accepted to almost not see me for six years,
and **my grandparents**,
especially **Janusz Jędrzejczak** who would never imagine
that 30 years later my life will be in Poland,
and **Christiane Jamault**, who is, I am sure, kindly watching me from above.

And most importantly,
I would like to thank my wife, **Zuzanna** and our son **Jeremi**,
who were always there when there was nobody else.
Vraiment.

This doctoral thesis was supported by the National Science Centre SONATA BIS grant (UMO-2012/07/E/NZ2/04098) “Plant secondary metabolites control the colonization of plants by microorganisms.”

I was additionally supported by a fellowship from Poznan RNA Research Centre (Leading National Research Centre; KNOW)

Table of Contents

Abbreviations

4CL: 4-coumarate-CoA ligase

AADC: Aromatic L-amino acid decarboxylase

ADC: Arginine decarboxylase

ACT: Agmatine coumaroyltransferase

AHT: Agmatine hydroxycinnamoyl transferase

ANOVA: Analysis of variance

BAHD: Enzyme family named after the first letters of its members (Benzyl alcohol *O*-acetyltransferase, Anthocyanin *O*-hydroxycinnamoyltransferase, *N*-Hydroxycinnamoyl/benzoyltransferase, and Deacetylvindoline 4-*O*-acetyltransferase)

BLAST: Basic local alignment search tool

bp: Base pair

BX: Benzoxazinoid

Bx1-10: Benzoxazinoneless1-10

C3H: *p*-coumarate 3-hydroxylase

C4H: 4-cinnamic acid hydroxylase

cDNA: Complementary DNA

CDP: Copalyl diphosphate

CG: Cyanogenic glycoside

CHS: Chalcone synthase

CoA: Coenzyme A

COMT: Caffeic acid-*O*-methyltransferase

CafSer: *N*-caffeoylserotonin

CouAgm: *N*-*p*-coumaroylagmatine

CouPut: *N*-*p*-coumaroylputrescine

CouSer: *N*-*p*-coumaroylserotonin

CouTry: *N*-p-coumaroyltryptamine

ABBREVIATIONS

CPS: Copalyl synthase

CYP: Cytochrome P450

DAM: Differentially accumulated metabolite

DIBOA: 2,4-dihydroxy-1,4-benzoxazin-3-one

DIBOA-Glc: DIBOA glucoside

DiFerPut: *N*,*N*-Diferuloylputrescine

DIMBOA-Glc: 2,4-dihydroxy-7-methoxy-1,4-benzoxazin-3-one glucoside

DMSO: Dimethyl sulfoxide

DNA: Deoxyribonucleic acid

EC50: Half maximal effective concentration

EDTA: Ethylenediaminetetraacetic acid

ETI: Effector triggered immunity

F5H: Ferulate 5-hydroxylase

FDP: Farnesyl diphosphate

FDR: False discovery rate

FerAgm: *N*-feruloylagmatine

FerSer: *N*-feruloylserotonin

FerTry: *N*-feruloytryptamine

FerPut: *N*-feruloylputrescine

FLR: Fluorescence

FW: Fresh weight

FWHM: Full width at half maximum

GGDP: Geranylgeranyl diphosphate

HCA: Hydroxycinnamic acid

HCAA: HCA amide

HCT: Hydroxycinnamoyltransferase

HCN: Hydrogen cyanide

HDMBOA-Glc: 2-hydroxy-4,7-dimethoxy-1,4-benzoxazin-3-one glucoside

HHT: Hydroxycinnamoyl-CoA:hydroxyanthranilate HCT

hpi: Hours post-inoculation

HR: Hypersensitive response

IAA: Indole-3-acetic acid

ABBREVIATIONS

IGP: Indole-3-glycerol phosphate

IPP: Isopentenyl pyrophosphate

LRR: Leucine reach repeat

MAMP: Microbe-associated molecular pattern

MAPK: Mitogen-activated protein kinase

MBOA: 6-methoxy-2-benzoxazolinone

mRNA: Messenger RNA

MS: Mass spectrometry

MUSCLE: Multiple sequence comparison by log-expectation

NB: Nucleotide binding

NMR: Nuclear magnetic resonance

NMT: *N*-methyltransferase

ODC: Ornithine decarboxylase

OSC: Oxidosqualene cyclase

O-threonyl-CafSer: *N*-caffeoyl-*O*-threonyl-serotonin

PAL: Phenylalanine ammonia-lyase

PAMP: Pathogen-associated molecular pattern

PCA: Principal component analysis

PCR: Polymerase chain reaction

PDA: Potato dextrose agar

PHT: Putrescine hydroxycinnamoyltransferase

PHYLIP: Phylogeny inference package

PR: Pathogen-related

PR10: Pathogenesis-related gene 10

PRR: Pattern recognition receptor

PTAL: Phenylalanine/tyrosine ammonia-lyase

PTI: PAMP-triggered immunity

qPCR: Quantitative PCR

rDNA: Ribosomal DNA

RLK: Receptor-like kinase

RLP: Receptor-like protein

RNA: Ribonucleic acid

ABBREVIATIONS

RNA-Seq: RNA sequencing

ROS: Reactive oxygen species

RT: Retention time

RT-qPCR: Quantitative reverse transcription PCR

sad1: *saponin-deficient1*

SD: Standard deviation

SDS: Sodium dodecyl sulfate

sl: Sekiguchi lesion

SnToxA: *Parastagonospora nodorum* Toxin A

SPHT: Spermidine hydroxycinnamoyl transferase

STS: Stilbene synthase

T-DNA: Transfer DNA

T5H: Tryptamine 5-hydroxylase

TAL: Tyrosine ammonia-lyase

TBT: Tryptamine benzoyl transferase

TDC: Tryptophan decarboxylase

TFT: Tyramine feruloyl-CoA transferase

THT: Tyramine HCT

TPS: Terpene synthase

TYDC: Tyrosine decarboxylase

UBC18: Ubiquitin-conjugating enzyme 18

UDP: Uridine diphosphate glucose

UPLC: Ultra performance liquid chromatography

UV: Ultraviolet

VJ: Vegetable juice

y1: *yellow seed1*

ZmAN2: *Anther Ear 2*

Introduction

1 *Brachypodium distachyon*: a model grass

Humankind bases the majority of its food income from plants, but only 75 000 of the 400 000 known flowering plant species are edible, from which 7000 are eaten by humans (1). Moreover, only three of these species, rice (*Oryza sativa*), maize (*Zea mays*), and wheat (*Triticum spp.*), provide more than half of calories consumed by human population (2). These three species belong to the Poaceae family, commonly called grasses, making this plant family the most agronomically important one. Moreover, grasses are not only important for human alimentation but are also used in biofuel production and animal feeding. The emergence of developing countries together with environmental concerns, like greenhouse-gas emission, raise new challenges for world food production (3, 4).

Since Mendel researches on genetic inheritance, the study of living organisms relies on model systems whose key characteristics did not fundamentally change. A model plant is defined nowadays as being easy to handle (small stature and robust), easy to grow (short generation time and high fertility), easy to manipulate genetically (easy crossing, small genome size, ease of mutagenesis and transformation), sharing biology with species of interest, and uniting an active research community (5). The search for a grass model plant started with the use of maize to investigate inheritance due to its ease to be crossed, along with barley (*Hordeum vulgare*) and wheat because of their agricultural significance, or sorghum (*Sorghum bicolor*) to help the study of sugarcane (*Saccharum* sp.). However, these plants were chosen for specific purposes and lacked some of the requirements defining convenient model plant. For example, maize and rice are sizable plants, uneasy to grow in research facilities, rice possesses long generation cycles, and maize is difficult to manipulate genetically (Table 1). For these reasons, the plant community went on the search of a plant, which could be studied to better understand grass family members.

Table 1: Feature comparison of selected plants in regards to model organism requirements. Adapted from Brkljacic *et al.* (6).

	Arabidopsis	Barley	Brachypodium	Maize	Rice	Sorghum	Wheat
Height (cm)	15-20	50-120	15-20	120-300	100	50-250	50-100
Planting density (plants/m²)	2000	80-120	1000	4	36	50	50
Growth requirements	Simple	Intermediate	Simple	Demanding	Demanding	Demanding	Intermediate
Generation time (weeks)	8-12	10-20	8-12	8-15	12-24	13-18	10-20
Seeds per plant	>1000	150-200	100-1000	200-1000	>1000	>1000	50-150
Transformation	Extremely easy	Efficient but labor intensive	Highly efficient	Efficient but labor intensive	Highly efficient	Inefficient	Inefficient
Genome size (Mb)	119	5500	272	2300	382	700	16000
Assembled genome sequence	Finished genome sequence (2000)	Finished genome sequence (2012)	Finished genome sequence (2010)	Draft genome (2009)	Finished genome sequence (2005)	Finished genome sequence (2009)	Finished genome sequence (2018)
T-DNA resources	Extensive	None	>20000 lines	Transposon mutants available	Extensive	None	None

Purple false brome (*Brachypodium distachyon*; hereafter called Brachypodium) belonging to the Pooideae subfamily of Poaceae has been proposed as a new model grass. This plant species is closely related to rice, oat (*Avena sativa*), barley, wheat, and rye (*Secale cereale*), but more distant to sorghum and maize (Figure 1A). *Brachypodium* genus contains so far 17 perennial species distributed worldwide and three annual species restricted to the Mediterranean basin (Figure 1C). Brachypodium is one of the few annual species representing this genus and is growing at high altitudes, in a rather cold and wet environment, consistent with the vernalization required for certain lines to flower (7). This species possesses several features making it a suitable model plant. Mature Brachypodium measures 15-20 cm, with pedicels carrying 1-7 spikelets featuring long awns giving up to 1000 seeds per plant (Figure 1B), and has a relatively short generation time, making it a plant easy to grow for research purposes, compared to other grass species (Table 1).

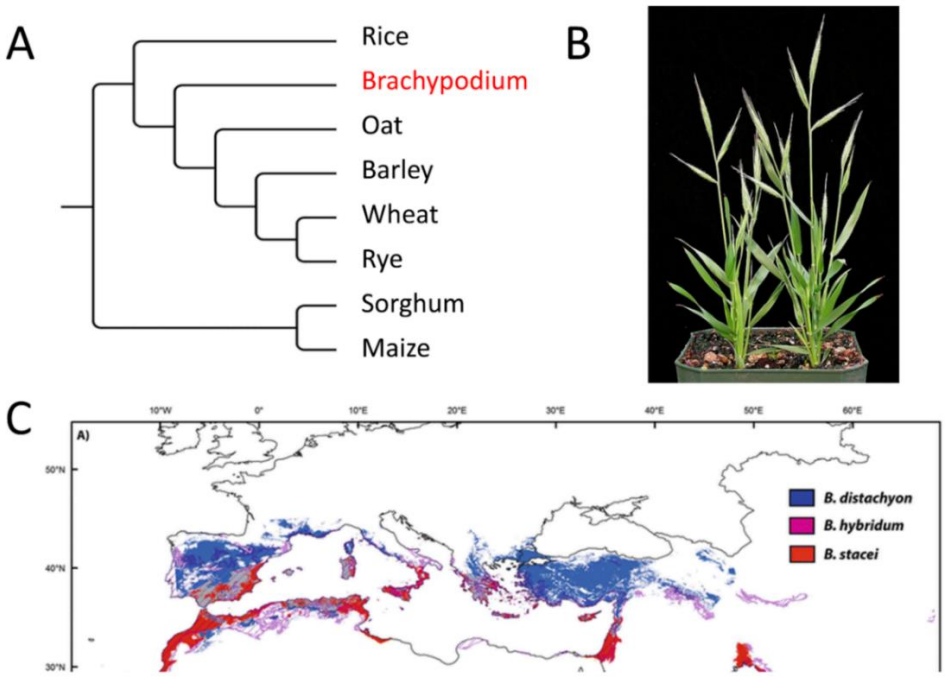

Figure 1: Brachypodium as a model plant. A: Phylogenetic relationships between selected crop grasses and Brachypodium. Simplified phylogenetic tree drafted based on maximum likelihood phylogenetic trees of complete plastomes (8, 9), and chloroplast DNA (10, 11); B: Mature Brachypodium plants (from Neil Harris, University of Alberta/Wikimedia Commons); C: Geographic occurrence of Mediterranean Brachypodium species, (from Catalan *et al*. (7)).

The first version of Brachypodium genome was released in 2010 (12), with the most recent version (v3.1) released in 2017 (13). Genomes of other crops model species have also been released, with most recently barley genome in 2012 and wheat genome in 2018 (Table 1) (14, 15). Brachypodium genome is relatively small, with approximately $272x10^6$ base pairs (bp) including nearly 25000 coding genes, and is less complex than other grass genomes, with fewer clusters, and shorter intergenic distances (Table 1) (16). Different resources were provided following Brachypodium genome sequencing, including accession and Transfer Deoxyribonucleic acid (T-DNA) line collections, as well as bacterial artificial chromosome, expressed sequence tag and yeast two-hybrid libraries, which is not the case for all other grass models (Table 1). Tools and protocols were also developed by the community to make Brachypodium easy to handle for genetic manipulations, like the establishment of *Agrobacterium*-based transformation protocols (17).

2 Mechanisms of plant immunity

In the environment, plants are constantly in contact with numerous organisms including deleterious herbivores and pathogens. Infectious agents and microorganisms include viruses, bacteria, oomycetes, and fungi. Pathogenic microorganism evolved into different lifestyles and feeding strategies. For instance, necrotrophic pathogens feed on dead cells they previously killed by secreting toxins, while biotrophic pathogens can take nutrients exclusively from living cells. Hemibiotrophic pathogens start infection with a biotrophic phase, before switching to the necrotrophic mode. Despite their lifestyle, all these pathogens represent a threat causing major crop losses. It is estimated that taken together, pathogens, animals, and weeds are responsible for a loss of approximatively 70% of global agricultural production. Fungal pathogens alone are responsible for approximatively 8% of the annual loss of crop production worldwide (18). In addition, pathogens representing necrotrophic and hemibiotrophic lifestyles can impact the quality of food, by the presence of toxins in amounts that could be difficult to assess (19). That is why understanding the mechanisms of defense of plants is important for sustaining the increasing demand for food, by improving the yield and the quality of existing crop production.

During their evolution, plants evolved sophisticated and efficient immune responses that can be triggered by recognition of unique molecules produced by the pathogen. This may occur either at the surface or in the cytoplasm of plant cells and is followed by an array of responses meant to completely avoid or at least restrict colonization of plant tissue by the pathogen.

2.1 Pattern recognition

One of the two types of pathogen recognition occurs at the interface with the external environment, from where the pathogen arrives, and is mediated by so-called Pattern Recognition Receptors (PRRs). These plasma membrane-localized proteins recognize unique molecules indicating the potential threat of the pathogen. Molecules recognized by PRRs could be of different origin including microbial molecules called Microbe-Associated Molecular Patterns (MAMPs). These are, amongst others, peptides, polysaccharides or lipids that are conserved among a bigger microbial phylogenic clade.

In addition to MAMPs, some PRRs can recognize molecules resulting from the pathogen-triggered enzymatic degradation of plant cell wall or cuticle, which are called Danger-Associated Molecular Patterns. Depending on their functional domains PRRs can be of two different kinds. The first type are Receptor-Like Kinases (RLKs), formed by an apoplastic Leucine Reach Repeat (LRR) domain binding the respective MAMP, and a cytosolic part harboring a kinase domain that can initiate a complex signaling cascade (20). The second type of PRRs are Receptor-Like Proteins (RLPs), which do not have intracellular kinase domains (20) and consequently need to interact with particular RLKs to transmit the signal (21). Recognition of different Pathogen-Associated Molecular Patterns (PAMPs) by PRRs leads to PAMP-triggered immunity (PTI). This type of immunity relies on the activation of a complex signaling cascade leading to gene expression changes mediated by different transcription factors. This signaling cascade usually involves Mitogen-Activated Protein Kinases (MAPKs; Figure 2) (22).

2.2 Effector recognition

The second type of recognition occurs in the cytoplasm and is mediated by receptors called Effector Recognition Receptors. They are polymorphic proteins possessing a Nucleotide Binding (NB) and an LRR domain, which gave the name of these NB-LRR proteins. These receptors can recognize proteins, called effectors, that are produced by the pathogen and released into the cytoplasm to interfere with plant immune responses, for example to hamper PTI. NB-LRRs can be specific to a certain effector or may target a broader spectrum of them. Plants learned to recognize effectors either directly, or indirectly by the perception of modified targets of these effectors (23, 24). This recognition leads to the Effector Triggered Immunity (ETI), and is usually involved in defense against adapted pathogens. Effectors can interfere with both PTI and ETI, leading to a chain of responses and interferences. This resistance adaptation characterizes the never-ending arms race between the plant and the pathogen (23).

The processes leading to downstream signaling after effector recognition is not as well recognized as those following MAMP recognition. Experimental evidence suggests that at least some NB-LRRs are transported in the nucleus and play a role in the transcription of genes involved in immunity, by interacting with particular transcription factors (Figure 2) (25).

2.3 Responses following recognition

Downstream signaling triggered by MAMP and effector recognition, converge to the regulation of immunity-related gene transcription. This results in the deployment of an array of responses aiming to stop pathogen development. To restrict pathogen intrusion, plant cell wall can be reinforced at the points of attempted entrance. This could be achieved with the incorporation of different compounds into the cell wall structure. Callose, a β-1,3-glucan, and lignin are the most studied polymers involved in cell wall reinforcement (26). Lignin is a phenolic polymer that has molecular properties making its degradation by microbial enzymes difficult. Moreover, lignin layer can prevent exchanges between the cell and the pathogen. The pathogen can neither spread toxins and enzymes into the host, nor feed on water and nutrients from the plant cell (27).

In addition to the cell wall reinforcement, MAMP or effector recognition can trigger a programmed cell death called Hypersensitive Response (HR), which may restrict development of biotrophic pathogens that can feed only on living cells. Major actors in HR are Reactive Oxygen Species (ROS). These highly reactive molecules are present constitutively at low abundance in plant cells but are generated in higher amounts upon pathogen infection, in a process called oxidative burst. ROS can modify intracellular pH and membrane potential, and also have an influence on ion fluxes and protein conformation (28). They play a role in intracellular and intercellular communication, participate in cell wall reinforcement, and may also be directly harmful to pathogens (29). Transcriptional regulation that is triggered by pathogen recognition leads also to the biosynthesis and the release of specialized metabolites, which may function in restricting pathogen growth (Figure 2).

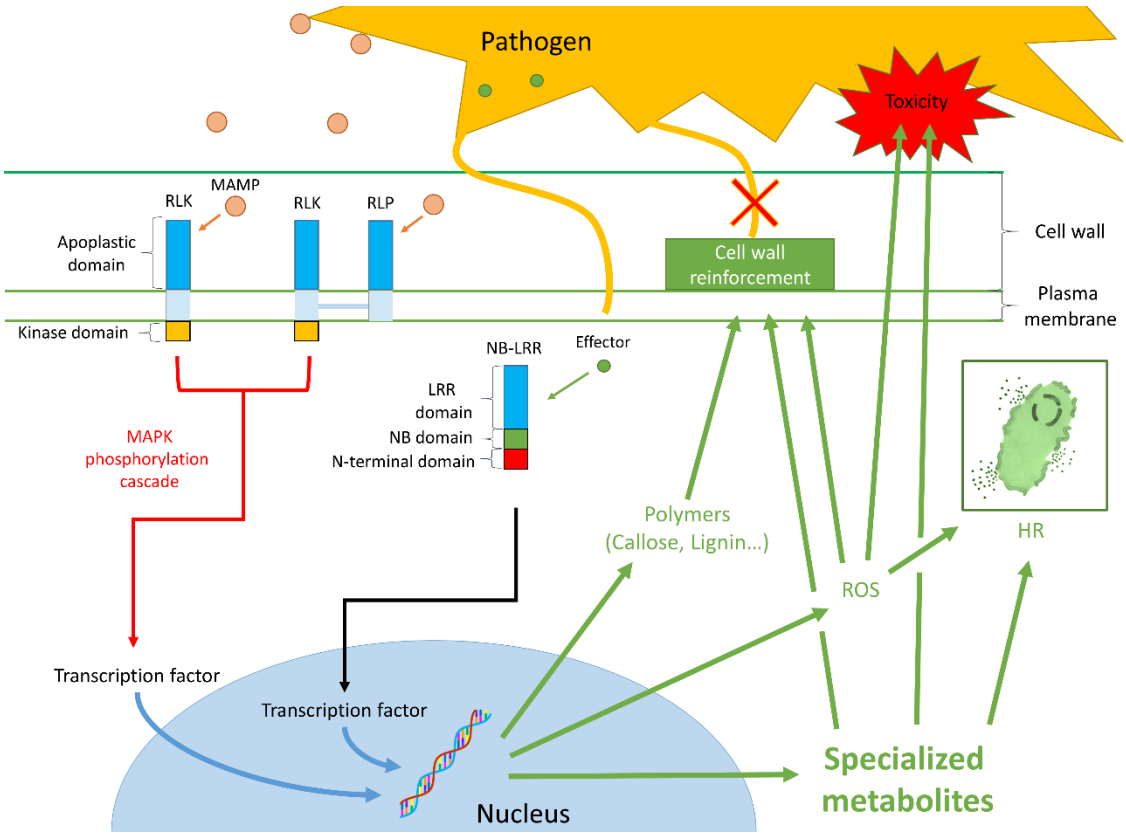

Figure 2: Simplified scheme of pathogen recognition and subsequent responses in plant immunity. HR: Hypersensitive Response; LRR: Leucine Reach Repeat; MAMP: Microbe-Associated Molecular Pattern; MAPK: Mitogen-Activated Protein Kinase; NB: Nucleotide Binding; RLK: Receptor-Like Kinase; RLP: Receptor-Like Proteins; ROS: Reactive Oxygen Species.

2.4 *Brachypodium distachyon*: a model to study grass immunity

As a model plant, Brachypodium has been used to study its interaction with fungal pathogens, in order to transfer the obtained knowledge to understand defense mechanisms in close related crop species (Figure 3). To this purpose, Brachypodium susceptibility has been tested, among others, against major crop pathogens which can cause more than 50% of yield loss in the most cultivated grasses worldwide. Among these major pathogens, Brachypodium was found to be susceptible to fungi infecting barley (*Bipolaris sorokiniana*, *Fusarium* spp., and *Ramularia collo-cygni*), wheat (*Fusarium* spp. and *Parastagonospora nodorum*, former *Stagonospora nodorum*) and rice (*Magnaporthe* spp.). The range of tested pathogens which succeed in infecting Brachypodium covers different lifestyles and infection strategies, being mainly necrotrophs and hemibiotrophs (Table 2). Necrotrophic pathogens feed on dead cells they previously killed using different toxic strategies, while hemibiotrophic pathogens start their development with a biotrophic phase, feeding on nutrient of living cells, before switching to a necrotrophic lifestyle. Due to their mode of feeding biotrophic pathogens cannot be cultivated *in vitro*, complicating their use to study plant-pathogen interaction. Hemibiotrophic and necrotrophic pathogens may be easier to cultivate *in vitro*, but carrying out inoculation experiment to study plant defense response requires spores, in order to simulate environmental conditions. Sporulation protocols were not successfully developed for several of these pathogens which make them more difficult to use in inoculation assays (Table 2). Because of the agronomical significance of these pathogens and their extensive use in research, different sequencing projects were initiated, and most of these pathogens have their genome completed, which facilitates potential gene expression analysis (Table 2). All these features should be taken into consideration in order to select a pathogen suitable for particular study needs.

Table 2: Selected fungal pathogens infecting Brachypodium (adapted from Fitzgerald *et al.* (30)). a, *in vitro* sporulation protocol available; b, genome available.

Pathogen	Host	Lifestyle
Bipolaris sorokiniana (30) [a,b]	Wheat, barley	Hemibiotroph
Colletotrichum cereale (30) [a,b]	Rye, wheat, oat, turfgrass	Hemibiotroph
Fusarium spp. (30, 31) [a,b]	Wheat, barley	Hemibiotroph
Gaeumannomyces graminis (30) [b]	Wheat, rice	Necrotroph
Magnaporthe spp.(30, 32) [a,b]	Rice	Hemibiotroph
Oculimacula spp. (30)	Wheat	Necrotroph
Ophiosphaerella spp. (30)	Turfgrass	Necrotroph
Parastagonospora nodorum (30) [a,b]	Wheat	Necrotroph
Puccinia spp. (30, 33) [b]	Wheat, oat, switchgrass	Biotroph
Pyrenophora teres (30) [a,b]	Barley	Hemibiotroph
Ramularia collo-cygni (30) [a,b]	Barley	Hemibiotroph
Rhizoctonia solani (30) [b]	Wheat, barley	Hemibiotroph
Sclerotinia homoeocarpa (34) [a,b]	Turfgrass	Hemibiotroph
Zymoseptoria tritici (35) [a,b]	Wheat	Necrotroph

3 Specialized metabolites in plant immunity

Historically, specialized metabolites had been named “secondary” metabolites and defined as small molecules differentiating from primary metabolites by the fact that they are not involved in basic molecular processes of the organism, like growth, development, and reproduction (36). Nevertheless, these compounds play crucial roles in host organisms and the term “secondary” may be misleading in the context of their importance. In order to not undermine their role, they are frequently referred to as specialized metabolites, natural products, or in plants as phytochemicals.

So far structures of at least 40 000 plant specialized metabolites are known (37). These compounds originate from primary metabolites or their biosynthetic intermediates. For instance, aromatic amino acids can be metabolized to phenolic compounds or alkaloids, while isopentenyl pyrophosphate (IPP) is the precursor of terpenoids. Importantly, in plants representing different phylogenetic clades the same biosynthetic precursor can be frequently metabolized through different core biosynthetic pathways. Obtained intermediates can be subjected to further modifications in pathway branches whose occurrence could be even more phylogenetically limited. This results in huge structural diversity of specialized metabolites and in the restriction of certain compounds to particular taxonomic groups of the plant kingdom (38). Different classifications are used in an attempt to organize the diversity observed among plant specialized metabolites. When the first plant specialized metabolites were identified at the beginning of the 20th century, scientists could only rely on the structure or molecular composition (e.g. presence of a heteroatom) to classify the newly discovered compounds. Started in 1950’s development of new techniques in biochemistry and molecular biology, and the later rise of genomics, enabled identification of precursors and characterization of natural product biosynthetic pathways. This allowed improving the structure-based classification, by taking the compound biosynthesis into consideration (36). Specialized metabolites can be first hierarchically grouped in large classes by their precursors. Then, they can be sub-classified according to their core biosynthetic pathways allowing separation of compounds sharing the precursor, but not the biosynthetic pathway. Finally, these specialized metabolite subclasses can be divided into smaller groups according to branch pathways leading to the formation of respective compounds. Metabolites formed as a

result of conjugation of compounds originating from different precursors and metabolic pathways can be grouped in their own separated subclasses. Nowadays the classification according to structure, precursor, and biosynthetic pathway is the most commonly used. However, one can still find the mention of groups of compounds, like alkaloids, remnants of classification based on other criteria.

Specialized metabolites have been suggested for the first time to have a role in the interaction with the environment at the end of the 19th century (39). Since then, these compounds have been proved to be engaged in the response to abiotic factors or in biotic interactions. Abiotic stressors can be of different kinds including presence of salts or heavy metal ions, drought, extreme temperatures, excess light or nutrient deficiency (40). In response to these factors, specialized metabolites can act as UV protectors, antioxidants, or chelating agents (41, 42). In the case of biotic interactions, specialized metabolites can be involved in mutualistic as well as antagonistic relationships. For instance, they can play a role in symbiotic associations between plants and microorganisms, as well as in the attraction of pollinators or natural predators of phytophagous insects (43, 44). In antagonistic interactions, they can restrict growth of competitive plants, or repel herbivores (44, 45). Additionally, specialized metabolites play also a role in defense against pathogens (46). To fulfill this function, they can be incorporated into the cell wall and linked to its components in order to reinforce this barrier against pathogen penetration attempts (47). They can also be involved in HR as signaling molecules (48). Finally, some plant specialized metabolites can act as direct anti-fungal agents (49). Mechanisms of toxicity of so far investigated in this context compounds suggest that pathogen plasma membrane and enzymes are the most common targets (49).

3.1 Immunity-related specialized metabolites in grasses

Specialized metabolites involved in plant immunity can be classified according to their mode of production. Phytoanticipins are compounds constitutively synthesized and stored ahead of pathogen attempt of colonization. Upon pathogen attack, these compounds can be quickly released at the infection site. On the other hand, phytoalexins are compounds synthesized *de novo* following infection (50). However, as these definitions rely on the mode of synthesis, and not on the chemical structure, the same molecule can be both a phytoanticipin and a phytoalexin, depending on the species or even the organ. For example, sakuranetin is a phytoalexin in rice produced in response to rice blast fungus (51, 52), but is classified as a phytoanticipin in leaves of blackcurrants (*Ribes nigrum*) (53). Moreover, in rice, momilactone A is a phytoalexin produced in leaves in response to rice blast fungus (54), but accumulates constitutively in seed husks (55), making it a phytoanticipin in this tissue.

3.1.1 Anthranilate-derived compounds

Anthranilate is produced from chorismate, the precursor of aromatic amino acids, and is an intermediate in the biosynthesis of tryptophan that is formed from indole-3-glycerol phosphate (IGP), by the tryptophan synthase. This enzyme is composed of two subunits, α and β, respectively responsible for the conversion of IGP into indole, and the condensation of indole and serine into tryptophan. Numerous specialized metabolites involved in plant immunity can be derived directly from this amino acid. Alternatively some compounds could be produced from tryptophan precursors, for instance benzoxazinoids (BXs) whose biosynthesis branch from IGP.

3.1.1.1 Serotonin

Different tryptophan-derived compounds have been shown to play a role in the immune response in different plant species, a notable example being camalexin in the model plant Arabidopsis (*Arabidopsis thaliana*) (56). The most frequently investigated tryptophan-derived compound in the context of grass immunity is serotonin. Apart from its immune function, this compound is involved in other plant processes, including growth regulation and reproduction (57). Serotonin together with structurally related compounds including

tryptamine, 3-(2-aminoethyl)-3-hydroxyindolin-2-one (a putative derivative of tryptamine) and 5,5′-dihydroxy-2,4′-bitryptamine (serotonin dimer), have been found to accumulate in higher amounts in rice leaves upon infection with fungal pathogen *Bipolaris oryzae* (Figure 3) (58, 59). When wheat leaves were infiltrated with *P. nodorum* Toxin A (SnToxA), an effector produced by this necrotrophic fungal pathogen, serotonin was observed to accumulate in higher amount compared to non-treated plants (60). Serotonin and 5,5′-dihydroxy-2,4′-bitryptamine accumulated in higher amounts upon inoculation of foxtail millet (*Setaria italica*) leaves with *Bipolaris maydis*, and inoculation of cultivated barley leaves with *B. sorokiniana*, the fungal pathogen responsible for spot blotch of barley leaves. Under the same conditions, barley also accumulated higher amounts of 3-(2-aminoethyl)-3-hydroxyindolin-2-one (59). In Brachypodium, serotonin was also shown to accumulate in higher amount in spikes infected with *Fusarium graminearum* than in uninfected ones (61).

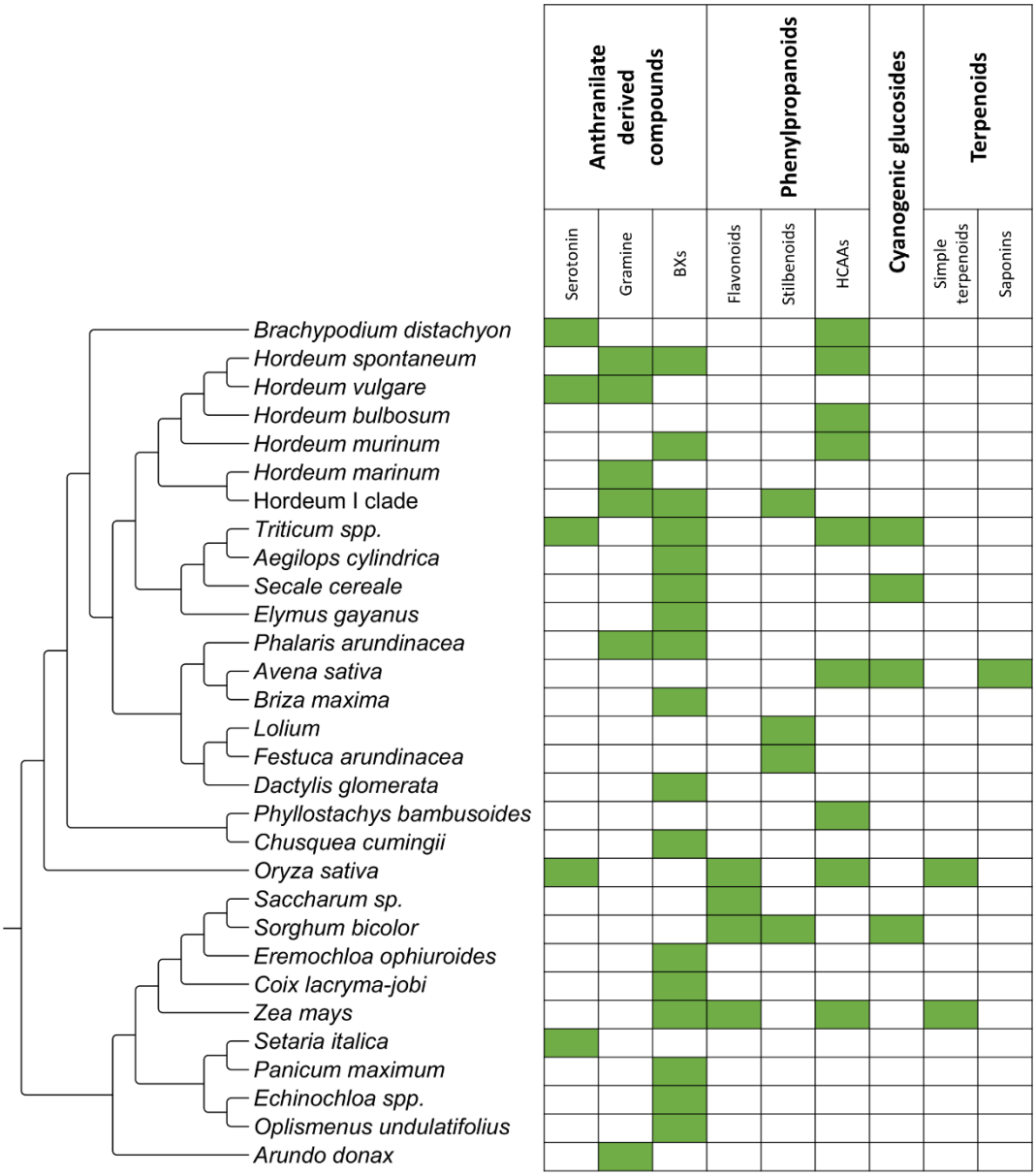

Figure 3: Distribution of immunity-related specialized metabolites in grasses. Maximum likelihood phylogenetic tree without scale based on complete plastomes, according to Saarela *et al.* (8), Teisher *et al.* (9), and chloroplast DNA, according to Mason-Gamer *et al.* (10), Arthan *et al.* (11). Hordeum phylogenetic subtree based on nuclear ribosomal DNA (rDNA) internal transcribed spacer region according to Blattner *et al.* (62, 63). Confirmed presence of specialized metabolites in particular species or in some species representing Hordeum I clade is indicated with green. BXs: Benzoxazinoids; HCAAs: Hydroxycinnamic acid amides. Hordeum I clade includes: *H. bogdanii*, *H. brachyantherum*, *H. chilense*, *H. flexuosum*, *H. pusiluum*, *H. jubatum*, *H. brevisubulatum*, *H. roshevitzii* and *H. lechleri*.

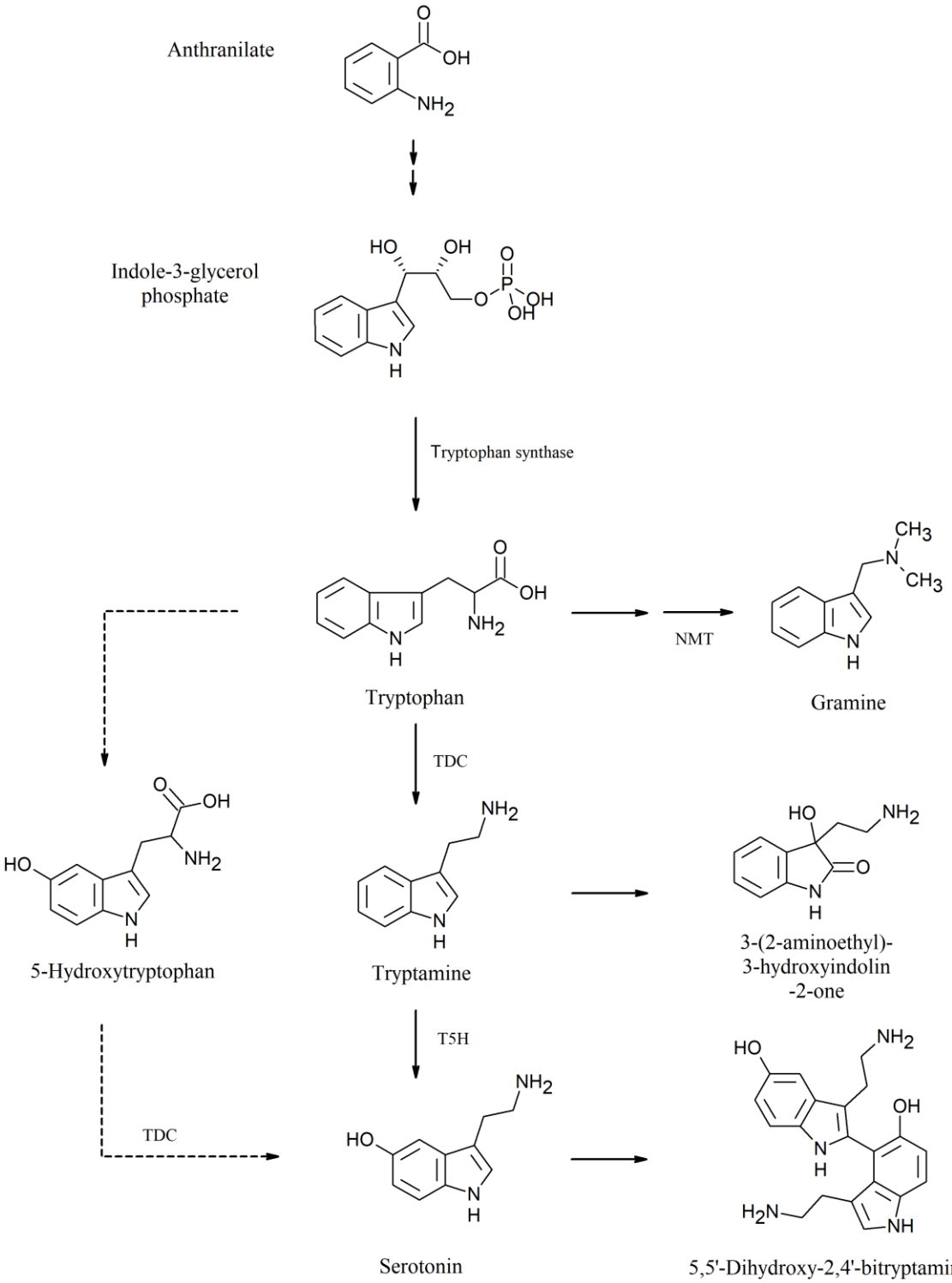

Figure 4: Simplified biosynthetic pathway of tryptophan-derived compounds. NMT: *N*-methyltransferase; T5H: tryptamine 5-hydroxylase; TDC: tryptophan decarboxylase. Dashed arrows indicate hypothetical biosynthetic steps.

So far serotonin biosynthesis was mainly investigated in rice. This biosynthetic pathway starts with the conversion of tryptophan to tryptamine, a reaction that is catalyzed by a tryptophan decarboxylase (TDC; Figure 4). Together with tyrosine decarboxylases (TYDCs), TDCs belong to the family of aromatic L-amino acid decarboxylases (AADCs), which are enzymes involved in the biosynthesis of an array of specialized metabolites. AADC family includes also closely related aromatic acetaldehyde synthases that additionally possess oxidase activity and can convert aromatic amino acids directly to the corresponding aldehydes (64).

Seven *AADC*-like genes have been identified in the sequenced rice genome. In order to functionally characterize these genes, three of them were heterologously expressed and obtained proteins showed TDC activity *in vitro* (65, 66). Corresponding genes were accordingly named *TDC1*, *TDC2*, and *TDC3*. T-DNA-tagged rice mutant or transgenic rice plants overexpressing these *TDC*s accumulated higher amounts of tryptamine, serotonin and serotonin dimer than wild-type rice (65, 66). These results suggest that these three TDCs are candidate enzymes for tryptamine biosynthesis in rice. Seven *AADC*-like genes were investigated in Brachypodium. Yeast transformants heterologously expressing two of these *AADC*-like genes were shown to produce tyramine, unlike not transformed yeast, suggesting that these two genes are coding for TYDCs (67). The expression of the five remaining genes was induced upon spike inoculation with *F. graminearum* (61), and the expression of two of them was induced upon seedling infection with *Fusarium pseudograminearum* (31). Phylogenetic analysis of *TDC* homologs in various monocots suggested existence of two *TDCs* in barley, and four in sorghum (68). Taken together, these results indicate that *AADCs* form multigene families in different grass species. However, for a long time it was not known if specificity of these enzymes towards tryptophan or tyrosine can be predicted based on unique conserved amino acid residues. Recently, crystal structural characterization of *Catharanthus roseus* TDC, *Papaver somniferum* TYDC, Arabidopsis phenylacetaldehyde synthase, and *Rhodiola rosea* 4-hydroxyphenylacetaldehyde synthase, combined with phylogenomic analysis allowed to identify conserved residues of the substrate-binding pocket (Figure 5). Among these, glycine from the position 370 of *Cr*TDC is strongly conserved in TDC clade, while a serine or a threonine is present at the corresponding position within TYDC clade (Figure 5) (64). Structural comparison between *Cr*TDC and *Ps*TYDC showed that this

substitution modifies the size of the substrate-binding pocket, therefore facilitating binding of either tryptophan or tyrosine (64).

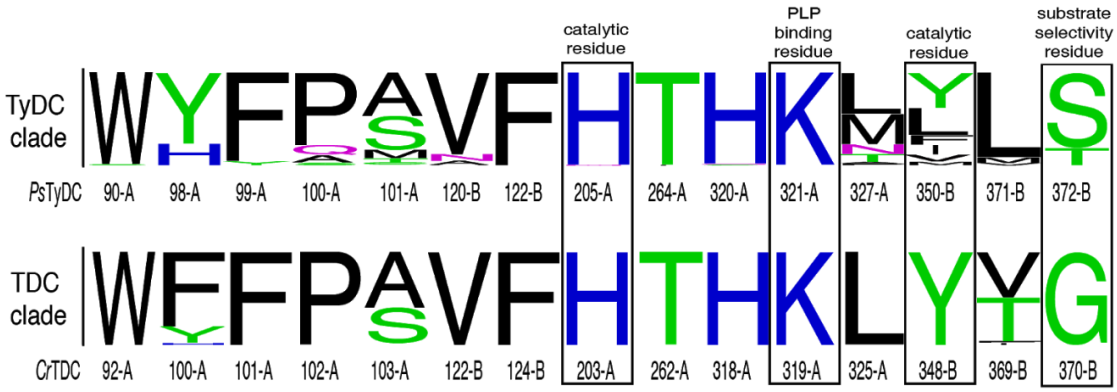

Figure 5: Conserved residues of the substrate-binding pocket from tyrosine decarboxylases (TYDCs) of 42 plant species or tryptophan decarboxylases (TDCs) of 29 plant species. Y-axis represents the relative amino acid frequency of a given amino acid. Key residues are framed and their function is annotated. Adapted from Torrens-Spence *et al.* (64).

After its formation from tryptophan, tryptamine is metabolized to serotonin by a cytochrome P450 (CYP) monooxygenase known as tryptamine 5-hydroxylase (T5H). Enzymes of the CYP family have been estimated to be encoded by a number of genes representing up to 1% of total genes annotations of each plant species. The recurring presence and the diversity of enzymes belonging to this family in natural product biosynthetic pathways contribute to plant specialized metabolite diversity (69). T5H function was investigated in rice using a *sekiguchi lesion* (*sl*) mutant cv. Sekiguchi-asahi, which is a lesion mimic mutant exhibiting unique orange colored spots induced by pathogen inoculation (70). This phenotype was shown to be linked with a mutation in a gene coding for a CYP monooxygenase (71). This enzyme was heterologously expressed, and enzymatic assays showed *in vitro* T5H activity (71). *sl* mutant was also found to accumulate tryptamine upon infection with *Magnaporthe grisea* when no tryptamine accumulation was detected in wild-type rice upon the same treatment (72). Moreover, the same mutant does not accumulate serotonin in higher amount upon infection with *B. oryzae*, unlike wild-type plants (58). Correspondingly, *T5H* expression was shown in rice to increase upon treatment with chitin or inoculation with *M. grisea* (71). In Brachypodium, expression of a putative *T5H* ortholog was induced in seedlings after

inoculation with *F. pseudograminearum* (31), and in spikes after inoculation with *F. graminearum* (61). Taken together these results confirm the role of T5H in serotonin biosynthesis.

Despite the lack of functional T5H, *sl* plants are still able to produce low levels of serotonin suggesting existence of an additional T5H homolog or an alternative serotonin biosynthetic pathway (73). In mammals, serotonin is produced from 5-hydroxytryptophan by TDC. To check if rice enzymes have also capacity to catalyze this reaction, *TDC1* was heterologously expressed in yeast and *Escherichia coli*, and ectopically expressed in rice leaves. The purified protein from *E. coli* showed a potential to metabolize 5-hydroxytryptophan into serotonin. Feeding experiment on cut transgenic rice leaves, and on yeast and *E. coli* cell cultures expressing *TDC1* lead to the same conclusion (74). Finally, when *T5H* expression was repressed in rice by Ribonucleic acid (RNA) interference, higher accumulation of 5-hydroxytryptophan than in the wild-type was observed, suggesting a partial rerouting of tryptophan metabolism pathway upon accumulation of tryptamine (75). Taken together, these results do not exclude the existence of an alternative serotonin biosynthetic pathway in rice.

Enhanced serotonin accumulation observed upon inoculation with fungal pathogens suggests that this compound plays a role in immunity. In order to verify if serotonin or biosynthetically-related metabolites may act directly as toxic agents, these compounds were tested for their antifungal activity. Serotonin inhibited *in vitro* sporulation of *P. nodorum*, but with no effect on vegetative growth (60). Antifungal properties of serotonin were also tested *in vitro* with *F. graminearum*, showing a slightly negative effect on growth and a delay in conidia germination (61). Also, serotonin- and tryptamine-derived compounds were tested for their fungicidal activity. 5,5′-dihydroxy-2,4′-bitryptamine, 3-(2-aminoethyl)-3-hydroxyindolin-2-one, along with serotonin, were shown *in vitro* to inhibit *B. sorokiniana* conidia germination. Interestingly, the inhibition rate measured for serotonin dimer was five times higher than for serotonin (59). These results suggest that 5,5′-dihydroxy-2,4′-bitryptamine, rather than the monomeric serotonin, acts as an antifungal compound.

3.1.1.2 Gramine

Tryptophan is also the precursor of gramine, a phytoanticipin found in *Hordeum* species, reed canary grass (*Phalaris arundinacea*), and giant cane (*Arundo donax*) (76, 77). This compound is constitutively present in leaves of cultivated barley seedlings and its accumulation increases in response to mechanical stress or inoculation with *Blumeria graminis* (Figure 3) (78). Gramine biosynthesis requires participation of *N*-methyltransferase (NMT) whose activity was observed *in vitro* in barley leaf extract after long-term heat stress (Figure 4). Enzymatic assays indicated that a single NMT is probably responsible for the last two steps of gramine biosynthesis in barley (79). It was found that gramine-deficient barley cultivars lack a single gene, which was suggested to code for an NMT. This assumed function was addressed with enzymatic assays confirming NMT activity for the heterologously expressed protein (80).

3.1.1.3 Benzoxazinoids

BXs are the most common phytoanticipins reported in Poaceae crop plants (81). They are produced in maize, wheat, rye, *Chusquea cumingii*, *Elymus gayanus* and members of *Hordeum* genus including wild barley (*Hordeum spontaneum*), but so far were not identified in close relatives, like oat, rice, cultivated barley and Sorghum (Figure 3) (76, 82-84). Recent metabolic analyses of 64 Poaceae species indicated the presence of BXs also in cat grass (*Dactylis glomerata*), *Briza maxima*, reed canary grass, jointed goatgrass (*Aegilops cylindrica*), Centipedegrass (*Eremochloa ophiuroides*), Guinea grass (*Panicum maximum*), wavyleaf basketgrass (*Oplismenus undulatifolius*) and two species of *Echinochloa* (77). BXs are constitutively stored as glucosides. The prominent form of BX glucosides in maize and wheat is 2,4-dihydroxy-7-methoxy-1,4-benzoxazin-3-one glucoside (DIMBOA-Glc), whereas in rye and wild barley 2,4-dihydroxy-1,4-benzoxazin-3-one glucoside (DIBOA-Glc) is found in the highest amount. In addition, 2-hydroxy-4,7-dimethoxy-1,4-benzoxazin-3-one glucoside (HDMBOA-Glc) has been identified in maize (85), wheat (86) and Job's tears (*Coix lacryma-jobi*) (87). BXs are not exclusively present in monocots but were also found in other plant families like Acanthaceae, Ranunculaceae, Scrophulariaceae, and Lamiaceae (82).

BX biosynthetic pathway starts with the conversion of IGP to indole, catalyzed by Benzoxazinoneless1 (Bx1), a close homolog of the tryptophan synthase α-subunit (Figure 6). *Bx1* from maize was heterologously expressed and *in vitro* enzymatic assays showed that the obtained protein was catalyzing formation of indole (88). Leaf extract from *bx1*, a maize line bearing a mutation in *Bx1* gene, was shown to lack tryptophan synthase α monomer activity unlike extract from the wild type plants (89). This mutant also accumulates significantly lower amounts of BXs as compared to wild type plants (90). These results confirm the role of Bx1 in IGP conversion into indole in BX biosynthesis. During the next steps four CYP monooxygenases, Bx2 to Bx5, subsequently oxidize indole into DIBOA. Genes coding for these enzymes in maize were heterologously expressed, and enzymatic assays confirmed the specificity of the obtained proteins for each subsequent step in BX biosynthesis (88). Orthologs of maize *Bx2* - *Bx5* were identified in *Hordeum lechleri* and in wheat based on sequence homology and subsequent enzymatic assays of heterologously expressed proteins (84, 91). Phylogenetic analyses in

Brachypodium, foxtail millet, maize, sorghum, rice, wheat, and *H. lechleri* indicated existence of four separate clades, corresponding to *Bx2*-*Bx5* genes, constituted almost exclusively by genes from maize, *H. lechleri*, and wheat (92). The exception were two sequences from rice grouped in the clade gathering *Bx2* orthologs coding for P450s which are not yet biochemically characterized. The remaining sequences from rice and from other tested species were distant from the clades comprising enzymes involved in DIBOA biosynthesis supporting the idea that these species are not capable to produce BXs (Figure 3).

BX biosynthetic pathway continues with DIBOA glucosylation either by Bx8 or Bx9, which are redundant uridine diphosphate glucose (UDP)-glucosyltransferases. Activity of these enzymes was confirmed by enzymatic assays on heterologously expressed genes from maize (93). Orthologs of *Bx8*/*Bx9* have been also identified in wheat and rye by homology with maize genes (94). The following steps in the pathway start with the conversion of DIBOA-Glc to DIMBOA-Glc mediated by dioxygenase Bx6 and methyltransferase Bx7. Recombinant Bx6 and Bx7 produced in *E. coli* were shown *in vitro* to possess activity corresponding to the formation of DIMBOA-Glc from DIBOA-Glc (95). Finally, HDMBOA-Glc is produced from DIMBOA-Glc by DIMBOA-Glc 4-*O*-methyltransferase (Bx10). This enzyme was purified from wheat leaves and *in vitro* enzymatic assays confirmed its activity (87). Three putative *Bx10* were identified by quantitative trait locus mapping, and the heterologously expressed proteins showed DIMBOA-Glc *O*-methyltransferase activity during *in vitro* enzymatic assays (96).

In maize, genes coding for Bx1-8 are located next to each other forming the first operon-like specialized metabolite gene cluster reported in plants (97). Only *Bx9* and *Bx10* are located separately on another chromosome (93, 96). Clusters of *Bxs* are also found in wheat and rye, but in these cases, *Bx1* and *Bx2* are grouped on one chromosome, while *Bx3*-5 on another one (98). This gene organization facilitates a common transcriptional regulation of genes coding for enzymes involved in the same metabolic pathway.

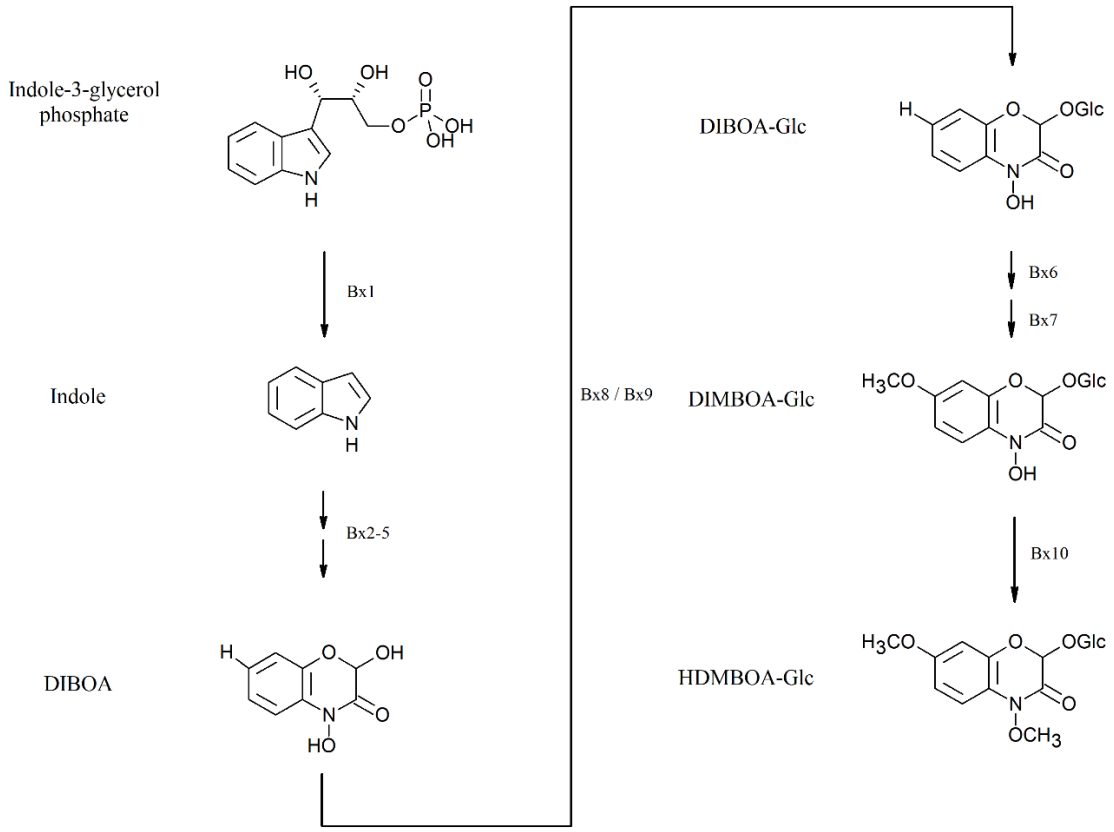

Figure 6: Simplified benzoxazinoid biosynthetic pathway. Bx1-10: Benzoxazineless1-10; DIBOA: 2,4-dihydroxy-1,4-benzoxazin-3-one; DIBOA-Glc: 2,4-dihydroxy-1,4-benzoxazin-3-one glucoside; DIMBOA-Glc: 2,4-dihydroxy-7-methoxy-1,4-benzoxazin-3-one glucoside; HDMBOA-Glc: 2-hydroxy-4,7-dimethoxy-1,4-benzoxazin-3-one glucoside.

Glucosylated forms of DIBOA and DIMBOA are biologically inactive and are stored in vacuoles prior pathogen attack. Certain β-glucosidases from maize (99), wheat (100), and rye (101) were purified from plant or heterologously expressed and have been shown to hydrolyze glucosylated BXs to their aglucone forms. One of these compounds, DIBOA, has been found to inhibit *in vitro* growth of *Gaeumannomyces graminis* var. *tritici*, the pathogen responsible for the root take-all disease of wheat (102). Another BX, DIMBOA can inhibit *in vitro* spore germination of *Setosphaeria turcica*, the causal agent of northern corn leaf blight in maize (103). It has been suggested that DIMBOA-Glc and HDMBOA-Glc can be further degraded to 6-methoxy-2-benzoxazolinone (MBOA) (85). This compound prevents *in vitro* growth of several fungal pathogens of maize including

Fusarium monoliform, *Gibberella zeae*, *Pyrenochaeta terrestris* and *Diplodia zeae*, (104). MBOA also inhibits *in vitro* conidia germination and germ tube growth of *B. maydis* (85). The inability to detect BX aglucones in intact plant tissue suggests a compartmentation of BX glucosides from β-glucosidases responsible for their conversion into potentially toxic metabolites (93, 105). Tissue damage could cause the release of BX glucosides and put them in presence of β-glucosidases, which hydrolyze these compounds to their aglucone forms, a mechanism also used by other plant species to activate different types of phytoanticipins (46).

3.1.2 Phenylalanine derived compounds

Phenylalanine is the precursor of a vast range of specialized metabolites called phenylpropanoids whose biosynthesis starts with the conversion of phenylalanine to cinnamic acid by the phenylalanine ammonia-lyase (PAL; Figure 7) (106). This entry-point enzyme is involved in stress response and developmental processes, and has been studied in many plant species (107). In monocots, certain PALs possess also tyrosine ammonia-lyase (TAL) activity and consequently are capable to convert tyrosine to *p*-coumaric acid (108, 109). As indicated by experimental evidence this broader substrate specificity depends on a single amino acid exchange (110). PAL is represented by different isoforms in grass species like sorghum (111), wheat (112), bamboo (*Bambusa oldhamii*) (113), barley (114), rice (115), and maize (116). In Brachypodium, eight genes putatively coding for PALs have been identified and heterologously expressed (108, 117, 118). Enzymatic assays carried out with the obtained proteins showed that one of them accepts phenylalanine and tyrosine as substrates, while remaining ones have exclusively PAL activity, which is consistent with the properties predicted from the amino acid sequences (108, 118). Expression of only two Brachypodium *PALs* was found to be induced in spikes inoculated with *F. graminearum* (61). In rice, treatment with different pathogens triggered expression of seven out of nine putative *PALs* genes (119). These results indicate that only particular PAL isoforms are linked with plant immunity.

Phenylpropanoid pathway continues with the conversion of cinnamic acid to *p*-coumaric acid by 4-cinnamic acid hydroxylase (C4H). In turn, *p*-coumaric acid can be activated to *p*-coumaroyl- Coenzyme A (-CoA) by 4-coumarate-CoA ligase (4CL). *p*-coumaric acid and *p*-coumaroyl-CoA are both precursors of compounds representing different

phenylpropanoid subclasses including hydroxycinnamic acids (HCAs), flavonoids, and stilbenes (Figure 7).

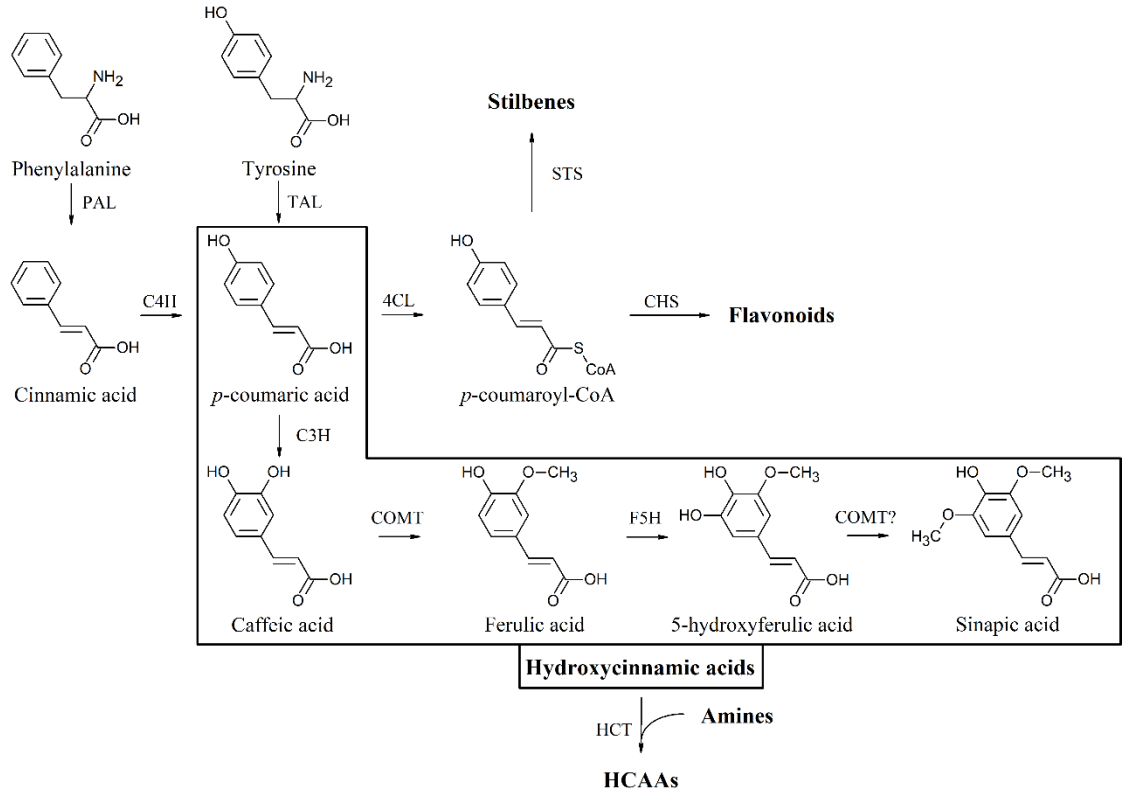

Figure 7: Simplified phenylpropanoid biosynthetic pathway. 4CL: 4-coumarate-CoA ligase; C3H: p-coumarate 3-hydroxylase; C4H: 4-cinnamic acid hydroxylase; CHS: chalcone synthase; COMT: caffeic acid-O-methyltransferase; F5H: ferulate 5-hydroxylase; HCAAs: hydroxycinnamic acid amides; HCT: hydroxycinnamoyltransferase; PAL: phenylalanine ammonia-lyase; STS: stilbene synthase; TAL: tyrosine ammonia-lyase.

3.1.2.1 Hydroxycinnamic acids and their conjugates

HCAs have a C_6-C_3 skeleton, and their phenol ring possesses one to three hydroxyl groups that can be methylated (Figure 7). The simplest representative of them is *p*-coumaric acid that can be converted by *p*-coumarate 3-hydroxylase (C3H) to caffeic acid. This compound can be metabolized to ferulic acid by caffeic acid *O*-methyltransferase (COMT). Ferulate 5-hydroxylase (F5H) is an enzyme that hydroxylates ferulic acid to form 5-hydroxyferulic acid. This compound can be further metabolized by COMT to give sinapic acid.

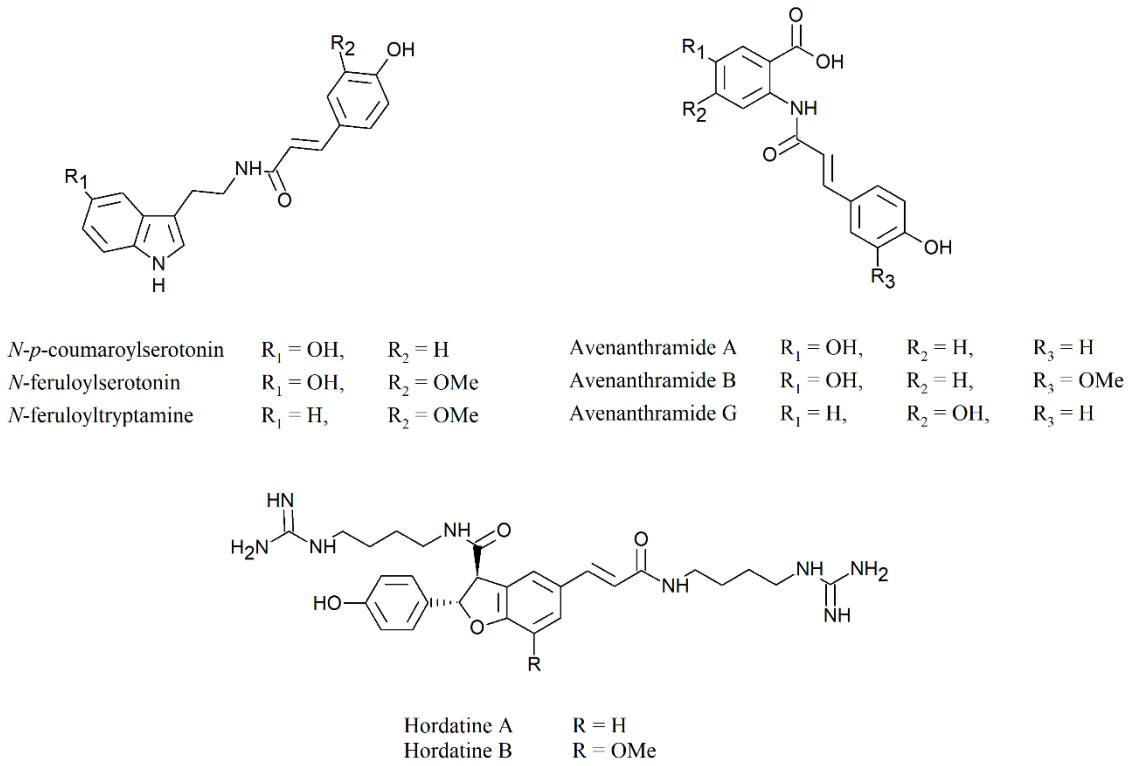

N-*p*-coumaroylserotonin	R_1 = OH,	R_2 = H	Avenanthramide A	R_1 = OH,	R_2 = H,	R_3 = H
N-feruloylserotonin	R_1 = OH,	R_2 = OMe	Avenanthramide B	R_1 = OH,	R_2 = H,	R_3 = OMe
N-feruloyltryptamine	R_1 = H,	R_2 = OMe	Avenanthramide G	R_1 = H,	R_2 = OH,	R_3 = H

Hordatine A	R = H
Hordatine B	R = OMe

Figure 8: Chemical structures of selected hydroxycinnamic acid amides.

In plants, HCAs are frequently found linked to other compounds, leading to a variety of conjugates including HCA amides (HCAAs) formed in a reaction between HCAs and amines. HCAAs are widely distributed in plant species, including grasses, and are involved in different growth and developmental processes, as well as in plant defense (Figure 3). *N*-*p*-coumaroylserotonin (CouSer) and *N*-feruloylserotonin (FerSer; Figure 8) were found to be more abundant in twigs of bamboo (*Phyllostachys bambusoides*) infected with *Aciculosporium take* (120), in rice leaves infected with *B. oryzae* or *Cochliobolus miyabeanus* (58, 121), and in Brachypodium spikelets infected with *F. graminearum* (61), as compared to uninfected organs of respective species. Metabolomic analysis performed on wheat leaves treated with SnToxA revealed higher quantities of FerSer and *N*-feruloytryptamine (FerTry) as compared to non-treated leaves (60). In maize, FerTry and *N*-p-coumaroyltryptamine (CouTry) had enhanced accumulation in leaves and roots inoculated with *Colletotrichum graminicola* (122). In barley, two pathogen-inducible HCAA dimers were identified including hordatine A, a dimer of *N*-*p*-coumaroylagmatine (CouAgm), and hordatine B, a conjugate of CouAgm and *N*-feruloylagmatine (FerAgm; Figure 8) (123). In addition, hydroxy-CouAgm has been

found in higher amounts in leaves of resistant barley line compared to a susceptible line, both inoculated with *B. graminis* (124).

Avenanthramides whose amide moiety comes from anthranilic acid are HCAAs unique for oat species. Four different representatives of these compounds, avenanthramide A, B, L and G (Figure 8), as well as their five dimers, were more abundant in oat leaves upon inoculation with *Puccinia coronata* sp. *avenae* and in oat cell suspensions treated with chitin or chitooligosaccharide (125-128).

To form HCAAs, HCAs are activated to CoA thioesters and then conjugated with amines by specific hydroxycinnamoyltransferases (HCTs), enzymes that transfer hydroxycinnamoyl units to an acceptor group to form an ester or an amide (Figure 7). HCTs involved in HCAA formation belong to the large BAHD acyltransferase family named after the first letters of its reported members (Benzyl alcohol *O*-acetyltransferase, Anthocyanin *O*-hydroxycinnamoyltransferase, *N*-Hydroxycinnamoyl/benzoyltransferase, and Deacetylvindoline 4-*O*-acetyltransferase) (129). Enzymes of the BAHD acyltransferase family possess two highly conserved domains. The HXXXD(G) motif is located in the central region of the protein sequence, is involved in substrate binding (130), and can be found in other acyltransferases using coenzyme A thioester as substrate. The other highly conserved domain is constituted by the DFGWG motif located near the carboxyl terminus, and has rather a structural than a catalytic role (131). HCTs using an amine as acceptor group are agmatine coumaroyltransferases (ACTs), agmatine hydroxycinnamoyl transferases (AHTs), hydroxycinnamoyl-CoA:hydroxyanthranilate HCTs (HHTs), putrescine hydroxycinnamoyltransferases (PHTs), serotonin hydroxycinnamoyltransferases, spermidine hydroxycinnamoyl transferases (SPHTs), tryptamine HCTs (THTs), and tyramine feruloyl-CoA transferases (TFTs) (129, 131).

In rice, *in vitro* assays with heterologously expressed enzyme combined with *in vivo* assays with overexpression of genes coding for respective enzymes allowed to identified two SPHTs (132), an AHT, three PHTs, two THTs, and one tryptamine benzoyl transferase (TBT), which can use *p*-coumaroyl-CoA as a substrate (133). *In vitro* assays conducted on another heterologously expressed HCT showed activity with both putrescine and agmatine as acyl acceptors and both *p*-coumaroyl-CoA and feruloyl-CoA as acyl donors (134). A putative *HCT* from maize was over-expressed in rice and the

obtained transgenic lines accumulated *N*,*N*-Diferuloylputrescine (DiFerPut), an HCAA absent in the wild type rice cultivar, indicating that this gene is probably coding for a PHT (135). Heterologously expressed Brachypodium HCT was able to use agmatine, cadaverine, putrescine as acyl acceptor, and caffeoyl-CoA, cinnamoyl-CoA, *p*-coumaroyl-CoA, and feruloyl-CoA as acyl donor, revealing the broadest *in vitro* substrate range among the so far investigated HCTs (136).

Expression of many HCTs has been found to be induced during the response to pathogen recognition. In barley, the activity of a PHT and TFT was found to increase upon inoculation with *B. graminis* (137). A complementary DNA (cDNA) library constructed using messenger RNA (mRNA) isolated from barley leaves inoculated with the same pathogen allowed to heterologously express three putative ACTs. Enzymatic assays showed that these enzymes had a higher specificity for *p*-coumaroyl-CoA than for feruloyl-CoA and caffeoyl-CoA. The affinity for agmatine, tyramine, and putrescine was also tested, and enzymatic activity was detected only with agmatine as acyl acceptor. This suggests a role of tested ACTs in barley defense response (138). Comparison between transcriptomes of Brachypodium control spikelets and spikelets infected with *F. graminearum* showed that the expression of five putative *HCT*s was upregulated upon infection (61). Four HHT cDNAs have been isolated in oat from a library constructed using mRNA isolated from leaves treated with crude extracts of *Pseudomonas fluorescens* (139). Expression of *HHT1* was induced in oat leaves upon inoculation with *P. coronata* f. sp. *avenae* in a resistant cultivar (140), and HHT activity was detected in crude protein extract from *E. coli* heterologoulsy expressing this gene (139). This variety of HCTs induced upon pathogen recognition may reflect the diversity of substrates used in HCAA formation, as well as different functions that these compounds may have in plant immunity.

Apart from the soluble fraction, HCAAs have been found to accumulate in the cell wall of potato tissue upon inoculation with various fungal pathogens, and to be covalently attached to the aliphatic domains of suberin, a polymer forming a protective layer of the cell wall (141, 142). This cross-linking has been postulated to reduce the digestibility of the cell wall and restrain pathogen colonization (124). Nevertheless, the production of HCAAs in response to pathogen attack exceeds the rate of incorporation into the cell wall, suggesting another role in defense mechanisms for this group of compounds (143). This

role could be linked with the antifungal properties of some HCAAs. For instance, CouSer and FerSer inhibited *C. miyabeanus* conidial germination *in vitro* (121). CouSer stopped *A. take* growth *in vitro* at a concentration higher than 100 µg/ml (120), but did not inhibit *B. oryzae* growth *in vitro* (144). Hordatine A and hordatine B have been found to possess *in vitro* antifungal activity against a range of fungal pathogens, including *Colletotrichum gloeosporioides* and *B. sorokiniana* (145). Hydroxy-CouAgm showed *in vitro* antifungal activity against *B. graminis* f. sp. *hordei* (124). Taken together, these results show that in addition to cell wall reinforcement HCAAs may act as antifungal compounds in grasses.

3.1.2.2 Flavonoids

Flavonoids constitute a large subfamily of phenylpropanoids, with more than 10 000 compounds reported so far (146). They are characterized by their chemical structure consisting of two phenyl rings and a central heterocyclic ring. Depending on the modification of the central ring, flavonoids are divided into different classes, including flavonols, flavanones, flavanols, anthocyanins, or isoflavones.

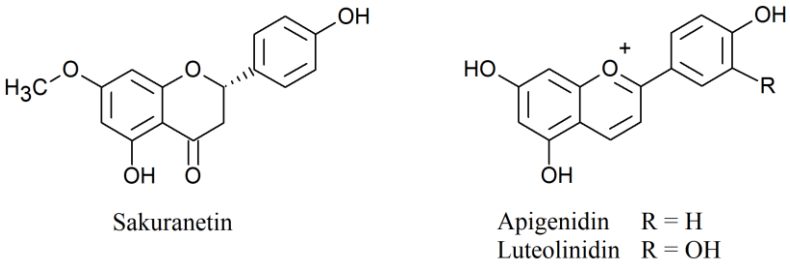

Figure 9: Chemical structures of selected flavonoids.

Despite the large structural diversity of flavonoids, only a few of them have been reported to be linked with plant immunity. Among those is sakuranetin (7-*O*-methylnaringenin; Figure 9), a flavone, which was found to accumulate in bigger amount in rice leaves after inoculation with *M. grisea (51)*. 3-deoxyanthocyanidins, including apigenidin and luteolinidin (Figure 9) are colored flavonoids found to be produced in leaves of a resistant cultivar of sorghum upon inoculation with *Colletotrichum sublineolum* or *B. maydis* (147, 148), in leaves and roots of maize upon inoculation with *C. graminicola* (122), or in sugarcane stalks upon inoculation with *Colletotrichum falcatum* (Figure 3) (147-149).

Biosynthetic pathway of flavonoids starts with the metabolization of *p*-coumaroyl-CoA by a chalcone synthase (CHS; Figure 7). This enzymatic activity was induced in sorghum

mesocotyls inoculated with *C. graminicola* (150) and the expression of a *CHS* gene was found to be induced in barley leaves upon inoculation with *B. graminis* f. sp. *hordei* (151). This suggests that flavonoids are synthesized to take part in plant defense mechanisms in these two grass species.

Investigation of the antimicrobial properties of sakuranetin showed that this compound inhibits spore germination of *M. grisea* (152). Sakuranetin has been also identified as a competitive inhibitor of β-hydroxyacyl-acyl carrier protein dehydratase from *Helicobacter pylori* (153). This enzyme is involved in fatty acid synthesis, and the disruption of this biosynthetic pathway by sakuranetin could explain its antifungal activity. 3-deoxyanthocyanidins possess *in vitro* anti-fungal properties against different fungal pathogens including *C. sublineolum* (154-156). Under particular pH conditions, 3-deoxyanthocyanidins can form self-aggregating structures in epidermal cells. These spherical microstructures called inclusions have been shown to disrupt lipid bi-layers. When the cell wall is partially hydrolyzed by the fungus these structures migrate to the site of penetration possibly to disrupt the plant cell membrane, and cause cell collapse. Subsequently, 3-deoxyanthocyanidin inclusions can be released into the apoplast, where they can target the fungal plasma membrane (157).

3.1.2.3 Stilbenes

Stilbenes are characterized by their structure consisting of two phenyl groups linked by an ethylene moiety, and they differ in their phenyl group substitutions. More than 450 different stilbene structures were identified so far in approximatively 30 plant families (158, 159).

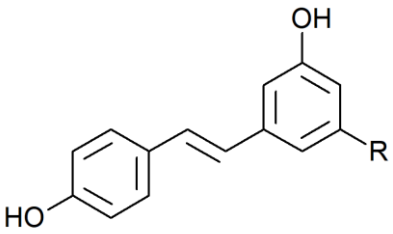

Resveratrol R = OH
trans-piceid R = OGlc

Figure 10: Chemical structures of selected stilbenes.

Colonization of aerial parts and/or seeds of tall fescue (*Festuca arundinacea*) and different species of *Lolium* and *Hordeum* infected with the *Acremonium* endophytes caused the accumulation of resveratrol (Figure 10) in higher amounts in the infected tissues than in non-infected ones (Figure 3) (160). Infection of sorghum seedlings with *C. sublineolum* revealed enhanced accumulation of glucosylated resveratrol, *trans*-piceid, in mesocotyl extract (161).

Resveratrol is synthesized from *p*-coumaroyl-CoA by the stilbene synthase (STS; Figure 7). In sorghum, *SbSTS1* was found to have its expression induced after mesocotyl inoculation with *Cochliobolus heterotrophus* or *C. sublineolum* (162).

Collectively, results obtained on the metabolic and transcriptomic level indicate involvement of stilbene biosynthetic pathway in defense against pathogens in sorghum and other plant species. In accordance with this assumption, resveratrol inhibited *in vitro Botrytis cinerea* conidia germination and mycelium growth (163). Overexpression of *STS* from *Polygonum cuspidatum* in Arabidopsis led to *trans*-piceid accumulation and enhanced resistance against *Colletotrichum higginsianum*, suggesting a role in defense mechanism of glucosylated resveratrol (164). However, no clear antifungal *in vitro* activity was observed for this compound against *C. sublineolum* (161). This suggests that *trans*-piceid either possesses antifungal activity against specific pathogens, or is the precursor of other compounds involved in immunity.

3.1.3 Polyamines

Polyamines are aliphatic compounds possessing two or more amine groups, and are constitutively present in all living organisms. The amount of these compounds has been found to increase in response to biotic and abiotic stresses in certain plant species (165, 166). For instance in grasses, increased accumulation of spermine and putrescine (Figure 11) have been observed in barley leaves inoculated with *B. graminis* (137, 167) and in "green islands" surrounding infection sites upon inoculation with *Puccinia hordei* (168). Putrescine, spermidine, and cadaverine amounts are accruing after inoculation of wheat heads with *F. graminearum* (169).

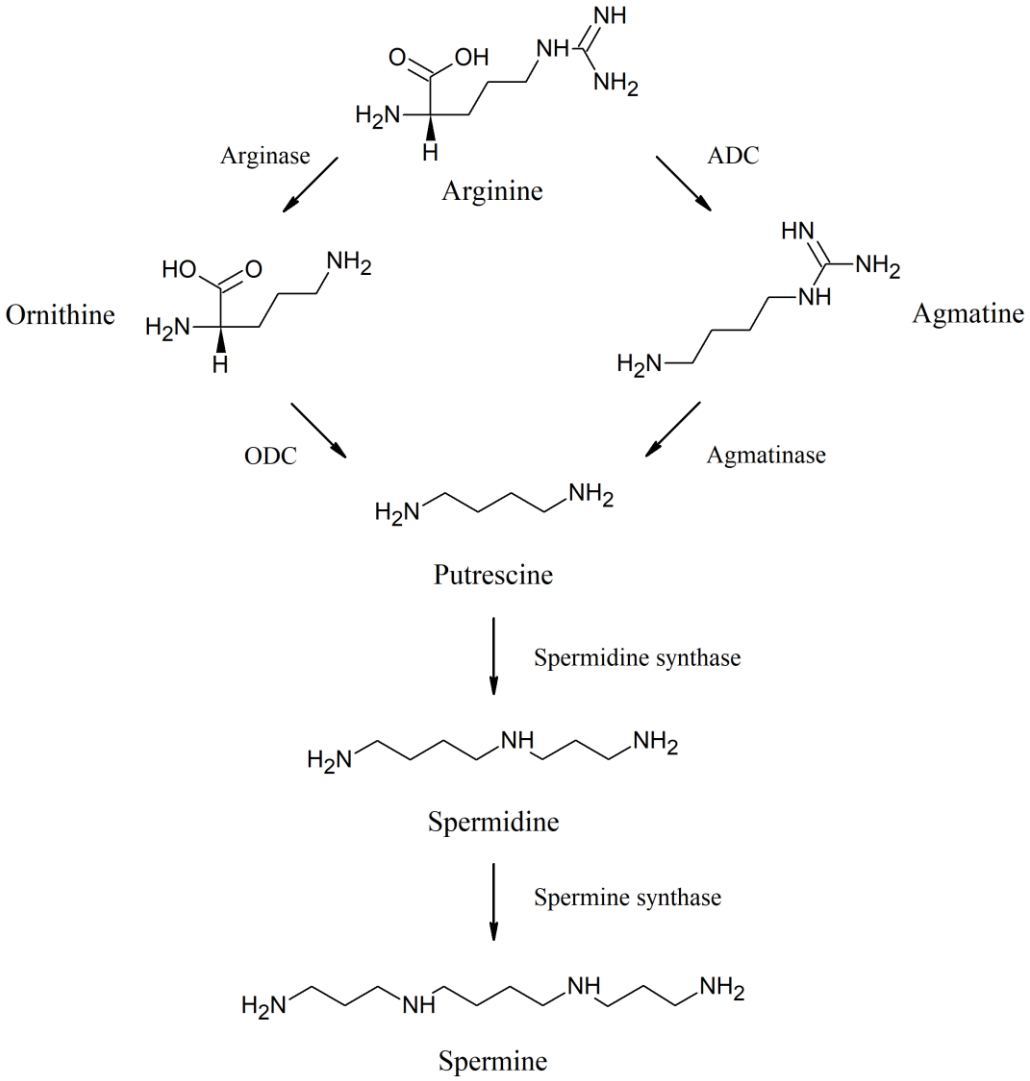

Figure 11: Simplified polyamine biosynthetic pathway. ADC: arginine decarboxylase; ODC: ornithine decarboxylase.

Putrescine, spermidine, and spermine are biosynthetically linked and synthesized from the same precursor, arginine (Figure 11). This amino acid is a branching point for two different biosynthetic pathways leading to putrescine. One of them involves metabolization of arginine to ornithine by an enzyme known as arginase. In turn, ornithine is converted to putrescine by ornithine decarboxylase (ODC). The other branch pathway leading to putrescine involves first arginine decarboxylase (ADC) to form agmatine, which is then converted to putrescine by agmatinase. The activity of ODC and ADC has been shown to increase in barley leaves upon infection with *B. graminis* (137). Additionally, expression of genes coding for these enzymes was induced in wheat upon inoculation with *F. graminearum* (169). Conversion of putrescine to spermidine is catalyzed by a spermidine synthase. In turn, spermidine can be metabolized into spermine by a spermine synthase.

The antifungal activity of free polyamines is not well documented, and these compounds are also produced by microorganisms, in which they fulfill important physiological functions (170). For this reason, it is likely that these compounds do not function directly as antimicrobial agents, but are rather involved in plant immunity through other mechanisms, e.g. HCAAs biosynthesis.

3.1.4 Cyanogenic glycosides

Cyanogenic glycosides (CGs) are phytoanticipins widely present in more than 2500 plant species, including grasses (171). These compounds are glycosylated forms of α-hydroxynitriles that could be derived from tyrosine, phenylalanine, valine, isoleucine or leucine. In barley, leucine is the precursor of epiheterodendrin and four structurally related non-cyanogenic cyano glucosides, while tyrosine is the precursor of dhurrin in sorghum (Figure 3 & 12) (172, 173).

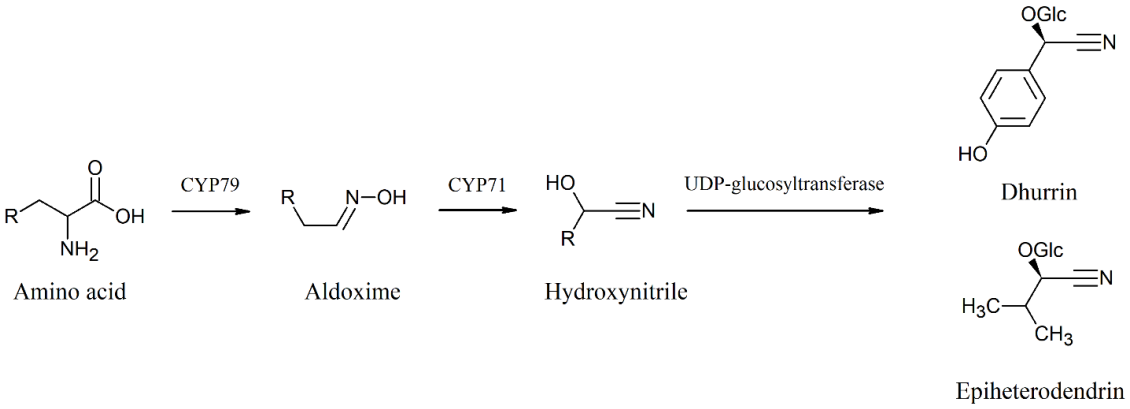

Figure 12: Biosynthetic pathway of cyanogenic glycosides (CGs). Tyrosine-derived dhurrin and leucine-derived epiheterodendrin are shown as CG exemplary structures.

CGs are synthesized in three enzymatic steps (Figure 12). In the first step, the precursor amino acid is metabolized to the corresponding aldoxime by a CYP monooxygenase from the CYP79 family. The aldoxime is converted into hydroxynitrile by a CYP monooxygenase representing the CYP71 family. Finally, the hydroxynitrile is glucosylated by an UDP-glucosyltransferase to yield a CG (171). Similarly to benzoxazinoid biosynthetic genes in maize, wheat, and rye, genes encoding enzymes responsible for CG biosynthesis were found to be clustered in distant species including sorghum, cassava (*Manihot esculenta*), and *Lotus japonicas*. This organization in the genome may facilitate a common transcriptional regulation of this biosynthetic pathway (174).

Intact CGs do not possess antimicrobial activity and have to be activated to fulfill their defensive function. To this end, they are first hydrolyzed by a specific β-glucosidase giving the corresponding hydroxynitrile, which in turn is hydrolyzed by a specific α-hydroxynitrile lyase resulting in the release of hydrogen cyanide (HCN). Cyanide anion is highly reactive and can effectively inhibit the activity of mitochondria cytochrome oxidase making HCN toxic to living organisms (175). In sorghum, dhurrin was found to accumulate predominantly in leaf epidermal cells, while dhurrin β-glucosidase and α-hydroxynitrile lyase localized exclusively in mesophyll tissue (172). The storage of substrate and hydrolytic enzymes in different cellular compartments may prevent spontaneous HCN release and subsequent self-poisoning. Upon tissue disruption, that can be caused by herbivores or eventually pathogens, CGs and both enzymes are put in

contact releasing HCN (171). In barley, epiheterodendrin, similar as dhurrin in sorghum, has been found in epidermal cell layer of seedling leaves. However, the corresponding cyanogenic β-glucosidase was detected only in the endosperm of germinating seeds. This could explain why detached barley leaves do not release HCN upon inoculation with *B. graminis* f. sp. *hordei*, despite the presence of epiheterodendrin (173).

3.1.5 Terpenoids

Terpenoids form the largest class of specialized metabolites gathering more than 20 000 known compounds (176). These complex molecules originate from the condensation of several IPP units. Terpenoids are conserved in plant kingdom and can fulfill different roles including photosynthetic pigments, electron carriers, development regulators, or membrane structural elements (177). In plant immunity, terpenoids may act as phytoalexins or phytoanticipins.

3.1.5.1 Simple terpenoids

The so far identified terpenoid phytoalexins originate from the condensation of either three IPP units, leading to sesquiterpenoid formation, or four IPP units, leading to diterpenoid formation, and have been reported in rice and maize (Figure 3) (46). Rice produces three classes of diterpenoid phytoalexins: phytocassanes, oryzalexins, and momilactones (Figure 13) (178). Phytocassanes have been found to be produced in accrued amounts in rice leaves infected with *M. grisea* and in rice stems treated with *Rhizoctonia solani* (179-181). Inoculation with *M. grisea* also induced the accumulation of higher amounts of oryzalexins in rice leaves (182), and momilactones in rice leaves and straws (54). Kauralexins, zealexins, and dolabralexins (Figure 13) are terpenoid phytoalexins identified in maize. Upon infection with *Rhizopus microsporus*, the amount of six kauralexins was induced compared to uninfected plants (183). Zealexins are sesquiterpenoids, which are produced in stems infected with *F. graminearum* (184). Maize roots inoculated with *F. graminearum* and *Fusarium verticillioides* accumulated dolabralexins, namely dolabradiene and two of its derivatives, in higher amounts than in control plants (185).

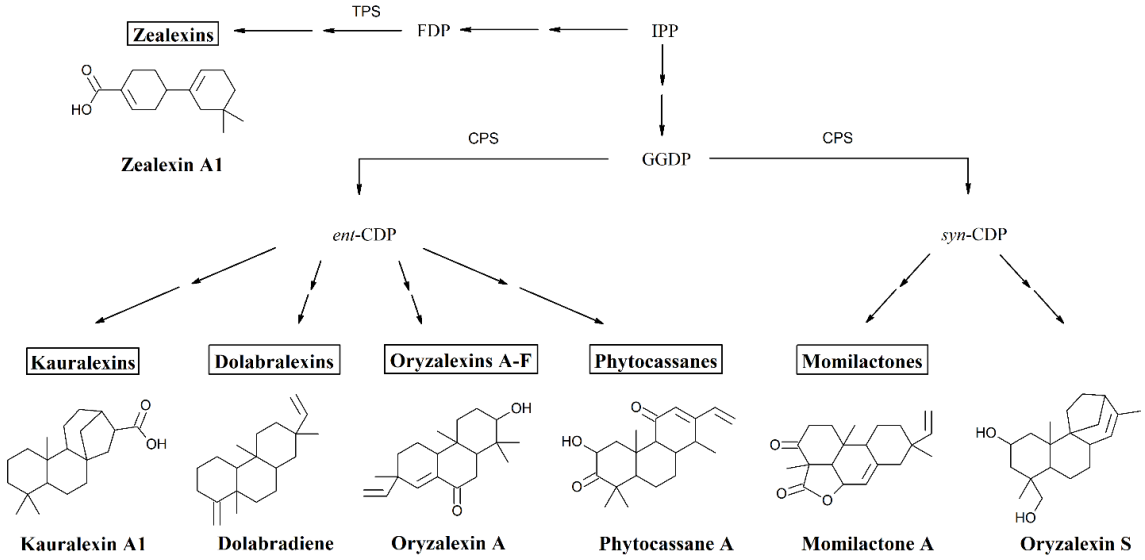

Figure 13: Simplified terpenoid phytoalexin biosynthetic pathway from rice and maize. Each phytoalexin class is illustrated by a representative compound. CDP: copalyl diphosphate; CPS: copalyl synthase; FDP: farnesyl diphosphate; GGDP: geranylgeranyl diphosphate; IPP: isopentenyl pyrophosphate; TPS: terpene synthase.

Biosynthesis of zealexins starts with condensation of three IPP units to form farnesyl diphosphate (FDP; Figure 13). Two genes coding for terpene synthases (TPSs) catalyzing the production of β-macrocarpene, a potential precursor of zealexin were identified in maize. *ZmTps6* and the nearly identical gene *ZmTps11* were found to have transcription levels increasing upon inoculation with different fungi (184). During the biosynthesis of the remaining groups of terpenoid phytoalexins, IPP condensation leads to geranylgeranyl diphosphate (GGDP) that is further metabolized by two different copalyl synthases (CPS) to stereoisomers of copalyl diphosphate (CDP), *ent*-CDP or *syn*-CDP. The CPS involved in kauralexin and dolabralexin biosynthesis in maize have been found to be encoded by the pathogen-inducible *Anther Ear 2* (*ZmAN2*) (185, 186). *ent*-CDP is the precursor to kauralexins, dolabralexins, oryzalexins A-F, and phytocassanes. *syn*-CDP is the precursor of momilactones and oryzalexin S. Like for benzoxazinoid and cyanogenic glucoside biosynthesis, genes involved in biosynthesis of some terpenoid phytoalexins are clustered. Two such clusters were identified in rice, for the biosynthesis of momilactone A (187) and phytocassanes respectively (188). No terpenoid phytoalexin was identified in wheat or barley, but putative *CPS* orthologs were identified in these species, suggesting another function for these genes (189, 190).

Members of the different terpenoid phytoalexin classes showed antifungal activity *in vitro*. For example, zealexin A4 inhibited *in vitro* growth of *Aspergillus flavus* (191), two kauralexins showed antifungal activity against *R. microsporus* and *C. graminicola* (183), two dolabralexins had *in vitro* inhibitory effect on *F. graminearum* and *F. verticillioides* growth (185), and phytocassanes and momilactones prevented spore germination and germ tube growth of *M. grisea* (180). This shows that the identified terpenoid phytoalexins may contribute to the protection against a variety of fungal pathogens.

3.1.5.2 Saponins

Saponins are glycosylated triterpenoids, steroids or steroidal alkaloids present constitutively in different plant species (192). These compounds possess characteristic structures consisting of a hydrophobic part linked to a hydrophilic sugar moiety. In grasses, oat is a model species to study saponin biosynthesis and function. This species produces two different saponin classes, which accumulate in a tissue-specific manner. Triterpenoid saponins named avenacins are present exclusively in roots (193), while steroidal saponins known as avenacosides are present in leaves and grains (Figure 3 & 14) (194, 195).

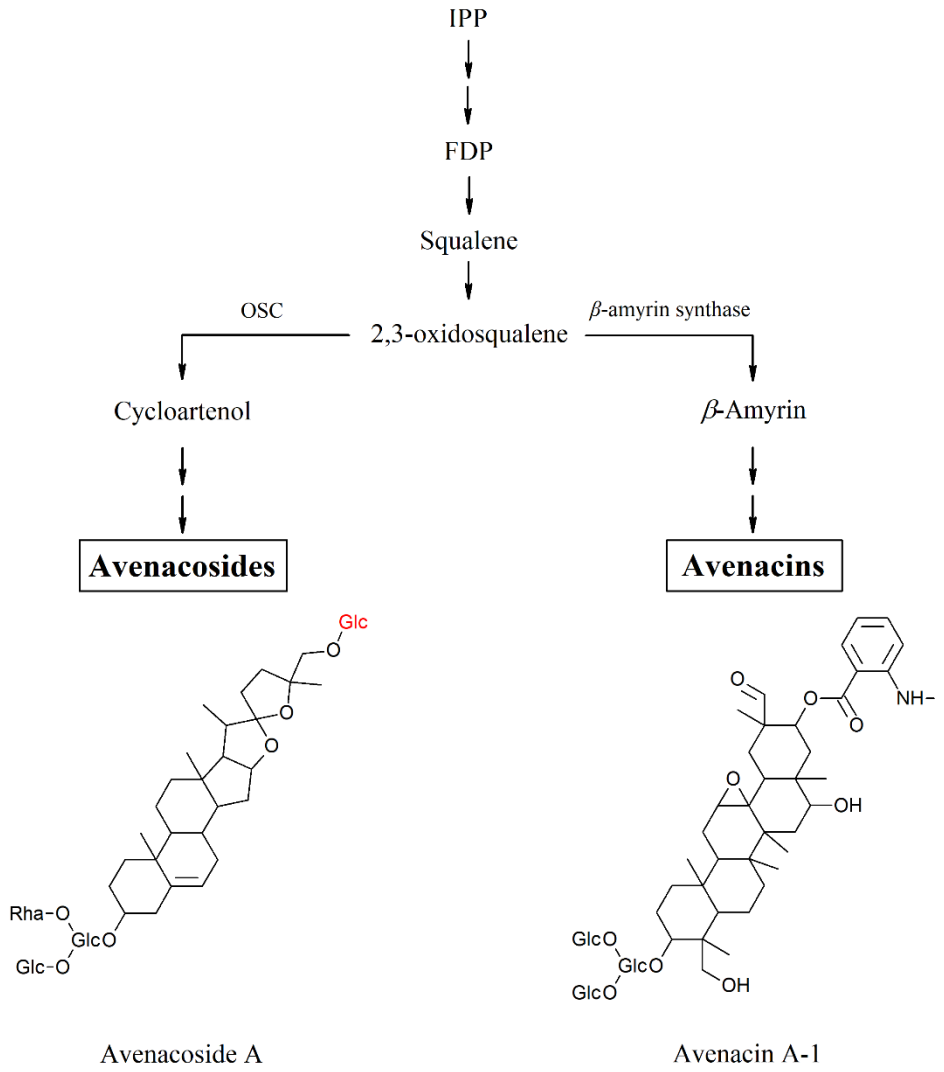

Figure 14: Simplified biosynthetic pathway of saponins from oat. FDP: farnesyl diphosphate; IPP: isopentenyl pyrophosphate; OSC: oxidosqualene cyclase. Each saponin class is illustrated by a representative compound. Glucose in C-26 position in avenacoside A is highlighted in red.

As other terpenoids, saponins are synthesized from IPP (Figure 14). Two FDP molecules are conjugated to form squalene, the precursor of 2,3-oxidosqualene. The pathway branches after 2,3-oxidosqualene to result in the synthesis of triterpenoid saponins, and in the synthesis of steroidal saponins. The first step leading to the biosynthesis of steroidal avenacosides in oat involves the formation of cycloartenol by an oxidosqualene cyclase (OSC). Avenacin biosynthesis starts with the cyclization of 2,3-oxidosqualene into *β*-amyrin by the *β*-amyrin synthase. The gene coding for oat *β*-amyrin synthase has been

identified and is clustered together with five out of seven genes known to be involved in avenacin biosynthesis (196).

Avenacins have been found to possess *in vitro* antimicrobial activity against *G. graminis* var. *tritici* and var. *avena*, and *Gaeumannomyces radicicola* (197). Their antifungal activity was also tested on inoculated detached leaves of barley or epidermis of onion bulb showing that exogenous addition of a mixture of these saponins inhibits the infection rate of *B. graminis*, and the growth of *B. oryzae* and *Magnaporthe oryzae* (198). Similarly as for other saponins, antimicrobial activity of avenacins has been suggested to be linked to their membranolytic activity. The hydrophobic region of saponins penetrates the lipid bilayer, while their hydrophilic parts associate and form pores in the membrane, resulting in cell death (199).

Avenacosides possess an additional glucose residue at the C-26 position, which interferes with the properties of the hydrophobic moiety (Figure 14), therefore avenacosides do not have direct antifungal activity. However, 26-desgluco-avenacosides inhibit *in vitro* *Sordaria macrospora* growth (194). A β-glucosidase named avenacosidase has been identified in oat to be capable to hydrolyze avenacosides to 26-desgluco-avenacosides (200). It has been suggested that to avoid self-poisoning, avenacosides and avenacosidase are stored in different compartments. However, tissue disruption caused by the pathogen is postulated to bring the enzyme and its substrate in contact resulting in the release of the toxic 26-desgluco-avenacosides (194).

3.2 Proving function of specialized metabolites in grass immunity

In order to address their potential function in plant immunity, specialized metabolites are typically tested for their *in vitro* antibiotic activity, frequently including calculation of their half maximal effective concentrations (EC50). However, there are no analytical methods to check if such concentrations are achieved *in vivo* at the plant-microbe interaction site. Therefore *in vitro* antimicrobial activity alone is not sufficient to unambiguously prove specialized metabolite function in plant immunity. Such proof can be delivered using genetic tools. For instance, plant lines with altered accumulation of metabolite of interest can be obtained using mutant screens or genetic engineering. If the accumulation changes of the selected compound in the obtained during these approaches

plant lines correlate positively with resistance against tested pathogens such a compound can be claimed to be important for plant immunity. Mutant plants obtained by screening mutagenized population or by targeted mutagenesis are most frequently used to prove metabolite function. These mutants can show changes in metabolite accumulation due to the absence, or the reduced activity of an enzyme involved directly in the biosynthesis of the compound of interest. Alternatively, plants can be modified to modulate selected gene expression and eventually induce changes in metabolite accumulation. Gene or genes can also be transferred from one species to another, modifying biosynthetic pathway in the transformed plant.

3.2.1 Deficiency in particular specialized metabolites may increase plant susceptibility

The above-mentioned approaches have been applied to investigate different specialized metabolism pathways in grass immunity. Among these pathways, flavonoid biosynthetic pathway was investigated in rice using a T-DNA insertion mutant with a knocked out Os*PAL06* (Figure 7). This line accumulates lower amounts of sakuranetin in roots in comparison to wild type plants (201). The same pathway was investigated in a sorghum mutant carrying a transposon in *yellow seed1* (*y1*) which has a decreased amount of 3-deoxyanthocyanidins compared to wild type plants (202). Terpenoid biosynthetic pathway was in turn investigated in a *saponin-deficient1* (*sad1*) oat line which has been isolated by screening a mutant collection for lack of autofluorescent avenacins. *sad1* mutation has been found in a gene coding for AsbAS1, a *β*-amyrin synthase responsible for avenacin biosynthesis (Figure 14) (193, 203). Additionally, in maize, *ZmTps6*/*11* and *an2* mutants were respectively altered in zealexin and kauralexin biosynthesis (Figure 13) (204, 205), and a rice mutant, *cps4-tos*, accumulated reduced levels of momilactone A and oryzalexin S (Figure 13) (206). Another rice mutant, *sl*, which lacks the functional T5H, was used to study serotonin biosynthetic pathway, as it did not accumulate higher amounts of serotonin and its derivatives upon pathogen inoculation compared to wild type plants, but instead, tryptamine and its derivatives were found in higher quantities (58). All these mutants have been found to be more susceptible than respective wild-type plants to pathogen infection, proving the immune function of specialized metabolites whose accumulation was changed in these mutant lines (58, 193, 201, 202, 204-206).

Genetic engineering in grasses was also used to address the putative function of cyanogenic glucosides and cyanogenesis in plant immunity. Despite the known toxic effects of HCN, it had been questioned if plants are capable to deliver this compound in fungicidal amount. To test this, barley leaf epidermal cells that despite the presence of epiheterodendrin (Figure 12) are not cyanogenic, have been transfected with a gene encoding sorghum cyanogenic β-glucosidase. Transfected cells were subsequently inoculated with *B. graminis* f. sp. *hordei* and the conidiophore formation rate was found to be reduced by 35-60% compared to not transfected cells (207). This proved that cyanogenic plants possess a potential to negatively impact pathogen growth.

3.2.2 Diversity in specialized metabolite immune functions

Investigation of mutants with defects in the biosynthesis of specialized metabolites indicated that at least some of these compounds may function in plant immunity without serving as antifungal compounds. For instance, serotonin-deficient *sl* rice mutant lacks the characteristic brown material accumulating in the cell wall at the site of infection with *B. oryzae* (58). Treatment of rice leaves inoculated with *B. oryzae* with (S)-α-(fluoromethyl)tryptophan, a TDC inhibitor, also suppressed the formation of these brown deposits additionally pointing at the link between these deposits and tryptophan metabolism (208). Feeding of *sl* plants with serotonin restored deposition confirming that formation of this brown material is serotonin-dependent (58). Metabolite analysis of transgenic lines overexpressing TDC1 or TDC3 under the control of ubiquitin promoter showed a positive correlation between color intensity of spontaneously formed brown spots and serotonin dimer amount (65). In addition, reduced amount of H_2O_2 was detected around the site of infection in wild type plants inoculated with *M. oryzae* than across the entire leaf, indicating a link between H_2O_2 scavenging and serotonin dimer formation (209). Based on these results, it was suggested that following infection, serotonin serves as a ROS-scavenger around infection site, preventing non-colonized surrounding cells from oxidative damages. Oxidation of serotonin leads to the formation of its dimer, which is incorporated in the cell wall, giving the brown color at the infection site. As serotonin dimer possesses higher antifungal activity than serotonin, it can better protect adjacent cells from fungal spread (59). Combined, these results suggest that serotonin can play two

different roles in immunity, as a ROS-scavenger and an antifungal agent in its dimeric form.

Another class of compounds which may combine antifungal activity with another function is constituted by BXs. *bx1*, a maize mutant lacking tryptophan synthase α monomer activity, accumulates these compounds in significantly reduced quantities as compared to wild type plants (Figure 6). This mutant showed a faster lesion enlargement upon inoculation with *S. turcica* indicating indispensability of BXs for proper immune response in maize (103). In addition, it has been shown that upon treatment with chitosan, *bx1* deposits lower amounts of callose than BX-producing line. Apoplast infiltration of wild type leaves with DIMBOA resulted in callose formation suggesting that this BX can act as a signaling molecule in triggering callose deposition (103, 210). These results combined with BX antifungal activity suggest that these compounds can have multiple functions in plant defense.

Interestingly, some metabolites may be involved in immunity without showing significant antibiotic activity. Recently, in Brachypodium, a T-DNA insertion mutant of an *ACT*, named *Bdact2a*, was found to accumulate constitutively significantly lower amounts of FerAgm as compared with wild type plants (Figure 7). Furthermore, the mutant plants were more susceptible to *F. pseudograminearum*. Strikingly, during *in vitro* assays, FerAgm showed inhibitory activity on spore germination only at non-physiological concentrations and no inhibitory effect on mycelium growth. This suggests that FerAgm role in Brachypodium immunity does not result from its antifungal activity (136).

Overall, genetic tools are helpful in proving the role of specialized metabolites in plant immunity. Moreover, analysis of lines with altered accumulation levels of selected specialized metabolites indicated that these particular compounds have various functions, not necessarily linked with antibiotic activity. We can speculate that new functions may also be found for compounds considered so far as exclusively antifungal, but which were not yet investigated for additional activities. To this mean, genetic engineering encompasses useful techniques to reveal and understand the diversity of specialized metabolite functions in plant immunity.

Objectives

The purpose of this doctoral project was to characterize metabolic pathways involved in the immunity of the model species *Brachypodium distachyon*. To achieve this goal we used *Parastagonospora nodorum*, a necrotrophic pathogen of wheat to trigger defense response in leaves of Brachypodium seedlings. We selected this particular pathogen because of its agronomical relevance, and the ease to cultivate in laboratory conditions and to obtain spores for inoculation (Table 2). In addition, the availability of its genome sequence allows assessing its biomass in planta by estimating relative fungal DNA amount in infected plant tissue.

To characterize metabolic pathways involved in Brachypodium immunity, we aimed to assess the global influence of pathogen recognition on the metabolome, and to identify particular metabolites and genes encoding enzymes, which catalyze key steps of the corresponding biosynthetic pathways. We also planned to investigate the evolution of these enzymes in grasses using phylogenetic analysis and examination of conserved amino acid motifs and residues.

In order to study global metabolome changes and to identify compounds accumulating in higher quantities upon pathogen recognition, we performed Ultra Performance Liquid Chromatography (UPLC) analysis combined with Mass Spectrometry (MS). This allowed us to determine, which biosynthetic pathways are activated during Brachypodium response to pathogen attack. Genes encoding enzymes putatively participating in these pathways in Brachypodium were identified *in silico* by homology with known enzymes from other grass species using dedicated programs and available databases. Subsequently, pathogen-induced changes in expression levels of these genes were investigated by quantitative reverse transcription polymerase chain reaction (RT-qPCR) to select particular orthologs that may function directly in biosynthesis of the identified compounds. Investigation of phylogenetic relationships between Brachypodium proteins and corresponding enzymes from other selected cereals shed light upon the evolutionary history of these enzyme families in grasses. Collectively, using these approaches we could obtain information about multiple molecular levels activated in Brachypodium by pathogen recognition.

Material and methods

1 Chemicals, media, and kits

P. nodorum cultivation, Brachypodium leaf inoculation, and leaf staining:

- Agar; BioShop
- Calcium carbonate ($CaCO_3$); BioShop
- Chloral hydrate; Sigma-Aldrich
- Glycerol; POCH
- Lactic acid; Fluka
- Phenol; BioShop
- Potato dextrose agar (PDA) medium; BioShop
- Trypan blue; Sigma-Aldrich
- Tween 20; Sigma-Aldrich
- Vegetable juice “Vega Prowansalskie Pola”; Tymbark

Metabolite extraction and chromatographic analysis:

- 1,7 diaminoheptane; Sigma-Aldrich
- 2,5 -dihydroxybenzoic acid; Sigma-Aldrich
- 4-aminobenzoic acid; Sigma-Aldrich
- Acetone; POCH
- Acetonitrile; VWR chemicals
- Anthranilic acid; Sigma-Aldrich
- Dansyl chloride; Sigma-Aldrich
- Deionized water by Mili-Q Plus system; Millipore

- Dimethyl sulfoxide (DMSO); BioShop
- DL-ornithine; Sigma-Aldrich
- Esculetin; Sigma-Aldrich
- Ethyl acetate; POCH
- Formic acid; Sigma-Aldrich
- Hexane; POCH
- Perchloric acid ($HClO_4$; 70%; w/v); POCH
- Proline; Sigma-Aldrich
- Putrescine (1,4-Diaminobutane dihydrochloride); Sigma-Aldrich
- Salicylic acid; Sigma-Aldrich,
- Serotonin; Sigma-Aldrich
- Sodium carbonate (Na_2CO_3); POCH
- Spermidine trihydrochloride; Sigma-Aldrich
- Spermine tetrahydrochloride; Sigma-Aldrich
- Toluene; POCH
- Trimethylamine; POCH
- Tryptamine; Fluka
- L-tryptophan; Sigma-Aldrich
- Tyramine; Sigma-Aldrich
- L-tyrosine; Sigma-Aldrich

RNA and DNA isolation, reverse transcription, and real-time polymerase chain reaction (PCR):

- Agarose; BioShop
- Chloroform; POCH

- Deionized autoclaved water
- Ethanol (96%; v/v); POCH
- Ethylenediaminetetraacetic acid (EDTA); Bioshop
- Hydrochloric acid (HCl; 35%; w/w); POCH
- Isopropanol; POCH
- Oligo(dT); Genomed
- Purple gel loading dye; New England Biolabs
- Real-time PCR reagent iTaq^{TM} Universal SYBR Green Supermix; Bio-Rad
- Reverse transcription kit, Omniscript RT Kit; Qiagen
- Ribonuclease inhibitor, RNasin Plus RNase Inhibitor; Promega
- RNA extraction kit, RNeasy Plant Mini Kit; Qiagen
- RNase-Free DNase; Qiagen
- RNasin® Plus RNase Inhibitor; Promega
- Sodium Chloride (NaCl); CHEMPUR
- Sodium dodecyl sulfate (SDS); Bioshop
- Tris(hydroxymethyl)aminomethane (Tris); Bioshop
- β-mercaptoethanol; Fluka

2 Brachypodium and *Parastagonospora nodorum* cultivation

Seeds of Brachypodium inbred line Bd3-1 (211) were sown with their awns up in peat pellets (Jiffy) and placed in controlled conditions (22°C, 60% humidity, 10h day length) for 4 weeks.

P. nodorum strain SN15 (212) was kindly provided by Prof. Dr. Christian A. Voigt, University of Hamburg. The fungus was grown on vegetable juice-potato dextrose agar

(VJ-PDA) according to Friesen *et al.* (213) (150 ml/l Tymbark vegetable juice, 3 g/l $CaCO_3$, 30 g sucrose, 10 g/l PDA, 10 g/l agar) at 18°C and 12 h day length. Conidia appearance indicated sporulation, usually after around 10 days of cultivation. The inoculum was prepared by adding water to the plate and gently scratching the plate surface to harvest spores. The suspension was centrifuged (4000 rpm, 10 min), the supernatant was removed and the pellet was dissolved in sterile water. Spore concentration was measured using a Bürker counting chamber, adjusted to 6 x 10^6 spores/ml in 20% (v/v) glycerol and stored in 1 ml fractions at -80°C.

3 Leaf inoculation

Leaves of 4 weeks old Brachypodium plantlets were cut and laid on square plates containing 0,8% (w/v) agar. Inoculum at a concentration of 6 x 10^6 spores/ml was supplemented with Tween 20 to achieve the final concentration of 0,01 % (v/v). 1 ml of spore suspension was sprayed on leaves per plate using a small cosmetic atomizer. Control plates were sprayed with the same volume of a water solution containing 0,01% (v/v) Tween 20 and 20% (v/v) glycerol. To keep humidity, plates were sealed with parafilm and left at 20°C and 12 h day length until sampling.

4 Leaf staining

To observe development of fungal hyphae and plant cell death, leaves were collected from plates at 12 h, 24 h, 48 h, and 72 h after treatment. A trypan blue stock solution (10 g phenol, 10 ml glycerol, 10 ml lactic acid, 10 ml water and 0,02 g trypan blue) was diluted (1:2 v/v) with 96% (v/v) ethanol. Leaves were submerged in the staining solution in screw-cap tubes. Tubes were partially closed and placed in a heated water bath until boiling of the solution, left for one minute, closed and left overnight at room temperature. The next day, leaves were successively put in 2,5 g/ml chloral hydrate solutions until distain.

5 Metabolite analysis

5.1 Metabolite extraction

Leaves were collected from plates at 24 h, 48 h, and 72 h after treatment to obtain samples between 80 mg and 150 mg of fresh weight (FW), frozen in liquid nitrogen and stored at -80°C before extraction. Samples were homogenized in 2,5 µl DMSO per 1 mg of FW, using zirconia beads (1 mm diameter, Carl Roth) in a Precellys Evolution tissue homogenizer (Bertin Instruments) at 10000 rpm and a cycle of 4 x 30 s with 5 s pause between each crushing step. Homogenates were centrifuged 20 min at 15000 rpm and 4°C, and the obtained supernatants were kept for Ultra Performance Liquid Chromatography (UPLC) analysis.

5.2 Amine extraction and derivatization

To enable analysis of amines using UPLC with fluorescence detection (UPLC-FLR), specific extraction and derivatization with dansyl chloride were performed. Leaves were collected in 2 ml tubes (Eppendorf) Tubes containing collected leaves (as described above) were put in tube holder frozen in liquid nitrogen and crushed in an MM400 mixer mill (Retsch) with metal beads (5 mm diameter) at 1800 rpm. Samples were immediately put shortly back in liquid nitrogen and transferred for 10-15 min into ice. 1 ml of 4% (w/w) $HClO_4$ was added per 225 mg of sample FW and samples were incubated for 1 h at 4°C, shaken at 300 rpm. The extract was centrifuged (10000 rpm, 4°C, 15 min), 200 µl of supernatant was collected, mixed with 400 µl of dansyl chloride solution (15 mg/ml of acetone), 200 µl of saturated Na_2CO_3 in H_2O, and 10 µl of internal standard (0.02 mg/ml 1,7 diaminoheptane in 70% (w/v) $HClO_4$). Tubes were wrapped in aluminum foil to protect samples from light until the end of the procedure. The solution was shortly vortexed and shaken at 100 rpm 1 h at 60°C. Next, 100 µl of proline (100 mg/ml) was added to remove the excess of dansyl chloride, and the mix was shortly vortexed and incubated for 30 min at room temperature. Liquid-liquid extraction with toluene was performed by manual shaking for 2 min, and the emulsion was centrifuged (3000 rpm, 5 min). The upper phase was transferred in a new glass tube and mixed with 1 ml of hexane. This solution was loaded onto a Discovery ® silica column (3 ml, 500 mg, Supelco),

previously activated by the addition of 2 ml of toluene followed by 2 ml of toluene:trimethylamine (20:1 v/v). The derivatized amines were eluted from the column with 2 x 1 ml of ethyl acetate. This fraction was evaporated using a Savant SPD121P speedvac (Thermo Fisher Scientific) and the obtained dry pellet was dissolved in 200 µl of 80% (v/v) DMSO.

5.3 Ultra Performance Liquid Chromatography conditions

Preliminary untargeted metabolite analysis was carried out on Acquity UPLC system from Waters Corporation, using Syncronis reverse phase column (100 x 2,1 mm, 5 µm; Thermo Fisher Scientific), and a diode-array detector (spectra were collected from 210 nm to 400 nm). Derivatized amine separation and detection were performed using the same UPLC system, Synergi Polar-RP column (100×2,0 mm, 2,5 µm; Phenomenex) and FLR detector (excitation/emission wavelengths 350/525 nm). Detailed untargeted metabolite analysis including identification of selected compounds was performed using the Acquity UPLC system hyphenated to a micrOToF-Q mass spectrometer (MS; Bruker Daltonics). Separation was carried out on Syncronis reverse phase column (100 x 2,1 mm, 5 µm; Thermo Fisher Scientific). Conditions of chromatographic separation are summarized in Table 3. Calibration of the mass spectrometer with sodium formate salts clusters was done prior to each analysis in positive and negative ionization mode. MS operated upon following settings: the ion source voltage -4,5 kV or 4,5 kV, nebulization of nitrogen at a pressure of 1,2 bar and a gas flow rate 8 l/min. Ion source temperature at 220°C. The spectra were scanned in positive and negative ion mode at the range of 50-1000 *m/z* at a resolution higher than 15 000 full width at half maximum (FWHM).

Table 3: Conditions of chromatographic separation used during UPLC analysis.

		UV-detection based untargeted metabolite analysis		MS-detection based untargeted metabolite analysis		Amine analysis	
Temperature		22°C				16°C	
Injection volume		5 µl				5 µl	
Flow rate		0,350 ml/min				0,250 ml/min	
Phase composition	A	0,1% formic acid in H_2O (v/v)				H_2O	
	B	98% acetonitrile and 0,1% formic acid in H_2O (v/v)				98% acetonitrile in H_2O (v/v)	
Gradient		Time (min)	% A	Time (min)	% A	Time (min)	% A
		0	100	0	100	0	65
		1	100	10	75	2	65
		4	95	15	70	30	0
		25	78	20	0	35	0
		28	20	24	0	36	65
		29	0	24,5	100	49	65
		34	0	32,5	100		
		35	100				
		51	100				

5.4 Data processing

5.4.1 UV-detection based untargeted metabolite analysis

Data from UV-detection based untargeted metabolite analysis were collected and processed using Empower 3.0 (Waters) software. Selection of peaks representing compounds with accumulation affected by pathogen recognition was performed using UV chromatograms registered at 275 nm and 310 nm wavelengths. Peaks whose area was significantly bigger (Student's t-test; $P < 0,01$) in samples from *P. nodorum*-inoculated leaves compared to the corresponding control samples, were selected for classification based on their UV spectra.

Solutions containing 10 µg/ml of tryptophan and serotonin standards were injected and analyzed using the same conditions as for sample analysis. Compounds present in analyzed samples were putatively classified as tryptophan derivatives or hydroxycinnamic acids based on their registered UV spectra, by comparison to the registered tryptophan and serotonin spectra and published spectrum of caffeic acid (214). Serotonin was identified in analyzed samples using retention time and UV spectrum

obtained during analysis of the corresponding standard. Concentration of this compound in plant tissue was quantified using the following formula:

$$C_s = \frac{Area_s * (C_{st} * vol_{injstd})}{Area_{st}} * \left(\frac{vol_{ext}}{vol_{inj}}\right) * \left(\frac{1}{M_s}\right) * \left(\frac{1}{m_{ext}}\right)$$

With C_s: concentration of serotonin in plant tissue (µmol/g of FW); $Area_s$: Peak area (273 nm) of serotonin in investigated sample; $Area_{st}$: Peak area of serotonin standard; C_{st}: Standard concentration (µg/µl); vol_{ext}: volume of extract (µl); vol_{inj}: volume of sample injected (µl); vol_{injstd}: volume of standard injected (µl); M_s: Molar mass of serotonin (g/mol); m_{ext}: mass of sample FW (g).

5.4.2 Derivatized amine analysis

Data from derivatized amine analysis were acquired and processed using Empower 3.0 (Waters) software. The derivatization protocol described above was applied to 200 µl of amine standards including putrescine, spermidine, spermine, tryptamine, and tyramine (1 mg/ml of 0,1 M HCl, in HClO4, 1:100 v/v). This allowed to identify derivatized amines present in the obtained extracts based on their retention times, and to quantify their concentrations using the following formula:

$$C_a = \frac{\frac{Area_a}{Area_i}}{\frac{Area_s}{Area_{si} * m_s}} * \left(\frac{vol_{ext}}{vol_{inj}}\right) * \left(\frac{1}{M_a}\right) * \left(\frac{1}{m_{ext}}\right)$$

With C_a: concentration of derivatized amine of interest (nmol/g of FW); $Area_a$: Peak area of derivatized amine of interest; $Area_i$: Peak area of internal standard from sample; $Area_s$: Peak area of derivatized amine standard; $Area_{si}$: Peak area of internal standard from corresponding derivatized amine standard sample; m_s: mass of injected standard (ng); vol_{ext}: volume of extract (µl); vol_{inj}: volume of injection (µl); M_a: Molar mass of amine of interest (g/mol); m_{ext}: mass of sample FW (g).

5.4.3 MS-detection based untargeted metabolite analysis

Data acquisition for MS-detection based untargeted metabolite analysis was supervised by HyStar 3.2 software (Bruker Daltonics). UPLC-MS data were converted to *mzXML* format by MSConvert tool available in Proteowizard software (http://proteowizard.sourceforge.net/). Data sets from each experiment were processed separately for negative and positive ionization. Each of the following processing steps of UPLC-MS data analysis was conducted with MZmine 2.31 software (http://mzmine.github.io/) (215). Firstly, parameters of each processing step were set up experimentally on a randomly selected testing group of samples prior to optimization of each parameter. In the second step, lists of masses were generated by Mass detector module in each scan in the raw data files. Then chromatograms for each mass detected continuously over the scans were built by Chromatogram Builder algorithm. These chromatograms were deconvoluted using Wavelets algorithm relying on Bioconductor's XCMS package for R (http://www.bioconductor.org/packages//2.7/bioc/html/xcms.html) (216). Isotopic peaks grouper was used for isotope elimination followed by adduct and complex searching. Deviation of retention times between peak lists was reduced by Retention time normalizer. Such transformed peaks were aligned in all samples through a match score by Join aligner module. The resulting peaks list was completed by supplemental peak detection with Peak finder algorithm prior to missing value imputation (gap filling). Generated data table was subsequently exported in *csv* format for further post-processing and statistical analysis.

Post-processing was done by MetaboAnalyst (https://www.metaboanalyst.ca/) with missing values imputation, log transformation and interquartile range filtering (217). Then, results table were imported to MarVis – Suite 2.0 (http://marvis.gobics.de/) (218) toolbox for statistical analysis and selection of differentially accumulated metabolites (DAMs). Calculation was done jointly for three experiments. Firstly, one-way analysis of variance (ANOVA) followed by the Benjamini-Hochberg approximation was applied to achieve the false discovery rate (FDR or *q*-value). Then fold change in intensity of particular signals between control and treated samples were calculated by means difference. Only signals which fulfilled the conditions: q-value < 0.05 and $|\log_2$ fold change$|$ > 0,585 in all experiments were considered as DAMs. These signals were

visualized using principal component analysis (PCA), heat maps, volcano plots, Venn Diagrams, and boxplots created in MetaboAnalyst or MarVis.

Identification of selected DAMs was based on fragmentation scheme of ions obtained from MS/MS analysis in positive and negative ionization mode as well as literature data and available standard compounds, including 2,5-dihydroxybenzoic acid, 4-aminobenzoic acid, anthranilic acid, DL-ornithine, esculetin, salicylic acid, serotonin, L-tryptophan, and L-tyrosine. In addition, the following online databases were searched for automatic metabolites annotation: Metlin (219), KEGG Compound (220), BioCyc (221), PubChem (222), KNApSAcK (223), ChEBI (224), and ChemSpider (225).

6 Bioinformatic analysis

Brachypodium genes used for expression analysis and for sequence analysis were selected based on the homology of the corresponding encoded proteins with respective enzymes characterized in rice. Rice protein sequences used as templates were obtained from Phytozome 12 (Table 4) and their homologs in Brachypodium were searched using BLAST (Basic Local Alignment Search Tool) on Phytozome 12 website (https://phytozome.jgi.doe.gov/pz/portal.html). Brachypodium protein sequences were first selected on the basis of a BLAST Smith-Waterman alignment score higher or equal to 200. These sequences were then aligned with corresponding rice protein sequences by MUltiple Sequence Comparison by Log-Expectation (MUSCLE) method using Ugene software (http://ugene.net/), and alignment distance matrixes were calculated. Brachypodium protein sequence which had more than 60% identity with the corresponding rice protein sequence or for which rice protein sequence had more than 60% identity with were selected.

Table 4: Reference sequences used to identify respective Brachypodium homologs.

Investigated Brachypodium protein	Template protein
*Bd*ADC	LOC_Os04g01690 (226)
*Bd*HCT	LOC_Os01g47180 ; LOC_Os01g72210 ; LOC_Os04g56910 ; LOC_Os09g37200 ; LOC_Os10g23310 ; LOC_Os11g42370 ; LOC_Os06g08580 (133, 227, 228)
*Bd*ODC	LOC_Os02g28110 (229)
*Bd*PAL	LOC_Os02g41680 ; LOC_Os04g43800 (119)
*Bd*T5H	LOC_Os12g16720 (71)
*Bd*AADC	LOC_Os01g56380; LOC_Os08g04540; LOC_Os07g25590 (66)

Phylogenetic trees were generated to investigate the relationship between selected Brachypodium proteins and proteins from chosen cereal species. Used in this analysis protein sequences from Brachypodium, rice, sorghum, and maize were obtained from Phytozome 12. Barley and oat protein sequences were downloaded from UniProt (www.uniprot.org). Phylogenetic trees were built using PHYLogeny Inference Package (PHYLIP) neighbor joining method with Ugene software. Conservation of amino acid residues among enzymes of the same family was examined to classify these proteins, using MUSCLE sequence alignment achieved by Ugene software.

7 Nucleic acid analysis

7.1 DNA isolation

To estimate fungal DNA amount in plant tissue, total genomic DNA was isolated from Brachypodium leaves inoculated with *P. nodorum*. Two or three leaves of Brachypodium were sampled at 24 h, 48 h, and 72 h after treatment. DNA isolation was performed according to modified Edwards method. The collected material was ground with autoclaved plastic pestle in 300 µl of Edwards Buffer (200 mM Tris/HCl pH 7,5, 250 mM NaCl, 25 mM EDTA, 0,5% (w/v) SDS), shaken at 500 rpm, for 10 min at 65°C, and cooled down on ice for 10 min. 200 µl of cold chloroform was added and after gentle manual shaking the mix was centrifuged (5 min, 15000 rpm, 4°C). The supernatant was collected, mixed with 200 µl of cold isopropanol and centrifuged (5 min, 15000 rpm, room temperature). Pellet was washed two times with 500 µl of 70% (v/v) ethanol. Once dry, the pellet was dissolved in 100 µl of TE buffer (10 mM Tris/HCl pH 8, 1 mM EDTA). DNA concentration was measured using NanoDrop spectrophotometer (Thermo Scientific), and isolated DNA was stored at -20°C before further analysis.

7.2 RNA isolation and reverse transcription

Between 80-100 mg FW of control or *P. nodorum* inoculated leaves was collected from plates at 12 h, 24 h, and 36 h after treatment. Samples were put in liquid nitrogen, manually crushed with an autoclaved plastic pestle in RLT buffer (RNeasy Plant Mini Kit), and subsequent steps were performed according to RNeasy Plant Mini Kit protocol

including optional DNase digestion step to increase RNA purity. RNA of suitable quality showed three clear bands after migration on 1% agarose gel corresponding to 28S, 18S, and 5S ribosomal RNA. In the case of degradation, corresponding samples were discarded. RNA concentration, 260 nm / 280 nm ratio and 260 nm / 230 nm ratio were measured with NanoDrop spectrophotometer (Thermo Scientific). Isolated RNA was stored at -80°C. cDNA samples were obtained from 1 µg of RNA by mixing it with respective reagents from Omniscript RT Kit, 2 µl of 10 µM Oligo(dT) primer, and 10 units of RNasin® Plus RNase Inhibitor according to Omniscript RT Kit protocol, and incubating the mix 1 hour at 37°C. Synthesized cDNAs were stored at -20°C before further analysis.

7.3 Quantitative PCR analysis

Relative gene expression and relative fungal DNA amount were analyzed using quantitative PCR (qPCR). *Ubiquitin-conjugating enzyme 18* (*BdUBC18*) was used as a reference gene to calculate relative gene expression and relative fungal DNA amount (230). *Pathogenesis-related gene 10* (*BdPR10*) expression was assessed in each synthesized cDNA samples prior further analysis, to confirm response on gene expression level upon pathogen inoculation (61). Primers specific to targeted genes were designed using primer 3.0 software (http://bioinfo.ut.ee/primer3), by selecting pairs of primers of approximatively 20 base pairs (bp), for which the annealing temperatures did not differ more than 2°C, and which were giving a PCR product of approximatively 200 bp. Primer sequences were validated for their specificity using BLAST search in Brachypodium genome. Primers were ordered from Genomed, dissolved in 1 mM Tris/HCl pH 7,5 to a final primer concentration of 10 µM. qPCR reaction mix contained for each sample 0,5 µl of cDNA template, for relative gene expression analysis, or 100 ng of total DNA, for relative fungal DNA amount quantification, 10 µl of iTaq^{TM} Universal SYBR Green Supermix, 1 µl of solution of each primer specific to the target gene (Table 6), and 7,5 µl of autoclaved distilled water. For the semi-quantification of fungal DNA amount, *StagoUnique*, a pair of primers specific to *P. nodorum* genome (231), was used. The reaction was performed in CFX Connect™ Real-Time PCR Detection System (Bio-Rad), using a qPCR thermocycler program described in Table 5.

Table 5: qPCR thermocycler cycling protocol**.** Primer annealing temperature was set at 58°C for *BdHCT15* primers.

	Temperature	Time	
Initial denaturation	95°C	3 min	
Denaturation	95°C	30 sec	x 39
Primer annealing	54°C	1 min	
Extension	72°C	30 sec	

Data were collected and processed using Bio-Rad CFX Manager 3.1 program. Normalized gene expression for each sample was calculated as follow:

$$NE_i = 2^{Cq_{UBC18} - Cq_i}$$

With NE_i: normalized expression of gene of interest; Cq_{UBC18}: *UBC18* Cq value of corresponding sample; Cq_i: Cq value of gene of interest. Both Cqs are generated using threshold line value specific to the gene of interest.

Table 6: List of primers used for gene expression analysis by RT-qPCR.

Gene name	Gene id	Primer sequence	
BdADC	*Bradi1g50067*	F	CTGTCAGTGTTCACCTCCCT
		R	GAGGAACATGCCGAGGTAGT
BdACT2a	*Bradi4g36850*	F	ATCGTGGATGTCTCGTAGGG
		R	CGGATCGTGGATGTCTCGTA
BdACT2b	*Bradi4g36830*	F	CCTTCTCGATGGCGGCGGTG
		R	CCTGCGTGCAGTCCCCATGG
BdACT2c	*Bradi4g36820*	F	GTGGATAGCTGGCTCACGTT
		R	TTGAACGCTTGAAGGTTGTG
BdCOMT	*Bradi3g16530*	F	CTCAAGAACTGCTACGACGC
		R	CGAACTCCCTCTCGTACCTC
BdHCT1	*Bradi1g47180*	F	ACTACTCCCTGGAGGACCTG
		R	GGTCTCAAAGAAGAGGGCCG
BdHCT2	*Bradi1g47190*	F	TGGACGAACTGATGAGCGAG
		R	CATTGCCGAAGTAGCCCTGA
BdHCT3	*Bradi1g47232*	F	AGCGGTTCAGCAACCAAGTA
		R	GGAGTCGAACGGGACTCTTG
BdHCT4	*Bradi1g72210*	F	GGTCCATCGAATTCAAGGCC
		R	CACCGTCAACTTCTTCCACG
BdHCT5	*Bradi1g72220*	F	GATAGCTGGCTTGGGTTCAG
		R	CTACATCCTCGCTGGGAGAG
BdHCT6	*Bradi1g72230*	F	CAGCACCGACCACCTCTAC
		R	CGGTGAAGAAGGTGCTCATG
BdHCT7	*Bradi1g72237*	F	CCATGGGCTTGTTCTTCACC
		R	GCACCGTGAAGTTCCTGATC
BdHCT8	*Bradi3g02310*	F	TAAGGGATGTGTTGTGCCCT
		R	GGAGATGGAGTAGCAGCACT
BdHCT9	*Bradi3g23280*	F	CGGCCCACTCCTACAACAGGG
		R	CGTGACCTTCTTCCAGGTGT
BdHCT10	*Bradi3g48530*	F	GTTGAGGTCGGGTGCTACTT
		R	AGCTTGAAGATGTCCACGGC
BdHCT11	*Bradi4g24210.2*	F	CCAGTCCATGAGCGTCTTCT
		R	GGTCTTGATCGTCCTGTCCA
BdHCT12	*Bradi5g14720*	F	CTCATGGTCGGATCTCTGCC
		R	GTGTGAGCTCCTCGAACCAA
BdHCT13	*Bradi5g25166*	F	ACGCAGCATATAGTGTCCGA
		R	GGTTCCATTGTCGCCATTGT
BdODC1	*Bradi4g36810*	F	CCTCAGCTGCATCCCCAT
		R	AGCCGTTAAAGTTTGAGCCG
BdODC2	*Bradi4g36840*	F	GAAAGGACTTACGCCTCGAC
		R	GGACGTCGAGAATCCGTTGA
BdODC3	*Bradi4g36870*	F	GGAGAGAAGACGTACGCCTC
		R	TTGAAGTTGGACCCTGACGA
BdPR10	*Bradi4g05040*	F	CCAAGCTCACGGTGGAGTAT
		R	CCTCGACCTTCTTGAGCAAC

BdPTAL1	*Bradi3g49250*	F	GGACTACGGTTTCAAGGGGA
		R	TGGAGGACATGAGCTTGAGG
BdPAL2	*Bradi3g49260*	F	GGCCTCATCTCATCCAGGAA
		R	CTCAGGGTTTTCTTGGCCAC
BdPAL3	*Bradi3g49270*	F	GCGAGAAAGACATGCTCCAG
		R	GCAGCTCCTCTTCGAATTGG
BdPAL4	*Bradi3g49280*	F	AGAACTCTGTGGCGGTTACA
		R	GAAATGACCTCGGCGAGAAC
BdPAL5	*Bradi3g48840*	F	GCTCCAAGAGATTGAGCGTG
		R	TCAAACTGAGCAACCTTGGC
BdPAL6	*Bradi3g47110*	F	CCAAACAATTAAGGAGATCAATTAGAA
		R	CCCGAATACTGGAAAGTAAGATACA
BdPAL7	*Bradi3g47120*	F	CGACGGCTATCTCATCCTGT
		R	TCTTCTCGCCGGTCAGATAC
BdPAL8	*Bradi5g15830*	F	CGAAACAGGACAGGTATGCG
		R	ACTGGGCAAACATGAGCTTG
StagoUnique		F	GTCACCGCATTACCAAAGTT
		R	GGAAACTGGAACTGGAACAA
BdT5H	*Bradi4g39240*	F	GTCGAGGAGCACATCAACGG
		R	CGGGGGATTTCTGGACACGG
BdTDC1	*Bradi1g28960*	F	TGAGGTCGACAATGGCCATA
		R	GGTGGCCTCATCTTGCAAAA
BdTDC2	*Bradi2g02370*	F	CGGCAGCGAAGGAGCACG
		R	GCGTACACGGTGAGCCTCGT
BdTDC3	*Bradi3g14730*	F	CATGGCCAAGATGTTCGAGG
		R	CTCCTCCTGTAGTGACGACC
BdTDC4	*Bradi3g14740*	F	CCATGCTTGTCACGCTAGTC
		R	CATAGTTGGTCTCAGGCCCA
BdTDC5	*Bradi3g14750*	F	GGAGTCATGACAGAGGACGAC
		R	ACTCCTCACGTGCCTCTCCT
BdTDC6	*Bradi3g14760*	F	CAAGCTCTGGATGGTGATGC
		R	GCTTCCGTTCGTCTTGATCC
BdTDC7	*Bradi3g14780*	F	CAAGCTCTGGATGGTGATGC
		R	CACCATTCGCCTTGATCCTG
BdTYDC1	*Bradi2g02360*	F	TGTCCAGCAGCATCCAATGG
		R	AGTAGTCGGCGATGAAGTCG
BdTYDC2	*Bradi2g51120*	F	GCGGCAGCGCAGAATGGC
		R	GCGGGGAGCAGGTTGCGG
BdTYDC3	*Bradi2g51170*	F	CGTCGCACTTCTCCAATGT
		R	AGCAGGTTGCGGAGGAAG
BdTYDC4	*Bradi5g21770*	F	GGCTCAACGTGAACCCTTTC
		R	CGCCGATCTTCAAGAGCTTC
BdUBC18	*Bradi4g00660*	F	ACCCTCTACGCTGGTGAGAC
		R	TTGCTGTAAATGTGCGGATG

Results

1 *Parastagonospora nodorum*-Brachypodium pathosystem

In order to trigger immunity-related biosynthetic pathways in Brachypodium we needed a fungal pathogen, which is capable to infect this grass species. Additionally, we searched for a fungus that is easy to handle in laboratory conditions. Finally, we considered availability of genome sequence as an asset allowing us to estimate fungal biomass and eventually supporting future experiments addressing mechanisms of fungal pathogenicity. For these reasons, we chose *P. nodorum* (Table 2) that was reported to colonize Brachypodium (232), for which the genome sequence was reported (212), and which is growing and sporulating *in vitro* on simple medium (213).

In order to induce a strong plant response, we aimed to spray a high amount of spores on leaves. However, due to leaf vertical orientation and their surface hydrophobicity, sprayed droplets of spore suspension were hardly retained on leaves. Therefore, we decided to inoculate detached Brachypodium leaves maintained horizontally on agar plates.

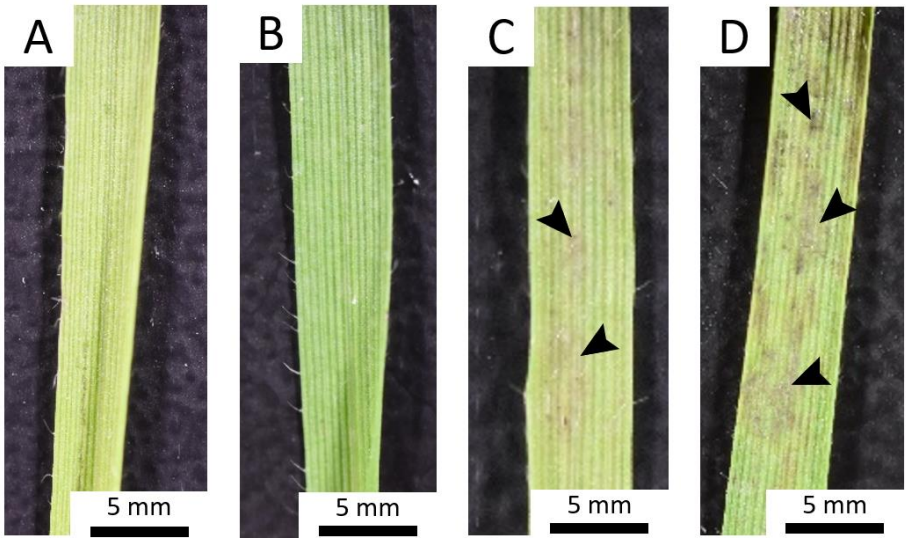

Figure 15: *P. nodorum*-triggered disease symptoms. Brachypodium non-inoculated leaf (A) and leaves collected 24 h (B), 48 h (C), and 72 h (D) post-inoculation (hpi) with *P. nodorum* spores. Necrotic lesions are visible (black arrowheads) at 48 hpi (C) and 72 hpi (D).

To check if this selected experimental setup supports interaction between *P. nodorum* and Brachypodium we monitored disease symptoms and fungal growth. No clear macroscopic difference was observed 24 hpi between inoculated leaves and control leaves (Figure 15). At 48 hpi we observed the presence of black spots, probably resulting from cell death. At 72 hpi these necrotic spots became darker and bigger, indicating a potential increase in the HR caused by the pathogen presence. To check if these disease symptoms correlate with *P. nodorum* development on leaves, we observed fungal growth at the microscopic level. To this purpose, inoculated leaves were stained with trypan blue to highlight fungal structures and dead cells (Figure 16). Fungal hyphae growing out of spores were visible at 12 hpi, and starting from 48 hpi, we could observe stained area which may indicate cell death resulting from plant HR. However, no clear difference in fungal growth could be observed between 12 hpi and 72 hpi using microscopic observation.

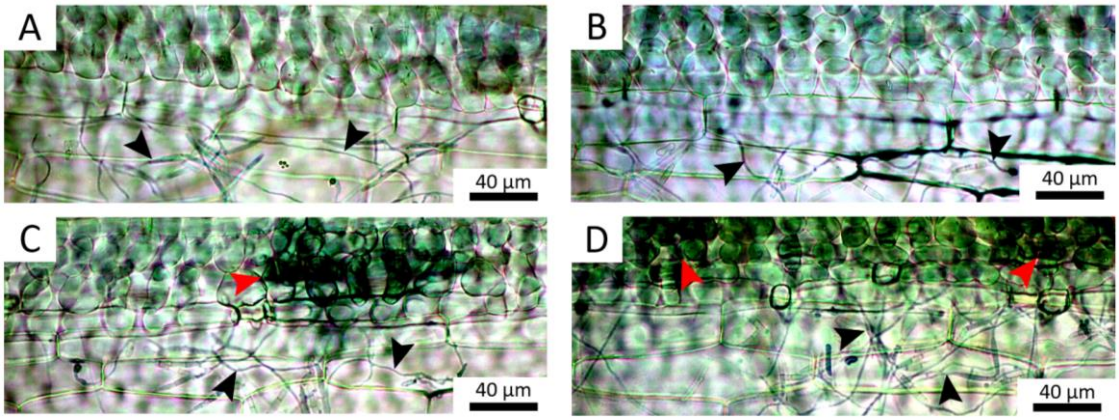

Figure 16: *P. nodorum* development on Brachypodium leaves. Microscopic pictures were taken at (A) 12 h, (B) 24 h, (C) 48 h, and (D) 72 h post-inoculation with fungal spores. Fungal structures (black arrowheads) and dead plant cells (red arrowheads) were stained with trypan blue.

To assess more in detail the biomass of *P. nodorum* developing on Brachypodium leaves, we decided to investigate the relative amount of fungal DNA. This semi-quantification was done by calculating the ratio between the amounts of qPCR products obtained using primers specific to *P. nodorum* (*StagoUnique*) and to Brachypodium (*UBC18*) genomic DNA (Figure 17). We did not observe any significant difference in relative fungal amount 24 hpi, 48 hpi, and 72 hpi. This suggests no fungal growth on Brachypodium leaves between these three time points.

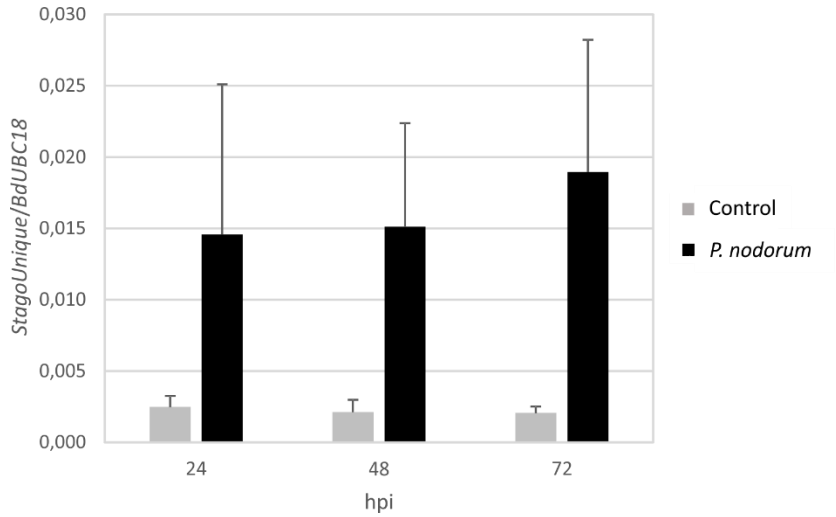

Figure 17: Biomass of *P. nodorum* in infected leaves collected at 24 h, 48 h and 72 h post-inoculation (hpi). Non-inoculated leaves were analyzed as controls at respective time points. Biomass was calculated as relative amount of the amplified fragment of *P. nodorum* genomic DNA (*StagoUnique*) to Brachypodium *ubiquitin-conjugating enzyme 18* (*BdUBC18*). Presented results are means ± SD from three independent experiments with three biological replicates in each (n = 9).

In order to check if presence of *P. nodorum* triggered plant defense response, we measured the expression of a defense-related marker gene. Expression of certain genes, called pathogen-related (PR) genes, is induced only in response to biotic stress and therefore these genes are considered as markers of plant immune response. Among them, we chose *pathogenesis-related gene 10* (*BdPR10*) whose expression was found to be induced in Brachypodium spikes upon inoculation with *F. graminearum* (61). We measured the expression of this marker gene upon *P. nodorum* inoculation (Figure 18). Our analysis revealed that *BdPR10* transcription was significantly induced at 24 hpi and 36 hpi, but not at 12 hpi, indicating that *P. nodorum* presence is recognized by Brachypodium and triggers defense mechanisms. Overall these experiments confirmed that *P. nodorum* initiates its development on Brachypodium leaves and triggers defense responses under our experimental conditions.

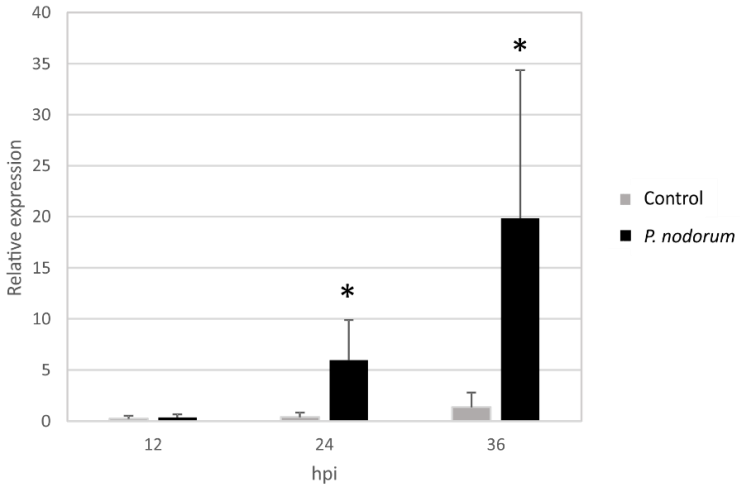

Figure 18: *Pathogenesis-related gene 10* (*BdPR10*) expressions in Brachypodium leaves upon inoculation with *P. nodorum* spores at 12 h, 24 h and 36 h post-inoculation (hpi). Non-inoculated leaves were analyzed as controls at respective time points. Presented results are means ± SD from three independent experiments with three biological replicates in each (n = 9). Values marked with asterisks are significantly different from respective controls (Student's t-test; $P < 0.01$).

2 Global metabolomic changes

Metabolomics changes triggered in Brachypodium leaves by *P. nodorum* recognition were initially investigated by Ultra Performance Liquid Chromatography (UPLC) analysis. First, we searched in UV chromatograms for peaks corresponding to compounds accumulating in significantly higher amounts in inoculated leaves than in control leaves. We calculated the area fold change of these peaks and we tried to classify them according to their UV spectra. Because tryptophan derivatives and HCA derivatives were reported to accumulate upon pathogen recognition in grasses, including Brachypodium (61), we compared obtained spectra with spectra of injected standards of serotonin and tryptophan, or a published spectrum of caffeic acid (214). Comparison was based on wavelengths of absorption maxima and the shape of the UV spectra (Figure 19). Compounds were classified as tryptophan derivatives if their spectra had the corresponding shape and absorption maxima at around 220 nm and 280 nm, or as HCA derivatives if their spectra shape matched the reference spectra and displayed absorption maxima at around 240 nm and 320 nm.

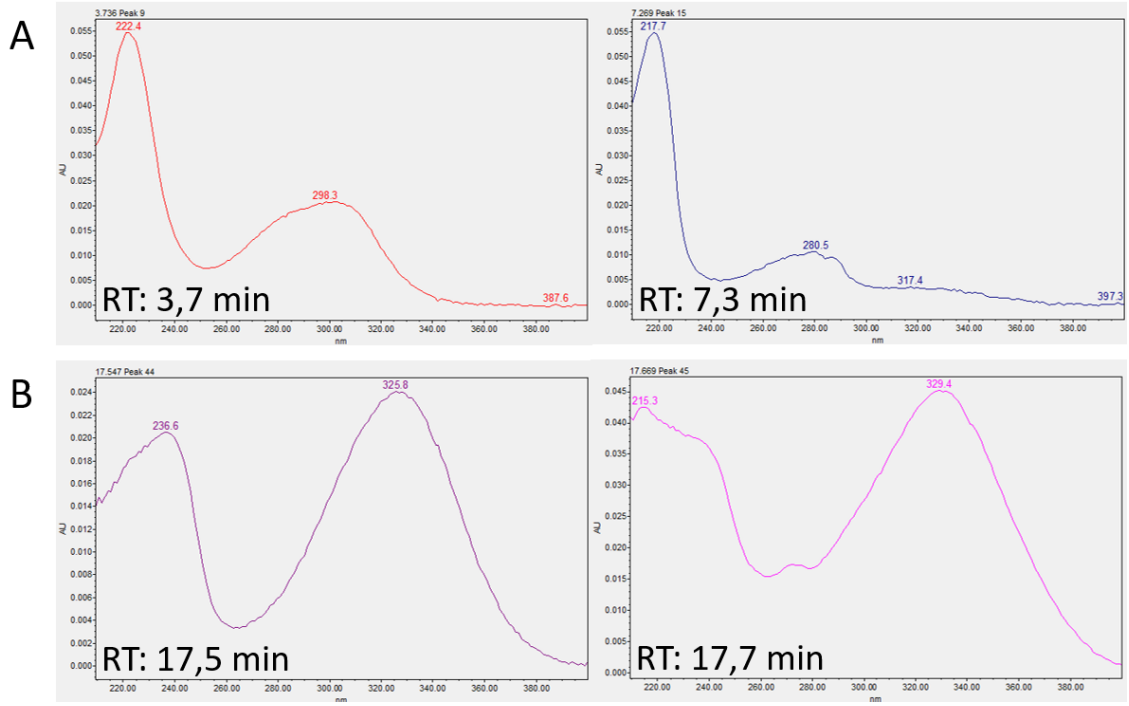

Figure 19: Exemplary UV spectra of selected compounds present in higher amounts upon inoculation with *P. nodorum* in Brachypodium leaves. Based on wavelengths of absorption maxima and shape of the spectra, compounds were classified as tryptophan derivatives (A) or hydroxycinnamic acid derivatives (B). RT: Retention time.

In addition to compounds classified as tryptophan and HCA derivatives, some compounds possessed spectra, which did not correspond to the reference spectra and consequently were not classified (Figure 20). From both classes of compounds, a higher number of tryptophan derivatives (7 compounds) was found to increase accumulation, as compared to HCA derivatives (4 compounds). However, compounds that were not classified were in larger number than compounds from both classes (13 compounds) suggesting that other biosynthetic pathways are involved in Brachypodium defense response.

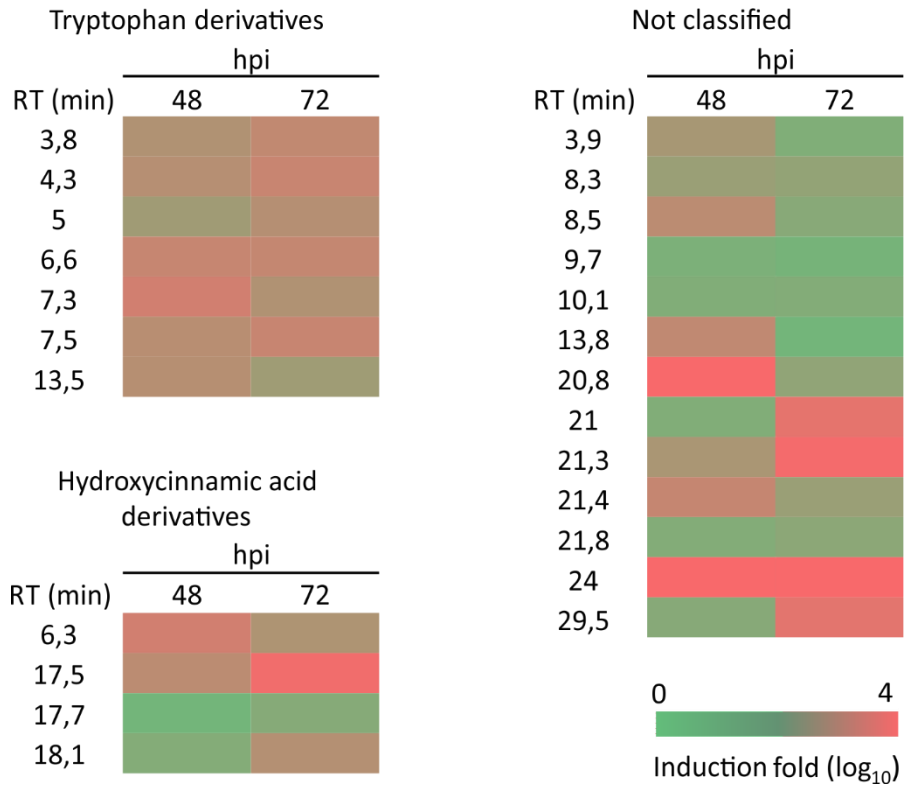

Figure 20: Induction fold of metabolites accumulating in significantly higher amounts (Student's t-test; $P < 0.01$) in Brachypodium leaves 48 h or 72 h post-inoculation (hpi) with *P. nodorum* spores. Compounds were classified according to their UV spectra as tryptophan or hydroxycinnamic acid derivatives. "Not classified" compounds possess UV spectra, which do not match with the two investigated classes. Presented results are means from three independent experiments with three biological replicates in each (n = 9). RT: Retention time.

Global metabolomic changes in Brachypodium leaves upon *P. nodorum* inoculation were investigated by UPLC-Mass spectrometry (MS) approach. Raw UPLC-MS data files from two experiments were processed jointly by available bioinformatics tools. In further parts of this work we used the term "signal" referring to bioinformatically and mathematically processed peak detected in UPLC-MS ion chromatograms, which represents single metabolite ionized in electrospray ionization source. On the other hand, one metabolite can be represented by few signals due to possibility of adduct formation in ionization source as well as possibility of occurrence of ions for particular metabolite in both positive and negative ionization mode. As a result of first part of our data processing we obtained a data table containing 17135 signals from positive and negative ionization modes.

After further processing, statistically and biologically important signals differentiating control and treated groups were selected on the basis of volcano plot analysis with following criteria: q-value < 0,05 and $|\log_2$ fold change$|$ > 0,585 separately for three studied time points in individual experiments (Figure 21). Only differentiating signals common to both experiments at particular time points were considered as statistically important and taken to further identification. Generally, number of signals with increased intensity was much higher than the number of signals with decreased intensity in all time points. Moreover, the number of differentiating signals increased with time from 186 at 24 hpi to 626 at 72 hpi which means more than a threefold increase in the course of two days. Only 75 signals (8,42% of all 891 differentiating signals) were common to three time points (Figure 22). Nevertheless, we observed higher similarity between 48 and 72 hpi (206 common differentially accumulated signals, 23% of total signals), whereas metabolomics response at 24 hpi was distinct from other time points. Only 33 signals (3,7% of total signals) were common for 24 and 48 hpi and 19 signals (2,1% of total signals) common for 24 and 72 hpi.

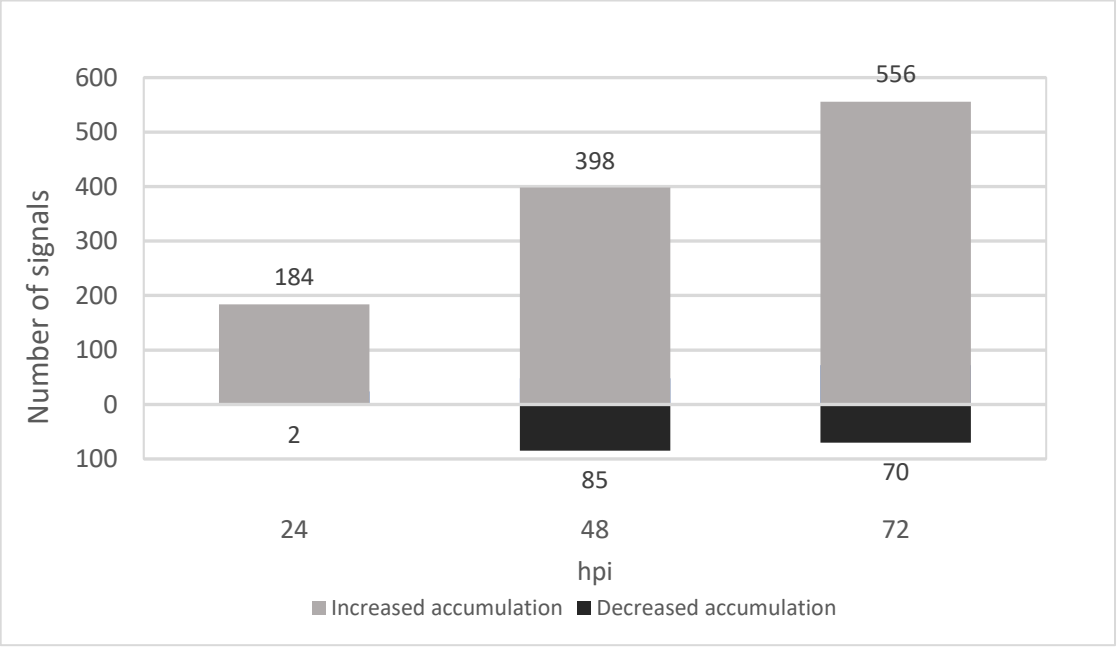

Figure 21: Number of differentiating UPLC-MS signals between Brachypodium leaves 24 h, 48 h, and 72 h post-inoculation (hpi) with *P. nodorum* spores and non-inoculated leaves, chosen on the basis of volcano plot analysis with following criteria: q-value < 0,05 and $\log_2$ fold change$|$ > 0,585). Selected signals met the described above criteria in two independent experiments with five biological replicates in each (n=10).

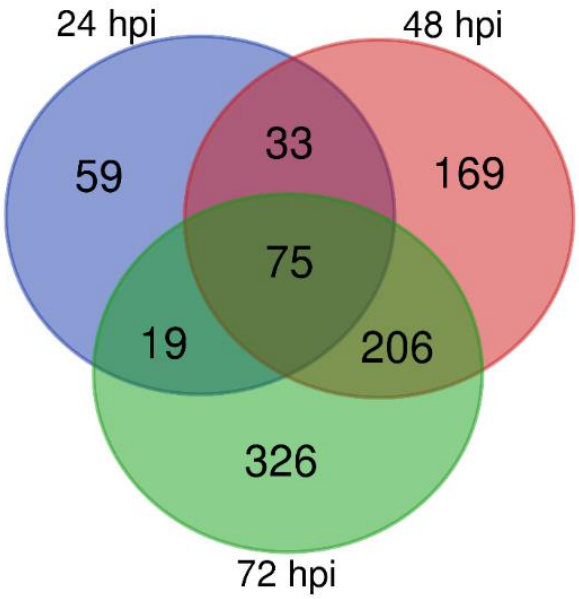

Figure 22: Venn diagram presenting similarities among differentiating signals between Brachypodium leaves 24 h, 48 h, and 72 h post-inoculation (hpi) with *P. nodorum* spores and non-inoculated leaves, chosen with criteria: q-value < 0,05 and $\log_2$ fold change| > 0,585. Selected signals met the described above criteria in two independent experiments with five biological replicates in each (n=10).

Identification of selected differentially accumulated metabolites (DAMs) detected in Brachypodium upon pathogen inoculation was based on UPLC-MS/MS mode with fragmentation of protonated ions. Fragmentation mode of MS analysis provided spectral information (exact mass of molecular ions and fragmentation patterns), which contributed to metabolite identification. Metabolomic database searches were also performed to support spectral analysis. However, Brachypodium metabolites are poorly known and information from databases was insufficient for complete annotation of metabolites.

Regarding the total number of signals representing DAMs, we focused identification of compounds on 75 signals common for all three time points assuming that the corresponding metabolites have important functions in Brachypodium immunity (Figure 22). UPLC-MS/MS analysis enabled tentative identification of 25 metabolites represented by some of these signals. Detailed list of identified compounds is presented in Table 7. These compounds have been identified at levels 2–4 according to the Metabolomic Standards Initiative (233). Among them, compounds from HCA and tryptophan metabolism were mainly observed as HCAAs. One flavonol and coumarin as

well as one lactic acid were also detected. In addition, three structures of saponins were also deduced on the basis of fragmentation scheme.

Identification of HCA derivatives (compounds 3, 5, 8, 9, 11, 18, 19, 20, and 22) was based on wide literature data concerning grasses, barley and wheat (61, 234). In general, the main product ions of HCA derivatives in positive ionization corresponded to *m/z* of dehydrated molecules of *p*-coumaric (147,04405 amu), caffeic (163,03896 amu), ferulic (177,05460 amu), and sinapic (207,06509 amu) acids. Masses and calculated chemical formula of main detached fragments in compounds 8 and 9 indicated putrescine and *N*-feruloylputrescine (FerPut), respectively. In addition, the $[M\text{ -feruloyl+H}]^+$ product ion at *m/z* = 89,108 amu in 8 and 9 corresponded to putrescine and confirm the presence of this HCAA among the studied structures. Thus, compounds 8 and 9 were assigned as FerPut and DiFerPut, respectively (Supplementary figure 1 & 2).

Analogical fragmentation scheme was observed for compounds 18, 20, and 22. The main product ion of these compounds was related with caffeic, ferulic and *p*-coumaric acid, respectively. Protonated molecules of 18, 20, and 22 yielded losses of 176,09461 amu corresponding to serotonin moiety as reported (61). Minor product ion produced after serotonin detachment at *m/z* = 160,0773 amu was also presented in compounds 18, 20, and 22 in lesser intensity. Chemical formula for the ion was calculated as $C_{10}H_{10}ON$ corresponding to serotonin moiety without amine group ($-NH_3$). Therefore, compounds 18, 20, and 22 were tentatively determined as *N*-caffeoylserotonin (CafSer), FerSer, and CouSer, respectively (Supplementary figure 3, 4, & 5).

For protonated molecule of compound 5 the most abundant product ions were the same as described above for compound 20, which correspond to dehydrated caffeic acid and serotonin. Additionally, losses of fragment 118,02599 amu indicated detachment of threonyl structure $C_4H_6O_4$ from ion of compound 5 (Supplementary figure 6). Threonic acid derivatives are constitutively presence in Brachypodium leaves as conjugates of this sugar acid with HCA.

Compounds 3 and 11 have abundant product ion at *m/z* = 177,05463 amu characteristic for ferulic acid (calculated chemical formula $C_{10}H_9O_3$ for dehydrated acidic moiety). Similarly, product ion of compound 19 with *m/z* = 207,06509 amu corresponded to dehydrated sinapic acid structure ($C_{11}H_{10}O_4$). However, fragments detached from $[M+H]^+$ ions of 3, 11 and 19 could not be determined at this moment. Thus, 3 and 11 were partially

described as ferulic acid derivatives and 19 was described as sinapic acid derivative. In addition, MS/MS spectra of protonated compounds 16 and 17 with $[M+H]^+$ ions at *m/z* = 211,05994 amu and 195,06511 amu were similar to 5-hydroxyferulic and ferulic acid, respectively (Supplementary figure 7 & 8) (234). Only those two compounds were observed as free HCAs.

On the other hand, the $[M+H]^+$ ion of compound 13 at *m/z* = 183,06549 amu with calculated chemical formula $C_9H_{11}O_4$ yields losses of abundant fragments 59,01335 and 78,03120 amu corresponding to structures of $C_2H_3O_2$ and $C_2H_6O_3$, respectively. Searching MS/MS data bases (Metlin and MassBank) confirmed similarity of studied spectrum to those generated by 3-(4-hydroxyphenyl)lactic acid which is the only free lactic acid observed in this study (Supplementary figure 9).

Differentiating signals 1 and 2 had the same retention time as ion related to serotonin standard. Main product ion of these compounds at *m/z* = 160.0773 amu was similar to product ions of compounds 18, 20, and 22, and correspond to serotonin without $–NH_3$ group. Molecular formula for the protonated ion of 1 was calculated as $C_{20}H_{22}N_4O_2$, which can indicate serotonin dehydrodimer. 5,5′-dihydroxy-2,4′-bitryptamine has been previously postulated as defence related metabolite in barley (59). Therefore we propose this structure for compound 1 (Supplementary figure 10). Signal 2 shared fragmentation scheme with 1. Molecular formula for signal 2 was calculated as $C_{20}H_{20}N_3O_2$ indicating dimer of serotonin with losses of $–NH_3$ amine group. Nevertheless, no literature data can confirm presence of such structure in plants. There is also lack of adequate deprotonated ion for the compound in negative ionization mode. Therefore, possibility that signal 2 was produced from compound 1 by in-ion source fragmentation during UPLC-MS analysis cannot be excluded and we did not consider it further as an independent compound.

Compounds 6, 12, 14, and 15 were tentatively assigned as serotonin derivatives on the basis of observed characteristic product ion at *m/z* = 160.0773 amu corresponding to serotonin without $–NH_3$ group. The losses fragments from protonated molecules of 6, 12, 14, and 15 cannot be described at the moment.

Compound 7 was annotated by database ChemSpider as serotonin derivative: 3-(2-aminoethyl)-5-hydroxy-1H-indole-2-carbonitrile (serotonin-2-carbonitrile) on the basis of $[M+H]^+$ masses at *m/z* = 202,0984 amu. Due to low abundance of the signal there was

lack of MS/MS spectra of 7 which could not confirm annotated structure (Supplementary figure 11). Therefore, additional UPLC-MS/MS analysis targeted with masses 202 amu was conducted. Losses of fragments corresponding to nitrile and amine group support the postulated structure. However, chemical synthesis of the compounds is planned to achieve the reference substance and to confirm presence of nitrile group in the molecule.

Compound 24 was identified as another serotonin conjugate. Product ions at m/z = 176,07045 amu with chemical formula calculated as $C_{10}H_{10}O_2N$ indicating indole-3-acetic acid (IAA) were observed simultaneously to ions characteristic for serotonin moiety. Abundant losses of $–NH_3$ and $–C_2H_5N$ fragments suggested presence of free 3-β-aminoethyl group of serotonin. Thus, IAA can be bound to serotonin via amide bond from pyrrole ring of serotonin (Supplementary figure 12).

The exact mass of protonated ion for compound 4 indicated $C_{10}H_9O_2$ chemical formula. The fragmentation scheme of compound 4 showed losses of carbonyl and methyl groups. In lesser intensity losses of $C_2H_2O_2$ which can be predicted as lactone-like chain was also observed. Such fragments are characteristic for coumarin derivatives. The presence of carbonyl as well as methyl group indicates methylcoumarin structure, which is in agreement with the molecular formula for protonated ion of 4 (Supplementary figure 13). However, the place of methylation could not be exactly determined. The literature describes accumulation of 5-methylcoumarin derivatives in barley upon *F. graminearum* infection (235). Therefore, this isomer can be considered to be also produced in Brachypodium as a defense-related metabolite.

Chemical formula $C_{17}H_{14}O_7$ generated on the basis of exact mass for compound 25 indicated flavonol core structure. Protonated ion with *m/z* = 331,0812 amu was matched in online databases with di-*O*-methylquercetin which can be confirmed by fragmentation of this ion with intensive losses of methyl groups in the structure (Supplementary figure 14).

For compounds 10, 21, and 23 with different fragmentation scheme saponin structure was postulated. The chemical formulas calculated on the basis of protonated molecules of those three compounds suggest a terpenoidal saponin structure. In addition, main product ions at m/z = 437,19281 amu, 469,243 amu, and 536,238 for compounds 10, 21, and 23 respectively, can indicate presence of terpenoid core structure for these compounds.

Table 7: Characterization of DAMs identified in Brachypodium by UPLC-MS/MS approach. MIL: metabolite identification level according to the Metabolomics Standards Initiative recommendation (233). Levels include: 1) Identified compounds, 2) Putatively annotated compounds without chemical reference standards, based upon physicochemical properties and spectral similarity with public spectral libraries, 3) Putatively characterized compound classes based upon characteristic physicochemical properties of a chemical class of compounds, or by spectral similarity to known compounds of a chemical class; nc: not calculated; RT: retention time.

N°	RT	*m/z* of [M+H]+ ions		Chemical formula	Error (ppm)	Fragmentation of [M+H]+ ions	Suggested identification	MIL	References
		Measured	Calculated						
1	4,9	351,1828	351,1816	$C_{20}H_{22}O_2N_4$	-3,5	351,1828; 275,082; 225,1007; 160,0773; 146,0611	5,5′-dihydroxy-2,4′-bitryptamine	2	(59)
2	4,9	334,1572	334,155	$C_{20}H_{20}O_2N_3$	-2,6	334,1572; 317,1272; 302,105; 288,0988; 275,0812; 259,0857; 247,0881; 225,1005; 172,0714; 160,0773; 146,0609; 144,0455	serotonin deaminodimer	2	(59)
3	5,5	486,222	486,221	$C_{22}H_{34}O_{10}N_2$	-0,898	486,3705; 317,1281; 293,031; 231,0432; 177,0328; 167,5811; 150,0845; 131,0704	ferulic acid derivative	3	(234)
4	8,1	161,06	161,098	$C_{10}H_9O_2$	-2,76	161,05981; 133,0649; 115,05465; 105,07039	5-methylcoumarin	3	(235)
5	6,7	473,1552	473,1555	$C_{23}H_{25}O_9N_2$	-0,606	454,29456; 355,12946; 320,09085; 208,06029; 177,10213; 160,07568	*N*-caffeoyl-*O*-threonyl-serotonin (*O*-threonyl-CafSer)	3	(234)
6	7,1	245,092	245,092	$C_{13}H_{13}O_3N_2$	-0,158	246,08835; 229,06082; 208,98073; 160,07597; 132,10204; 160,07597; 146,06000	serotonin derivative	3	(61)

7	7,64	202,098	202,098	$C_{11}H_{12}ON_3$	-2,706	201,1116; 185,071; 147,0654; 141,0503; 129,0549; 101,0603	3-(2-aminoethyl)-5-hydroxy-1H-indole-2-carbonitrile (serotonin-2-carbonitrile)	3	(61)
8	7,9	265,155	265,155	$C_{14}H_{21}O_3N_2$	0,004	265,15449; 248,1282; 177,0547; 145,0285; 115,0871; 89,108	*N*-feruloylputrescine (FerPut)	3	(234)
9	8,15	441,201	441,202	$C_{24}H_{29}O_6N_2$	-2,727	441,20081; 409,11032; 317,12970; 303,11273; 177,05449; 160,07581; 146,06026; 127,03909	*N*,*N*-di-feruloylputrescine (DiFerPut)	3	(234)
10	8,5	851,4006	885,2454	$C_{50}H_{59}O_{12}$	0,65	756,06714; 596,42450; 437,19281; 290,42969; 184,07324	saponin	4	(236)
11	8,92	476,176	nc	nc	nc	476,17609; 321,0949; 193,086; 177,05463; 166,0865, 161,0597; 132,1022; 86,0972	ferulic acid derivative	4	(234)
12	8,95	345,144	345,145	$C_{18}H_{21}O_5N_2$	1,3	346,11795; 330,12332; 328,10733; 255,10570; 215,14240; 197,07083; 160,07605	serotonin derivative	4	(61)
13	9	183,065	183,065	$C_9H_{11}O_4$	1,664	183,06549; 163,03899; 151,03900; 145,02831; 124,05214; 117,03393; 107,04960	hydroxyphenyllactic acid	3	(237)
14	9,11	368,161	nc	nc	nc	368,16101; 247,07535; 207,06509; 192,06525; 187,08633; 175,03893; 160,07571	serotonin derivative	4	(61)

15	9,51	627,255	nc	$C_{32}H_{39}O_{11}N_2$	nc	627,25524; 463,15765; 336,12265; 276,10266; 202,08618; 184,07584; 177,05457; 173,08365; 167,07016	serotonin derivative	4	(61)
16	10,5	211,06	2511,06	$C_{10}H_{11}O_5$	-0,758	211,05994; 193,08580; 177,05452; 149,05962; 121,06496; 106,04173; 91,05480	5-hydroxyferulic acid	2	(46)
17	10,7	195,065	195,065	$C_{10}H_{11}O_4$	-0,13	177,0546; 163,03868; 145,02843; 135,04437; 117,03390; 89,03937	ferulic acid	2	(234)
18	10,8	339,13378	339,1345	$C_{19}H_{19}O_4N_2$	-2,070	399,05774; 163,03888; 160,07559	*N*-caffeoylserotonin (CafSer)	3	(61)
19	11,45	659,19686	659,1970	$C_{32}H_{35}O_{15}$	-0,283	659,30225; 497,14301; 331,08096; 285,12418; 207,06509; 140,06874	sinapic acid derivative	4	(234)
20	12,49	353,149	353,15	$C_{20}H_{19}O_4N_2$	-1,285	353,14913; 336,12265; 227,08122; 177,05464; 145,02843; 117,03398; 89,03914	*N*-feruloylserotonin (FerSer)	2	(61)
21	12,5	887,4287	887,4271	$C_{43}H_{67}O_{19}$	1,785	887,4648; 607,2548; 469,243; 343,2064; 229,1419	saponin	4	(236)
22	12,7	323,139	323,139	$C_{19}H_{17}O_3N_2$	-1,08	231,13815; 203,08267; 231,13815; 177,10222; 160,07567; 147,04405	*N*-*p*-coumaroylserotonin (CouSer)	2	(61)

23	14,1	901,2191	901,2186	$C_{45}H_{41}O_{20}$	0,555	901,28407; 754,8716; 751,2567; 579,218; 536,1238; 303,8711; 299,5944; 184,0737; 147,0442; 140,0686; 127,0382; 123,4931	saponin	4	(236)
24	14,1	332,138	332,139	$C_{20}H_{18}N_3O_2$	-3,7	288,0887; 187,0898; 233,0917; 187,0898; 160,0777; 105,0731; 91,0517	serotonin–indolyl-3-acetic acid	3	(61)
25	15,5	331,081	331,081	$C_{17}H_{14}O_7$	-0,149	331,0812; 317,0591; 287,0551; 270,052	di-*O*-methylquercetin	3	(234)

3 Changes in accumulation of identified metabolites

We assessed the accumulation of compounds identified by UPLC-MS analyses by comparing their ion intensities (Figure 23). This showed that the majority of identified DAMs had a tendency to increase their accumulation with time upon pathogen inoculation.

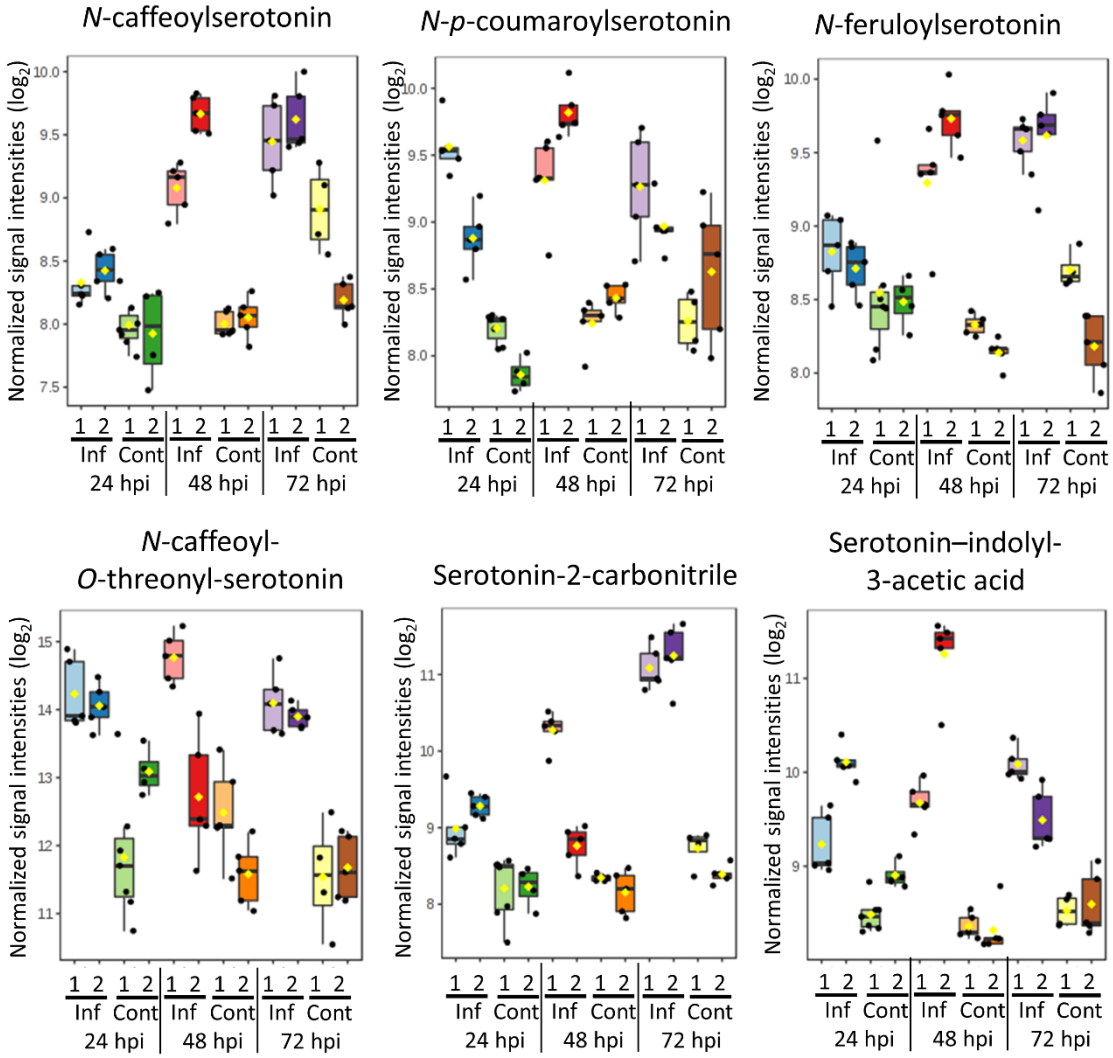

Figure 23 (following on next page): Changes in accumulation of selected DAMs in Brachypodium leaves 24 h, 48 h, and 72 h post-inoculation (hpi) with *P. nodorum* spores. Non-inoculated leaves were analyzed as controls at respective time points. Presented results from two independent experiments, respectively annotated 1 and 2, with five biological replicates in each (n = 5). Cont: control; Inf: infected; hpi: hours post-inoculation.

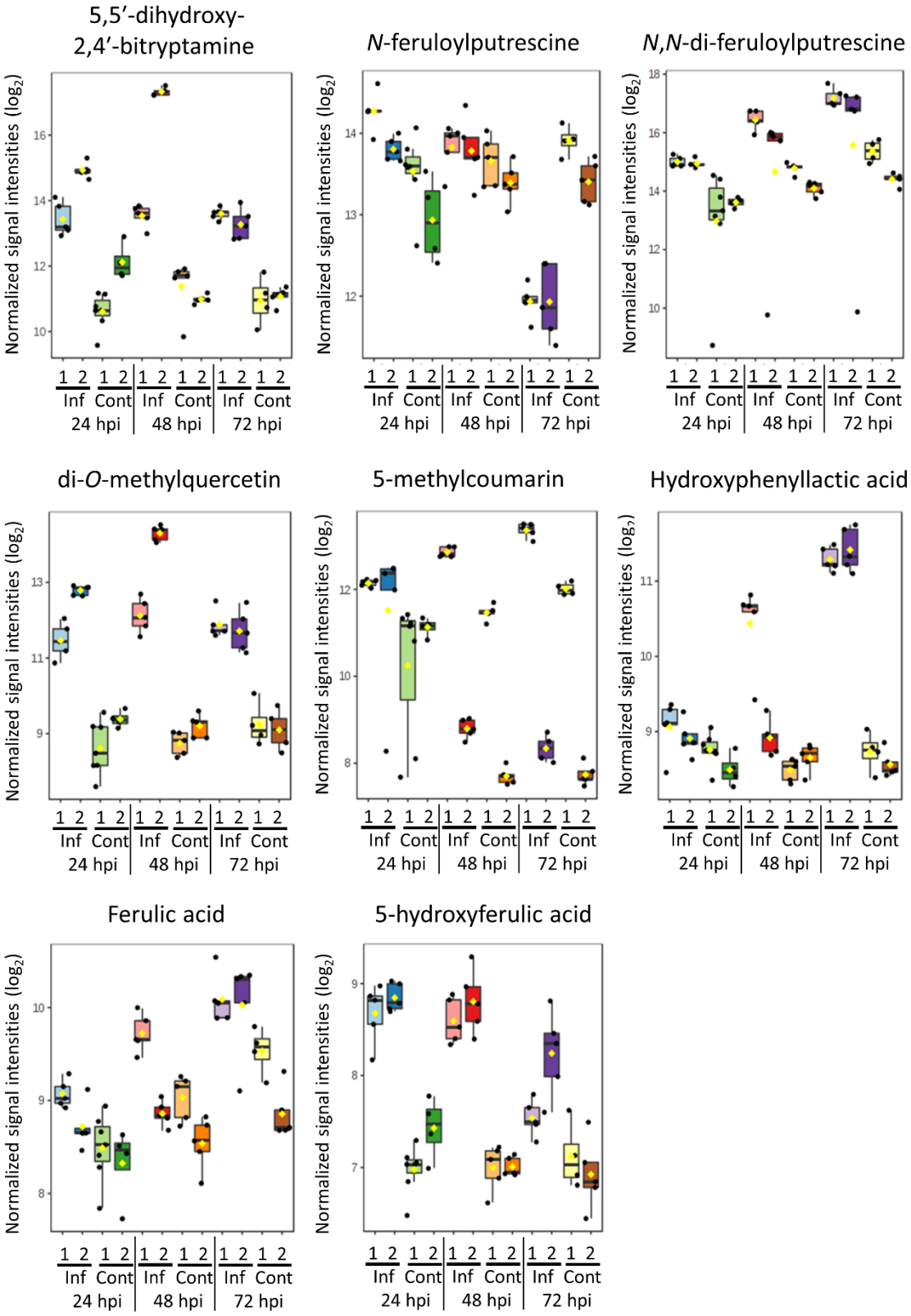
5,5′-dihydroxy-
2,4′-bitryptamine
N-feruloylputrescine
N,N-di-feruloylputrescine
di-O-methylquercetin
5-methylcoumarin
Hydroxyphenyllactic acid
Ferulic acid
5-hydroxyferulic acid
Normalized signal intensities (log2)
1 2 1 2 1 2 1 2 1 2 1 2
Inf Cont Inf Cont Inf Cont
24 hpi 48 hpi 72 hpi

Global UPLC-MS approach used in our experiments rely on comparison of ion intensity among samples and do not give the possibility to make precise quantitative analyzes. We used UPLC-UV-detection based analysis in order to obtain accurate quantification of serotonin accumulation (Figure 24). Serotonin was accumulating in higher amounts at 24 hpi, 48 hpi, and 72 hpi, with a tendency to increase its accumulation with time. In order to further investigate serotonin biosynthetic pathway, we assessed the amount of its precursor, tryptamine. This compound is present in plant tissue in lower quantity than serotonin, and therefore more difficult to quantify using UV detection. For this reason, we derivatized samples with dansyl chloride and analyzed them using FLR detection, which is more selective and sensitive than UV (Figure 24). Results of this analysis showed that tryptamine is increasing its accumulation as compared with control samples at 24 hpi, 48 hpi, and 72 hpi.

We identified putrescine derived HCAAs among compounds that had increased accumulation upon pathogen inoculation. For this reason, we decided to quantify the accumulation of this polyamine along with spermine and spermidine, two polyamines derived from putrescine, using the same derivatization procedure as for tryptamine (Figure 24). Putrescine was slightly more abundant in treated leaves 24 hpi, as compared with the respective control, but this difference was not observed at 48 hpi and 72 hpi. However, the seemingly higher accumulation of putrescine in samples from control leaves collected at 72 hpi as compared to inoculated leaves 24 hpi and 48 hpi suggests that other factors may induce accumulation of this compound. Spermidine was accumulating in significantly bigger quantity than in the control at 48 hpi and 72 hpi (Figure 24). However, the induction fold observed for this compound accumulated was lower than for serotonin and tryptamine. Spermine accumulation did not significantly change between control and inoculated leaves. We also investigated accumulation of tyramine, product of TYDC, for which no significant change was observed following pathogen inoculation (Figure 24).

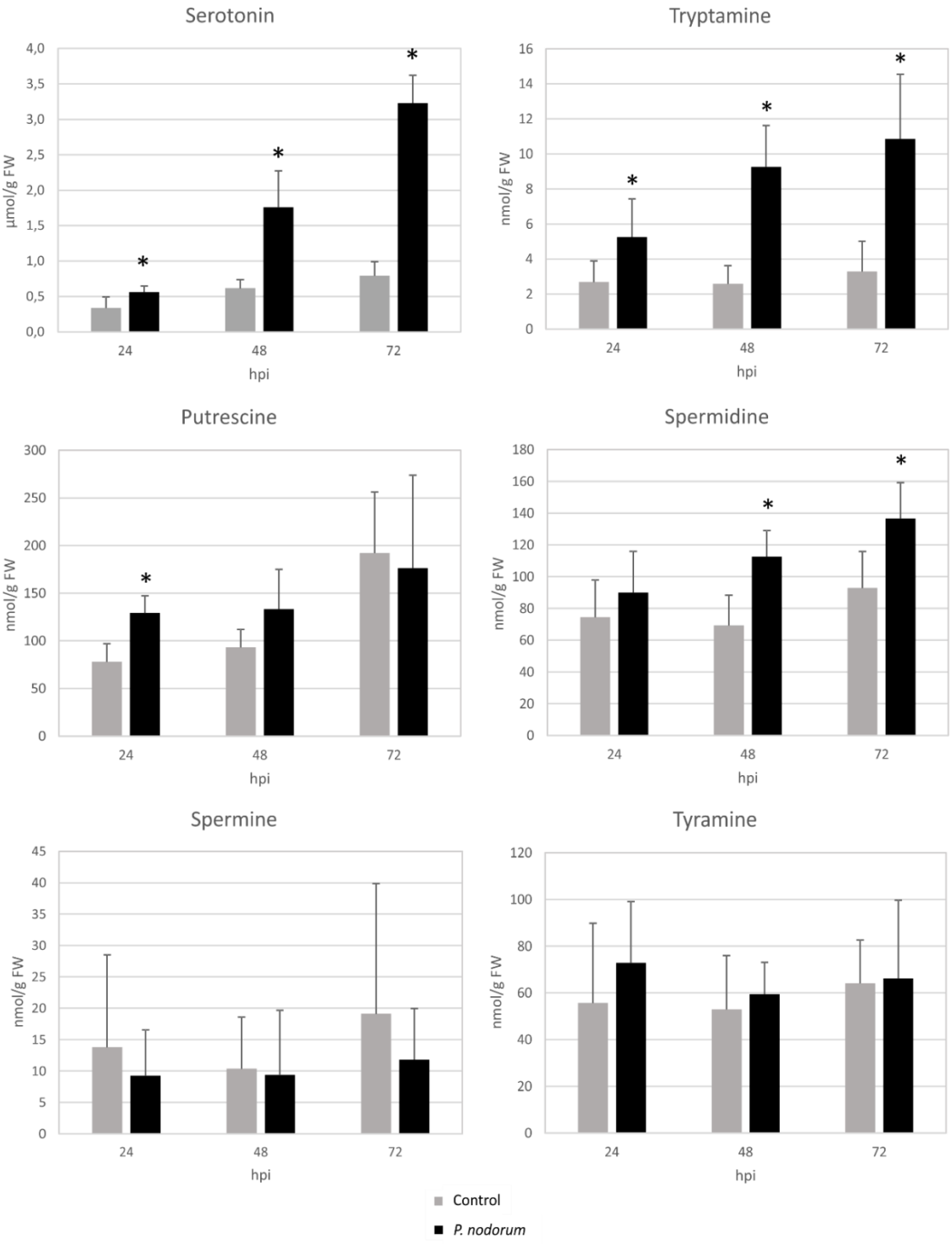

Figure 24: Accumulation of selected amines in Brachypodium leaves 24 h, 48 h, and 72 h post-inoculation (hpi) with *P. nodorum* spores. Non-inoculated leaves were analyzed as controls at respective time points. Presented results are means ± SD from three independent experiments with three biological replicates in each (n = 9). Values marked with asterisks are significantly different from respective controls (Student's t-test; $P < 0.01$).

4 Biosynthetic pathways activated in Brachypodium upon pathogen recognition

4.1 Polyamine biosynthesis

Based on the identified structures of metabolites whose accumulation was induced in Brachypodium leaves upon pathogen recognition, we selected biosynthetic pathways that could be activated during the immune response. These pathways include polyamine, serotonin, phenylpropanoid, and HCAA biosynthesis. Due to the pathway complexity and time constrains we decided not to investigate terpenoid pathway, which should lead to the biosynthesis of the identified saponins. In order to validate response of the selected pathways to the infection, we investigated pathogen-triggered changes in the expression of genes encoding corresponding enzymes in Brachypodium. We searched for these genes by homology of the encoded Brachypodium proteins with corresponding enzymes reported in rice.

The induced accumulation of FerPut, DiFerPut, and spermidine prompted us to investigate polyamine biosynthesis pathway in Brachypodium. From the enzymes involved in the two possible branches of putrescine biosynthesis (Figure 11), we selected ODC and ADC. We searched Brachypodium genes coding for homologs of rice ADC and ODC and we identified one *BdADC* (*Bradi1g50067*) and three *BdODC*s (*Bradi4g36810*, *Bradi4g36840*, and *Bradi4g36870*) named respectively *BdODC1*, *BdODC2*, and *BdODC3* according to the order of their localization in the genome, a rule we also followed for genes representing other investigated families. We measured changes in expression of these genes caused by pathogen inoculation in Brachypodium leaves and no significant induction was observed (Figure 25).

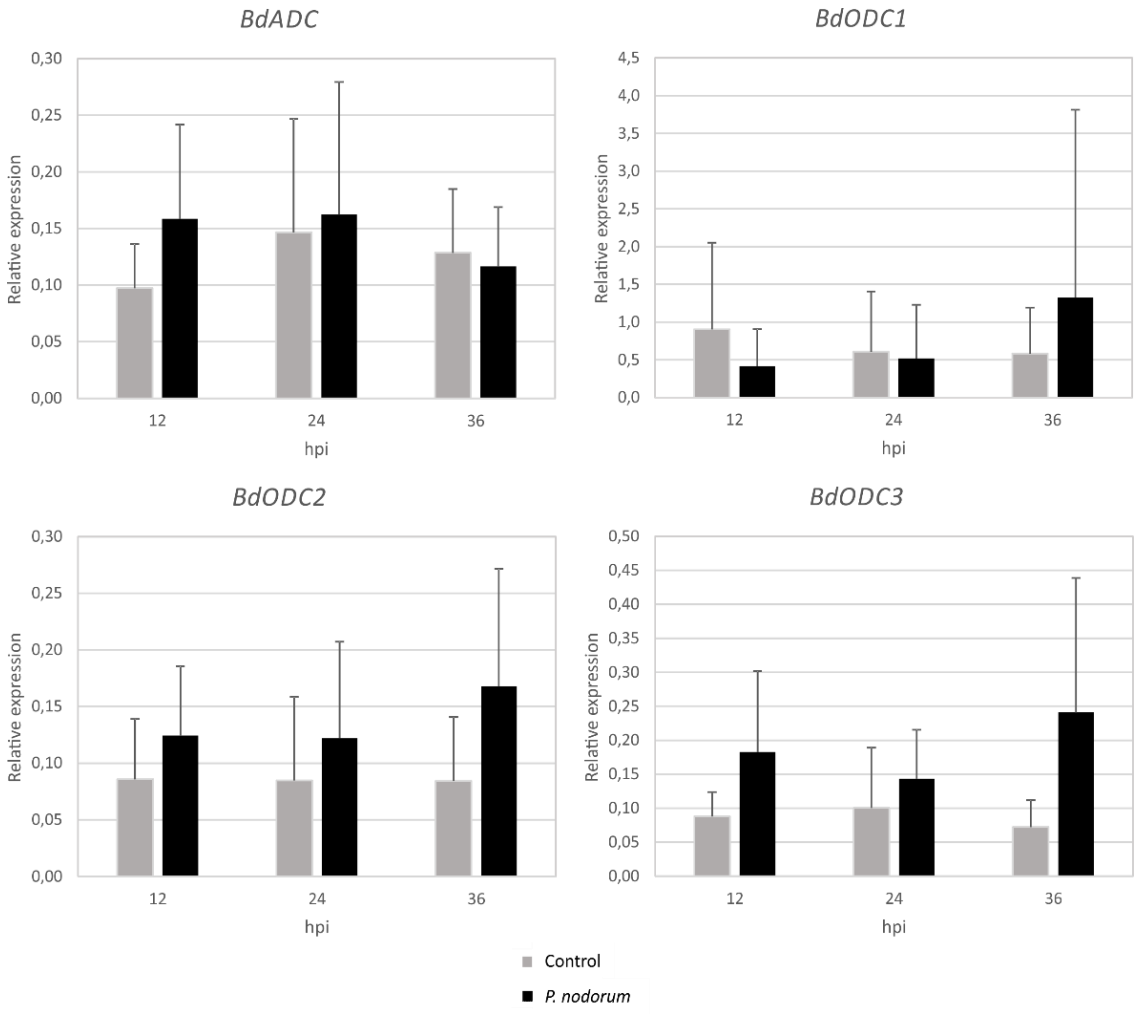

Figure 25: Expression of *arginine decarboxylase* (*ADC*) and *ornithine decarboxylases* (*ODC*s) in Brachypodium leaves upon inoculation with *P. nodorum* spores at 12 h, 24 h, and 36 h post-inoculation (hpi). Non-inoculated leaves were analyzed as controls at respective time points. Presented results are means ± SD from three independent experiments with three biological replicates in each (n = 9). Values marked with asterisks are significantly different from respective controls (Student's t-test; $P < 0.01$).

4.2 Serotonin biosynthetic pathway

Significant changes in the accumulation of tryptamine, serotonin, and its derivatives suggested that serotonin biosynthetic pathway was activated following pathogen recognition. Serotonin biosynthesis is initiated by TDC, responsible for the conversion of tryptophan to tryptamine (Figure 4). Because TDCs are highly homologous with TYDCs, we searched for genes coding for homologs of these two AADC types in Brachypodium

using sequences of two TDCs and one TYDC from rice as BLAST templates. This search led to the identification of 11 genes encoding homologous proteins, including seven *AADC*s already reported in Brachypodium (61, 67). A phylogenetic tree was generated to investigate the relationship between grass AADCs, including the proteins encoded by genes identified in Brachypodium (Figure 26). To build the tree, in addition to Brachypodium AADC sequences, we used published grass TDC and TYDC sequences. These include seven rice and two sorghum AADC sequences that came from genome-wide searches of respective homologs (65, 68). Activity of four of investigated rice AADCs had been confirmed in enzymatic assays (*Os*TDC1-3 and *Os*TYDC1) (65, 66). Other AADCs, including two from barley (68) and two from maize (238), were selected based on annotations from available databases. Our phylogenetic analysis separated protein sequences in two clades. Bradi2g02360.1, Bradi2g51120.1, Bradi2g51170.1, and Bradi5g21770.1 are closely related to *Os*TYDC1, therefore we assumed that these four Brachypodium AADCs are TYDCs, and we named them respectively *Bd*TYDC 1-4. The seven remaining *Bd*AADCs, Bradi1g28960.1, Bradi2g02370.1, Bradi3g14730.1, Bradi3g14740.1, Bradi3g14750.1, Bradi3g14760.1, and Bradi3g14780.1, are closely related to *Os*TDC1-3, suggesting that they are TDCs and we named them respectively *Bd*TDC1-7. Interestingly, our analysis revealed that opposite with AADCs from rice and Brachypodium, which can be found in both TDC and TYDC clades, putative AADCs from barley and sorghum are only found in TDC clade, while putative ADDCs from maize are present only in TYDC clade.

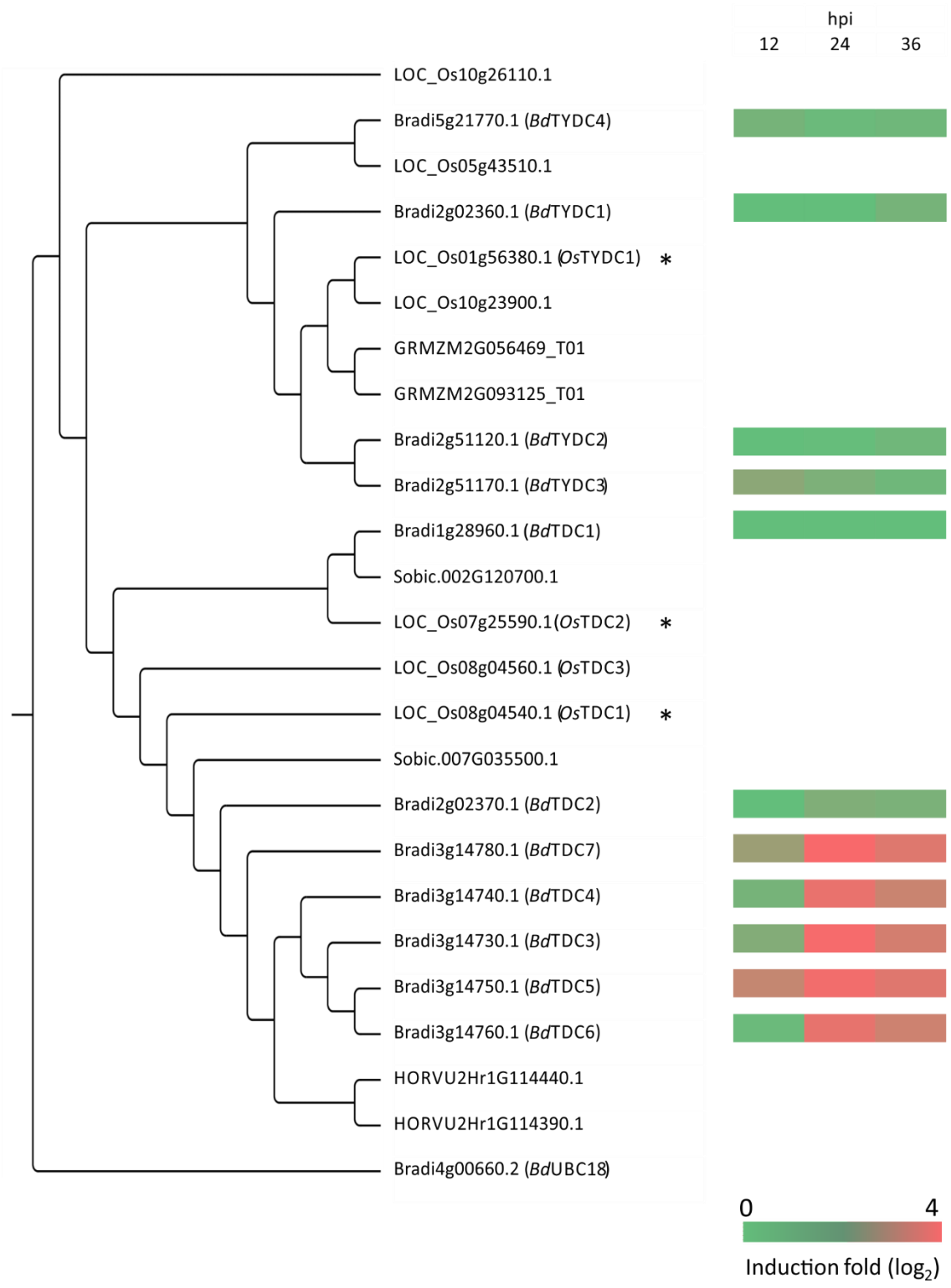
hpi
12
24
36
LOC_Os10g26110.1
Bradi5g21770.1 (BdTYDC4)
LOC_Os05g43510.1
Bradi2g02360.1 (BdTYDC1)
LOC_Os01g56380.1 (OsTYDC1) *
LOC_Os10g23900.1
GRMZM2G056469_T01
GRMZM2G093125_T01
Bradi2g51120.1 (BdTYDC2)
Bradi2g51170.1 (BdTYDC3)
Bradi1g28960.1 (BdTDC1)
Sobic.002G120700.1
LOC_Os07g25590.1(OsTDC2) *
LOC_Os08g04560.1 (OsTDC3)
LOC_Os08g04540.1 (OsTDC1) *
Sobic.007G035500.1
Bradi2g02370.1 (BdTDC2)
Bradi3g14780.1 (BdTDC7)
Bradi3g14740.1 (BdTDC4)
Bradi3g14730.1 (BdTDC3)
Bradi3g14750.1 (BdTDC5)
Bradi3g14760.1 (BdTDC6)
HORVU2Hr1G114440.1
HORVU2Hr1G114390.1
Bradi4g00660.2 (BdUBC18)
0
4
Induction fold (log2)

Figure 26 (previous page): Identification and analysis of *aromatic L-amino acid decarboxylases (AADC*s). Phylogenetic tree (left) displays relationship between identified *Bd*AADCs and AADCs from other grass species. Proteins marked with asterisks were used as BLAST templates in the search of homologs in Brachypodium. Protein sequence similarity tree was constructed by neighbor-joining distance. Ubiquitin-conjugating enzyme 18 (UBC18) protein sequence from Brachypodium was used as an outgroup. Heat map (right) indicates induction fold of *tryptophan decarboxylase* (*TDC*) expression in Brachypodium leaves 12 h, 24 h, and 36 h post-inoculation (hpi) with *P. nodorum* spores. Induction fold was calculated as ratio between relative gene expressions measured in inoculated and non-inoculated leaves at respective time points after inoculation. Presented results are means ± SD from three independent experiments with three biological replicates in each (n = 9). Bradi: Brachypodium; GRMZM: *Z. mays*; HORVU: *H. vulgare*; Os: *O. sativa*; Sobic: *S. bicolor*.

According to the published crystal structure of *Cr*TDC and *Ps*TYDC, TDCs can be differentiated from TYDCs by an amino acid substitution, which determines enzyme substrate specificity respectively for tryptophan or tyrosine (64). We decided to use this feature to confirm our *Bd*AADCs classification. By aligning AADC sequences from Brachypodium and selected grasses with reference sequences, we could examine the amino acid residue conservation among these enzymes (Figure 27). By comparison with *Cr*TDC and *Ps*TDYC sequences, we noticed that identified Brachypodium AADCs possess most of the conserved residues present in the substrate binding pocket. On one hand, all enzymes from the phylogenetic clade containing TDCs have a glycine conserved at the position 437 like *Cr*TDC, and on the other hand, enzymes from the clade containing TYDCs have either a serine (like *Ps*TYDC) or a threonine at the same position, which validates our classification based on the phylogenetic tree analysis (Figure 26).

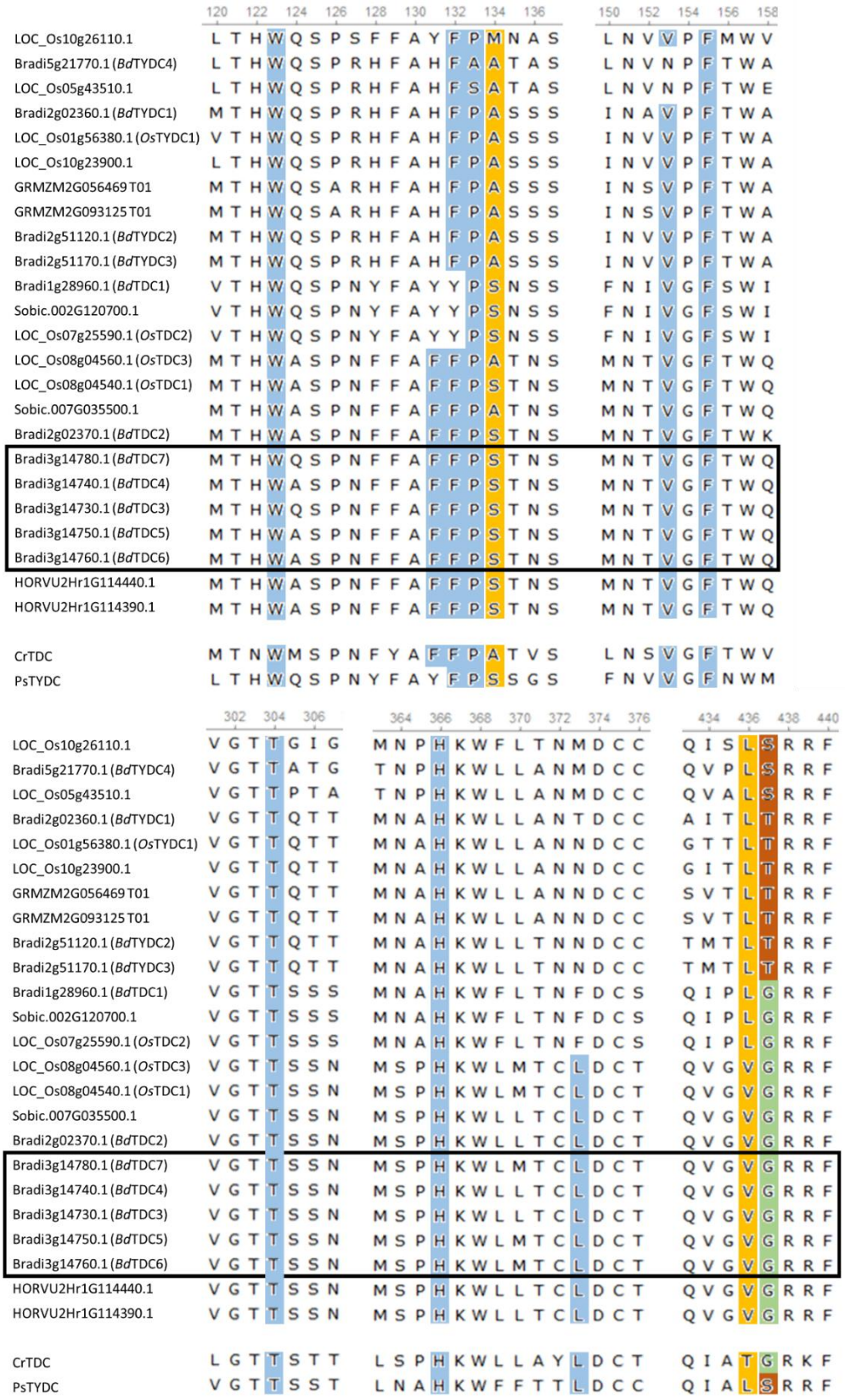
120 122 124 126 128 130 132 134 136 150 152 154 156 158
LOC_Os10g26110.1 L T H W Q S P S F F A Y F P M N A S L N V V P F M W V
Bradi5g21770.1 (BdTYDC4) L T H W Q S P R H F A H F A A T A S L N V N P F T W A
LOC_Os05g43510.1 L T H W Q S P R H F A H F S A T A S L N V N P F T W E
Bradi2g02360.1 (BdTYDC1) M T H W Q S P R H F A H F P A S S S I N A V P F T W A
LOC_Os01g56380.1 (OsTYDC1) V T H W Q S P R H F A H F P A S S S I N V V P F T W A
LOC_Os10g23900.1 L T H W Q S P R H F A H F P A S S S I N V V P F T W A
GRMZM2G056469 T01 M T H W Q S A R H F A H F P A S S S I N S V P F T W A
GRMZM2G093125 T01 M T H W Q S A R H F A H F P A S S S I N S V P F T W A
Bradi2g51120.1 (BdTYDC2) M T H W Q S P R H F A H F P A S S S I N V V P F T W A
Bradi2g51170.1 (BdTYDC3) M T H W Q S P R H F A H F P A S S S I N V V P F T W A
Bradi1g28960.1 (BdTDC1) V T H W Q S P N Y F A Y Y P S N S S F N I V G F S W I
Sobic.002G120700.1 V T H W Q S P N Y F A Y Y P S N S S F N I V G F S W I
LOC_Os07g25590.1 (OsTDC2) V T H W Q S P N Y F A Y Y P S N S S F N I V G F S W I
LOC_Os08g04560.1 (OsTDC3) M T H W A S P N F F A F F P A T N S M N T V G F T W Q
LOC_Os08g04540.1 (OsTDC1) M T H W A S P N F F A F F P S T N S M N T V G F T W Q
Sobic.007G035500.1 M T H W A S P N F F A F F P A T N S M N T V G F T W Q
Bradi2g02370.1 (BdTDC2) M T H W A S P N F F A F F P S T N S M N T V G F T W K
Bradi3g14780.1 (BdTDC7) M T H W Q S P N F F A F F P S T N S M N T V G F T W Q
Bradi3g14740.1 (BdTDC4) M T H W A S P N F F A F F P S T N S M N T V G F T W Q
Bradi3g14730.1 (BdTDC3) M T H W Q S P N F F A F F P S T N S M N T V G F T W Q
Bradi3g14750.1 (BdTDC5) M T H W A S P N F F A F F P S T N S M N T V G F T W Q
Bradi3g14760.1 (BdTDC6) M T H W A S P N F F A F F P S T N S M N T V G F T W Q
HORVU2Hr1G114440.1 M T H W A S P N F F A F F P S T N S M N T V G F T W Q
HORVU2Hr1G114390.1 M T H W A S P N F F A F F P S T N S M N T V G F T W Q
CrTDC M T N W M S P N F Y A F F P A T V S L N S V G F T W V
PsTYDC L T H W Q S P N Y F A Y F P S S G S F N V V G F N W M
302 304 306 364 366 368 370 372 374 376 434 436 438 440
LOC_Os10g26110.1 V G T T G I G M N P H K W F L T N M D C C Q I S L S R R F
Bradi5g21770.1 (BdTYDC4) V G T T A T G T N P H K W L L A N M D C C Q V P L S R R F
LOC_Os05g43510.1 V G T T P T A T N P H K W L L A N M D C C Q V A L S R R F
Bradi2g02360.1 (BdTYDC1) V G T T Q T T M N A H K W L L A N T D C C A I T L T R R F
LOC_Os01g56380.1 (OsTYDC1) V G T T Q T T M N A H K W L L A N N D C C G T T L T R R F
LOC_Os10g23900.1 V G T T Q T T M N A H K W L L A N N D C C G I T L T R R F
GRMZM2G056469 T01 V G T T Q T T M N A H K W L L A N N D C C S V T L T R R F
GRMZM2G093125 T01 V G T T Q T T M N A H K W L L A N N D C C S V T L T R R F
Bradi2g51120.1 (BdTYDC2) V G T T Q T T M N A H K W L L T N N D C C T M T L T R R F
Bradi2g51170.1 (BdTYDC3) V G T T Q T T M N A H K W L L T N N D C C T M T L T R R F
Bradi1g28960.1 (BdTDC1) V G T T S S S M N A H K W F L T N F D C S Q I P L G R R F
Sobic.002G120700.1 V G T T S S S M N A H K W F L T N F D C S Q I P L G R R F
LOC_Os07g25590.1 (OsTDC2) V G T T S S S M N A H K W F L T N F D C S Q I P L G R R F
LOC_Os08g04560.1 (OsTDC3) V G T T S S N M S P H K W L M T C L D C T Q V G V G R R F
LOC_Os08g04540.1 (OsTDC1) V G T T S S N M S P H K W L M T C L D C T Q V G V G R R F
Sobic.007G035500.1 V G T T S S N M S P H K W L L T C L D C T Q V G V G R R F
Bradi2g02370.1 (BdTDC2) V G T T S S N M S P H K W L L T C L D C T Q V G V G R R F
Bradi3g14780.1 (BdTDC7) V G T T S S N M S P H K W L M T C L D C T Q V G V G R R F
Bradi3g14740.1 (BdTDC4) V G T T S S N M S P H K W L L T C L D C T Q V G V G R R F
Bradi3g14730.1 (BdTDC3) V G T T S S N M S P H K W L L T C L D C T Q V G V G R R F
Bradi3g14750.1 (BdTDC5) V G T T S S N M S P H K W L M T C L D C T Q V G V G R R F
Bradi3g14760.1 (BdTDC6) V G T T S S N M S P H K W L M T C L D C T Q V G V G R R F
HORVU2Hr1G114440.1 V G T T S S N M S P H K W L L T C L D C T Q V G V G R R F
HORVU2Hr1G114390.1 V G T T S S N M S P H K W L L T C L D C T Q V G V G R R F
CrTDC L G T T S T T L S P H K W L L A Y L D C T Q I A T G R K F
PsTYDC V G T T S S T L N A H K W F F T T L D C C Q I A L S R R F

Figure 27 (previous page): Alignment of selected fragments of particular aromatic L-amino acid decarboxylases (AADCs) from grasses. Highly conserved amino acid residues of the substrate binding pocket are indicated in blue. Less conserved residues of the substrate binding pocket, are indicated in yellow. Residues in green are conserved among TDC clade, while residues in brown are conserved among tyrosine decarboxylase (TYDC) clade. Substrate binding pocket residues identified based on crystal structure of *Catharanthus roseus* TDC (*Cr*TDC) and *Papaver somniferum* TYDC (*Ps*TYDC) (64). Sequences of *BdTDC*s whose expression is induced in Brachypodium leaves upon *P. nodorum* spore inoculation are framed in black. Bradi: Brachypodium; GRMZM: *Z. mays*; HORVU: *H. vulgare*; Os: *O. sativa*; Sobic: *S. bicolor*.

We then investigated, which *Bd*TDCs were involved in the accumulation of tryptamine and serotonin observed upon pathogen inoculation. We also checked if the expression of genes coding for *Bd*TYDCs was affected by *P. nodorum* inoculation. To this purpose, we measured the impact of pathogen recognition on expression of identified *BdTDC*s and *BdTYDC*s (Figure 26). Among seven *BdTDC*s and four *BdTYDC*s that were investigated only expression of *BdTDC3*, *BdTDC4*, *BdTDC5*, *BdTDC6*, and *BdTDC7* was significantly induced upon *P. nodorum* recognition (Figure 29). Sequences of the proteins coded by these five genes are closely similar between them and with *Bd*TDC2, whose gene expression is not induced upon pathogen inoculation. These six TDCs share between 86% and 98% of identity and *Bd*TDC3-6 share more than 93% of identity. Furthermore, genes coding for these four enzymes are localized next to each other in the third chromosome, suggesting duplications of an ancestor gene in the course of evolution (Figure 28). *BdTDC5* and *BdTDC7* expression is significantly induced at 12 hpi, 24 hpi, and 36 hpi (Figure 29). In contrast, expression of *BdTDC3*, *BdTDC4*, and *BdTDC6* was significantly upregulated at 24 hpi and 36 hpi, but no induction was observed at 12 hpi. However, for all of them, we did not observe any clear expression changes between 24 hpi and 36 hpi.

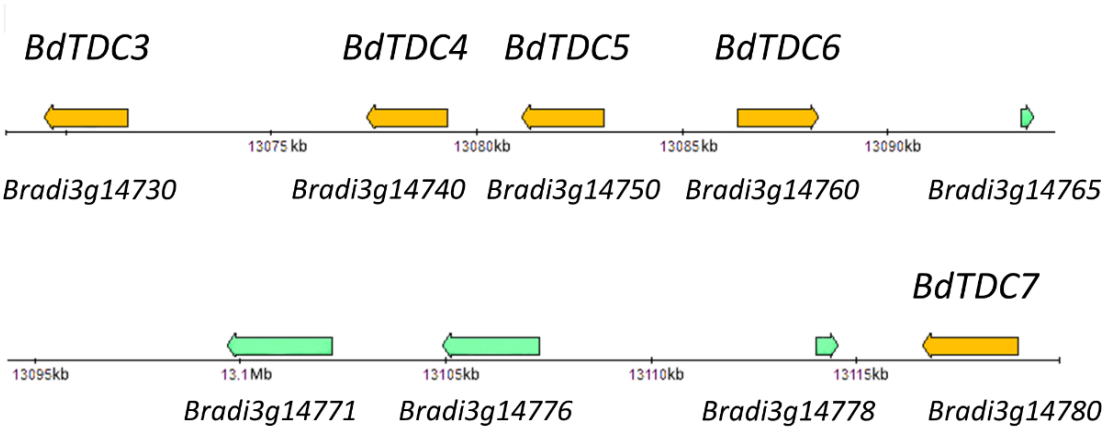

Figure 28: Organization of *BdTDC*s on Brachypodium chromosome III. *BdTDC*s are indicated in orange, other genes are indicated in green, and gene numbers and names are shown respectively below and above each gene. Arrows indicate gene transcription direction.

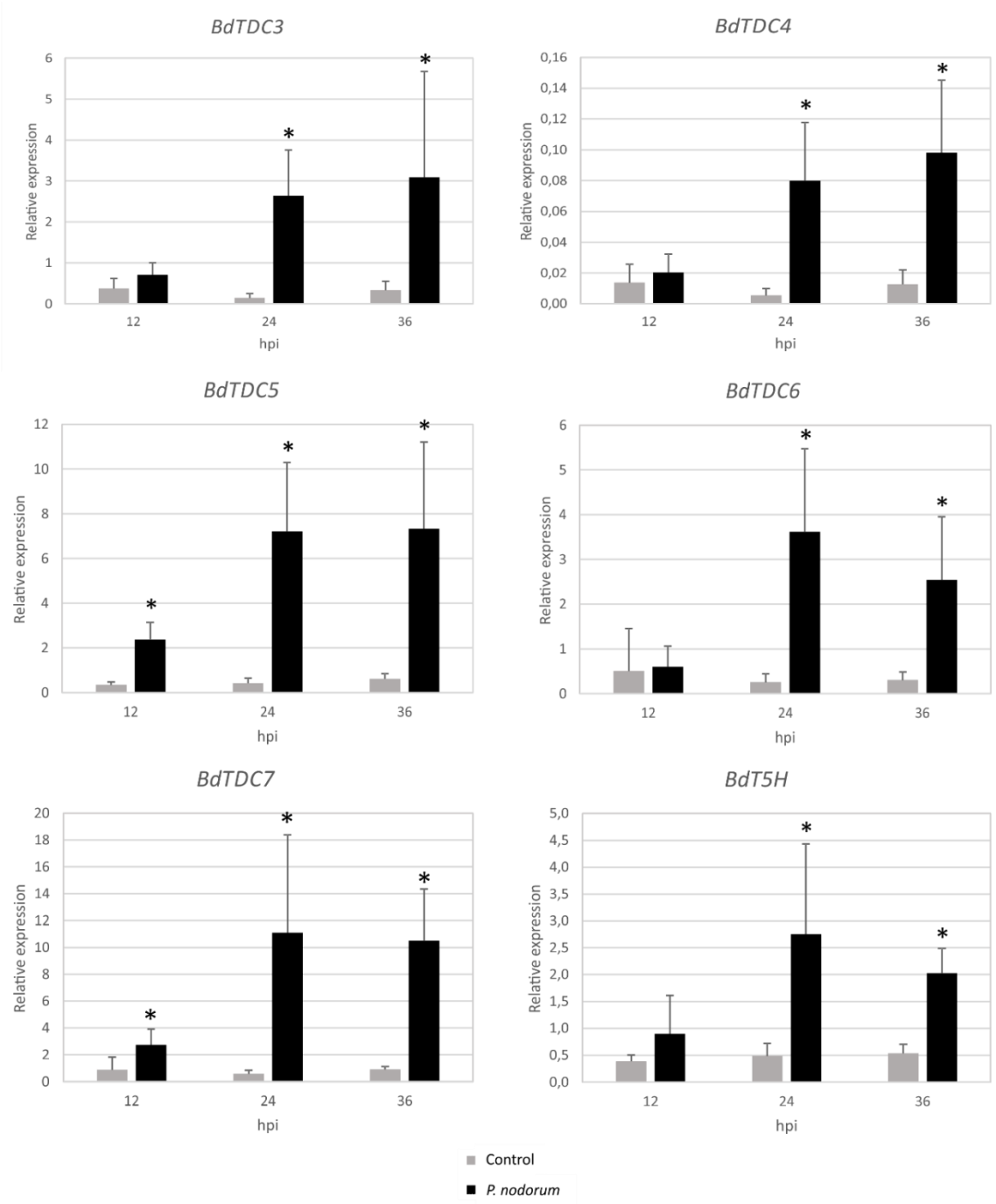

Figure 29: Expression of selected *tryptophan decarboxylases* (*TDC*s) and of *tryptamine 5-hydroxylase* (*T5H*) in Brachypodium leaves upon inoculation with *P. nodorum* spores at 12 h, 24 h, and 36 h post-inoculation (hpi). Non-inoculated leaves were analyzed as controls at respective time points. Presented results are means ± SD from three independent experiments with three biological replicates in each (n = 9). Values marked with asterisks are significantly different from respective controls (Student's t-test; $P < 0.01$).

The next step leading to serotonin biosynthesis involves T5H, which catalyzes the formation of serotonin from tryptamine (Figure 4). Searching for Brachypodium homologs of rice T5H, we found one gene, *Bradi4g39240*, which encoded a protein sharing 88% of identity with the reference rice enzyme. The second closest Brachypodium gene encoded a protein that was only 39% identical to rice T5H. For this reason, we assumed that Brachypodium possesses only one ortholog of T5H. Expression analysis of *BdT5H* showed significantly elevated transcription of this gene at 24 hpi and 36 hpi, but not at 12 hpi (Figure 29).

4.3 Phenylpropanoid biosynthetic pathway

As HCAs, HCAAs, and other phenylpropanoids were accumulating in higher amounts upon *P. nodorum* recognition (Table 7), we investigated the biosynthetic pathway leading to the formation of these metabolites. Phenylpropanoid biosynthetic pathway starts with the conversion of phenylalanine to cinnamic acid by PAL (Figure 7). Using the same approach as described for TDCs, we searched for Brachypodium genes coding for homologs of two rice PALs. As a result, we identified eight genes, *Bradi3g49250*, *Bradi3g49260*, *Bradi3g49270*, *Bradi3g49280*, *Bradi3g48840*, *Bradi3g47110*, *Bradi3g47120*, and *Bradi5g15830* that encode PAL homologs in Brachypodium. In the meantime, Barros *et al* published these genes and named them respectively *BdPTAL1* and *BdPAL2-8* (108). We, therefore, kept this nomenclature. In order to look for phylogenetic relationships between grass PALs, we build a protein similarity tree, based on published sequences (Figure 31). We included nine rice and seven sorghum protein sequences encoded by genes annotated as *PAL*s in the sequenced genomes of these species (239, 240). We add to our analysis other reported PAL sequences including four from bamboo (113), three from barley (114), three from wheat (112), and nine from maize (241).

We found that five *Bd*PALs (*Bd*PAL3, *Bd*PAL4, *Bd*PAL5, *Bd*PAL6, and *Bd*PAL7) are forming a clade among the analyzed grass PALs, and share between 91% and 98% of identity. The other three identified *Bd*PALs are not closely related to each other in the phylogenetic tree, despite sharing more than 72% of identity between them. Among them,

*Bd*PAL8 is closely related to the three identified PALs from wheat. Four *Bd*PALs (*Bd*PTAL1 and *Bd*PAL2-4) have their coding genes localized next to each other on Brachypodium third chromosome (Figure 30), suggesting that they originate from duplications of an ancestor.

To identify which *BdPAL*s could be responsible for the biosynthesis of HCAA precursors upon pathogen recognition, we measured *BdPAL* expression after inoculation with *P. nodorum*. This revealed that expression of four *Bd*PALs (*Bd*PAL2 and *Bd*PAL4-6) was significantly induced upon pathogen recognition (Figure 31 & 32). Out of them, *Bd*PAL4-6 are phylogenetically closely related. However, genes coding for *Bd*PAL3 and *Bd*PAL7, which are closely related to *Bd*PAL4-6, did not increase their expression upon treatment. Among genes whose expression was induced upon *P. nodorum* recognition *BdPAL2*, *BdPAL4*, and *BdPAL6* expression was significantly induced at 24 hpi, but not 12 hpi and 36 hpi (Figure 32). *BdPAL5* is the only homolog whose expression was significantly induced at 12 hpi, 24 hpi, and 36 hpi.

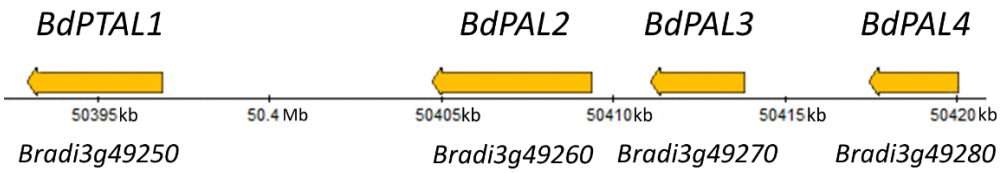

Figure 30: Organization *BdPAL*s on Brachypodium chromosome III. *BdPAL*s are indicated in orange and gene numbers and names are shown respectively below and above each gene. Arrows indicate gene transcription direction.

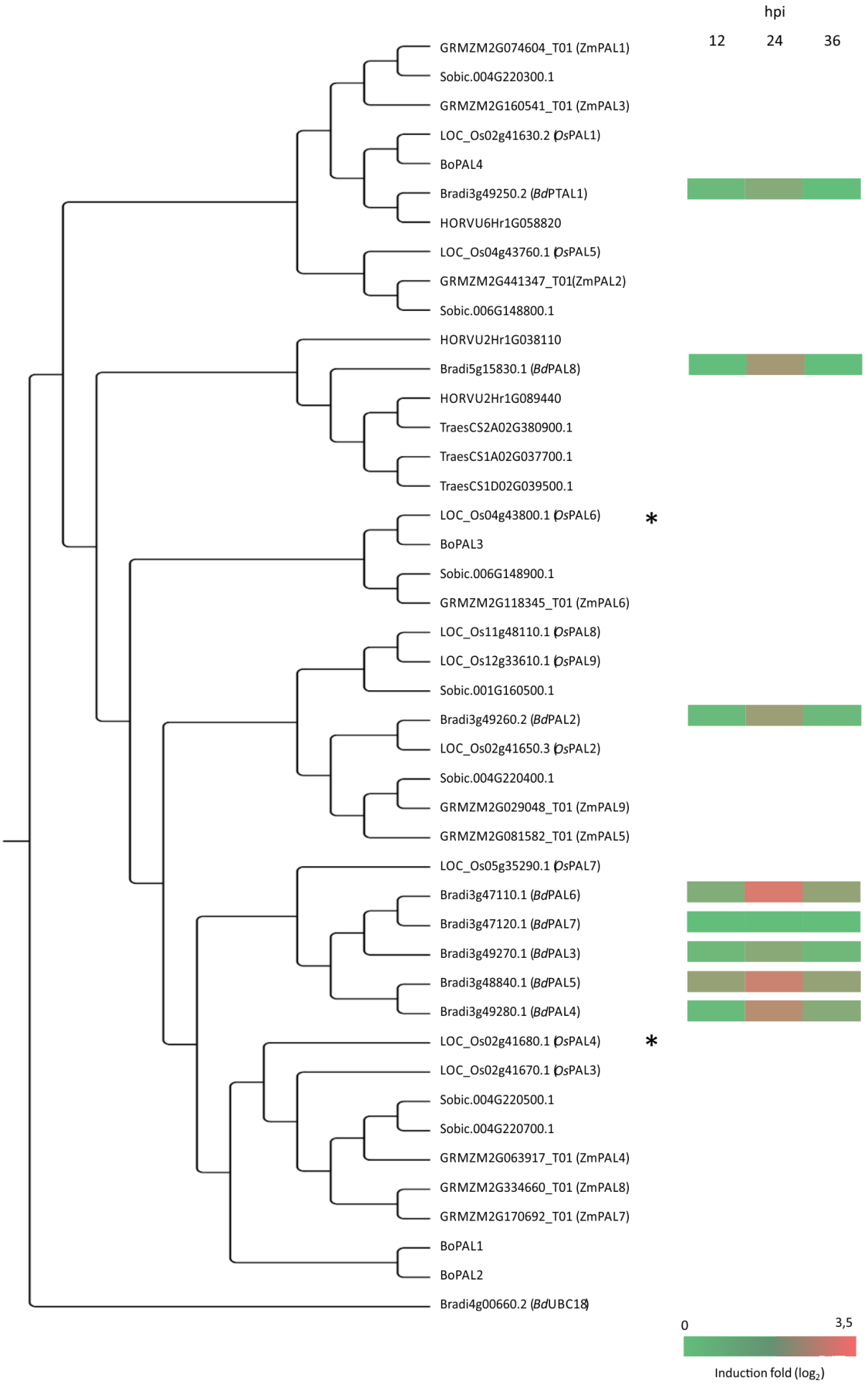
hpi
12
24
36
GRMZM2G074604_T01 (ZmPAL1)
Sobic.004G220300.1
GRMZM2G160541_T01 (ZmPAL3)
LOC_Os02g41630.2 (OsPAL1)
BoPAL4
Bradi3g49250.2 (BdPTAL1)
HORVU6Hr1G058820
LOC_Os04g43760.1 (OsPAL5)
GRMZM2G441347_T01(ZmPAL2)
Sobic.006G148800.1
HORVU2Hr1G038110
Bradi5g15830.1 (BdPAL8)
HORVU2Hr1G089440
TraesCS2A02G380900.1
TraesCS1A02G037700.1
TraesCS1D02G039500.1
LOC_Os04g43800.1 (OsPAL6)
*
BoPAL3
Sobic.006G148900.1
GRMZM2G118345_T01 (ZmPAL6)
LOC_Os11g48110.1 (OsPAL8)
LOC_Os12g33610.1 (OsPAL9)
Sobic.001G160500.1
Bradi3g49260.2 (BdPAL2)
LOC_Os02g41650.3 (OsPAL2)
Sobic.004G220400.1
GRMZM2G029048_T01 (ZmPAL9)
GRMZM2G081582_T01 (ZmPAL5)
LOC_Os05g35290.1 (OsPAL7)
Bradi3g47110.1 (BdPAL6)
Bradi3g47120.1 (BdPAL7)
Bradi3g49270.1 (BdPAL3)
Bradi3g48840.1 (BdPAL5)
Bradi3g49280.1 (BdPAL4)
LOC_Os02g41680.1 (OsPAL4)
*
LOC_Os02g41670.1 (OsPAL3)
Sobic.004G220500.1
Sobic.004G220700.1
GRMZM2G063917_T01 (ZmPAL4)
GRMZM2G334660_T01 (ZmPAL8)
GRMZM2G170692_T01 (ZmPAL7)
BoPAL1
BoPAL2
Bradi4g00660.2 (BdUBC18)
0
3,5
Induction fold (log2)

Figure 31 (previous page): Identification and analysis of *phenylalanine ammonia-lyases* (*PAL*s). Phylogenetic tree (left) displays relationship between identified *Bd*PALs and PALs from other grass species. Proteins marked with asterisks were used as BLAST templates in the search of homologs in Brachypodium. Protein sequence similarity tree was constructed by neighbor-joining distance. Ubiquitin-conjugating enzyme 18 (UBC18) protein sequence from Brachypodium was used as an outgroup. Heat map (right) indicates induction fold of *BdPAL* expression in Brachypodium leaves 12 h, 24 h, and 36 h post-inoculation (hpi) with *P. nodorum* spores. Induction fold was calculated as ratio between relative gene expressions measured in inoculated and non-inoculated leaves at respective time points after inoculation. Presented results are means ± SD from three independent experiments with three biological replicates in each (n = 9). Bo: *B. oldhamii*; Bradi: Brachypodium; GRMZM: *Z. mays*; HORVU: *H. vulgare*; Os: *O. sativa*; Sobic: *S. bicolor*; Traes: *Triticum aestivum*.

Among HCAs with increased accumulation in infected leaves we identified ferulic acid and its derivatives. Therefore we decided to investigate expression of *COMT* that encodes enzyme responsible for the conversion of caffeic acid to ferulic acid (Figure 7). Our BLAST search pointed at three homologs of COMT from rice in Brachypodium. However, phylogenetic analysis coupled with the search for conserved residues necessary for COMT catalytic activity was performed in the meantime by Daly *et al* (242), identifying among putative homologs a single *Bd*COMT, Bradi3g16530.1, which we selected for our gene expression analysis. *BdCOMT* expression was significantly induced at 24 hpi, but not at 12 hpi and 36 hpi (Figure 32). However, this significant induction could result from the reduced expression of this gene in the control samples at 24 hpi as compared with 12 hpi and 36 hpi. For this reason, this result should be considered carefully.

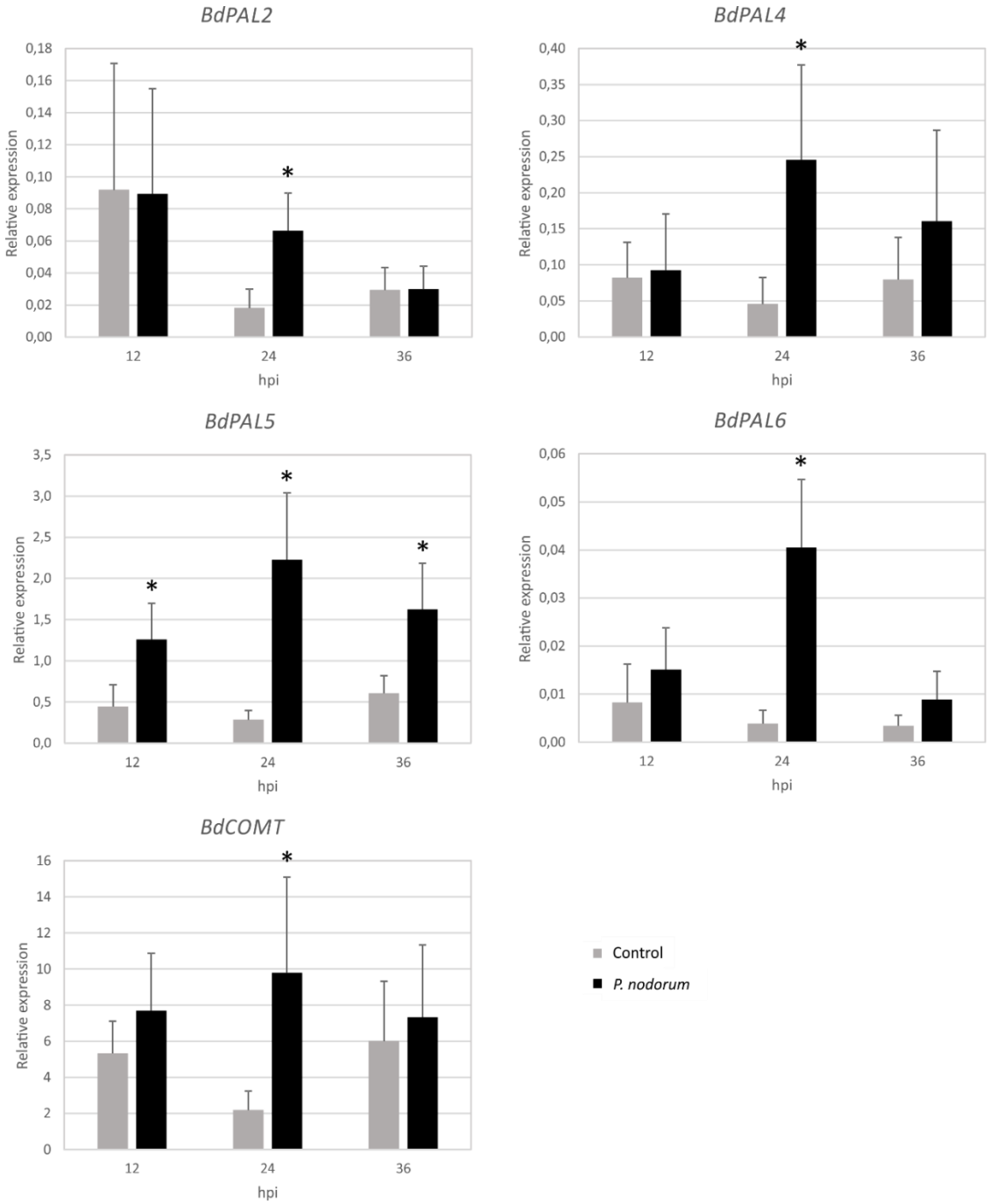

Figure 32: Expression of selected *phenylalanine ammonia-lyases* (*PAL*s) and *caffeic acid-O-methyl transferase* (*COMT*) in Brachypodium leaves upon inoculation with *P. nodorum* spores at 12 h, 24 h and 36 h post-inoculation (hpi). Non-inoculated leaves were analyzed as controls at respective time points. Presented results are means ± SD from three independent experiments with three biological replicates in each (n = 9). Values marked with asterisks are significantly different from respective controls (Student's t-test; $P < 0.01$).

4.4 Hydroxycinnamic acid amine biosynthesis

MS-detection based untargeted metabolite analysis led to the identification of FerPut, DiFerPut, FerSer, CouSer, CafSer, and *N*-caffeoyl-*O*-threonyl-serotonin (*O*-threonyl-CafSer) as metabolites accumulating in higher amounts upon *P. nodorum* recognition (Table 7). All these compounds are HCAAs, which are products of the conjugation between an HCA and an amine catalyzed by an HCT (Figure 7). To investigate this biosynthetic step leading to HCAA formation, we searched for genes coding for Brachypodium HCT homologs using as templates rice HCTs. Considering that HCTs from the same species can share less than 25% of identity, we decided to use seven rice HCTs, which shared between 24-54% of identity, as templates in order to minimize the chance to overlook any *BdHCT*s. This search led to the identification of 16 putative *BdHCT*s (*Bradi1g47180/90*, *Bradi1g47232*, *Bradi1g72210/20/30/37*, *Bradi3g02310*, *Bradi3g23280*, *Bradi3g48530*, *Bradi4g24210*, *Bradi4g36820/30/50*, *Bradi5g14720*, and *Bradi5g25166*). Among them six have been already reported (61, 136), including *Bradi4g36820/30/50* that were designated as *BdACT2c*, *BdACT2b*, and *BdACT2a* due to the identity (> 66%) with a putative wheat ACT (136). We kept this nomenclature of these three *BdHCTs*, and named the remaining genes *BdHCT1-13*. To study phylogenetic relationship between grass HCTs, we built a protein similarity tree based on sequence distances of published grass HCTs, including two from barley (138), one from maize (135), four from oat (139), 14 from rice (132-134), and one from wheat (243) (Figure 33). In the obtained tree we observed seven clades grouping proteins sharing at least 65% of identity, while proteins belonging to different clades have only between 20-50% of identity. Clade I includes *Bd*ACT2a which have been shown *in vitro* to preferentially use agmatine, cadaverine, and putrescine as acyl acceptors (136), and *Os*PHT3, which preferentially uses putrescine as substrate *in vitro* (134). In clade II we found ACTs from rice and barley together with *Bd*HCT13. Clade III is the largest clade and includes four closely related *Bd*HCTs (*Bd*HCT4-7), grouped with rice THTs and TBTs, which were reported to preferentially use respectively tryptamine, and tyramine and serotonin as substrates *in vitro* (133). *BdHCT4-7* are localized next to each other, which suggest that they originate from the same ancestor gene. Clade IV and V group three *Bd*HCTs with

three PHTs from rice, clade VI includes HHT from oat and two *Bd*HCTs, and clade VII includes only two SPHTs from rice.

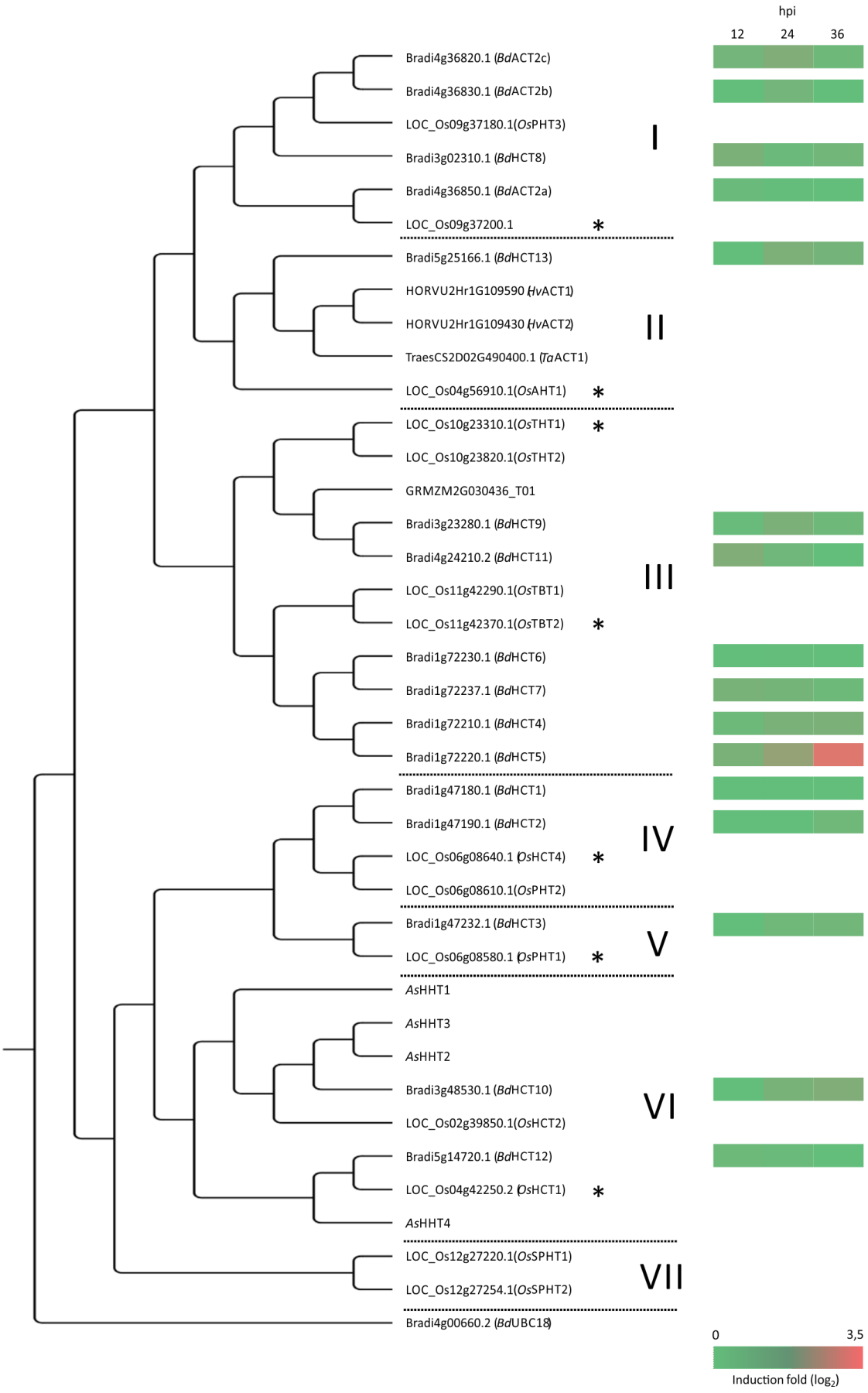
hpi
12
24
36
Bradi4g36820.1 (BdACT2c)
Bradi4g36830.1 (BdACT2b)
LOC_Os09g37180.1(OsPHT3)
Bradi3g02310.1 (BdHCT8)
Bradi4g36850.1 (BdACT2a)
LOC_Os09g37200.1 *
Bradi5g25166.1 (BdHCT13)
HORVU2Hr1G109590 (HvACT1)
HORVU2Hr1G109430 (HvACT2)
TraesCS2D02G490400.1 (TaACT1)
LOC_Os04g56910.1(OsAHT1) *
LOC_Os10g23310.1(OsTHT1) *
LOC_Os10g23820.1(OsTHT2)
GRMZM2G030436_T01
Bradi3g23280.1 (BdHCT9)
Bradi4g24210.2 (BdHCT11)
LOC_Os11g42290.1(OsTBT1)
LOC_Os11g42370.1(OsTBT2) *
Bradi1g72230.1 (BdHCT6)
Bradi1g72237.1 (BdHCT7)
Bradi1g72210.1 (BdHCT4)
Bradi1g72220.1 (BdHCT5)
Bradi1g47180.1 (BdHCT1)
Bradi1g47190.1 (BdHCT2)
LOC_Os06g08640.1 (OsHCT4) *
LOC_Os06g08610.1(OsPHT2)
Bradi1g47232.1 (BdHCT3)
LOC_Os06g08580.1 (OsPHT1) *
AsHHT1
AsHHT3
AsHHT2
Bradi3g48530.1 (BdHCT10)
LOC_Os02g39850.1(OsHCT2)
Bradi5g14720.1 (BdHCT12)
LOC_Os04g42250.2 (OsHCT1) *
AsHHT4
LOC_Os12g27220.1(OsSPHT1)
LOC_Os12g27254.1(OsSPHT2)
Bradi4g00660.2 (BdUBC18)
I
II
III
IV
V
VI
VII
0
3,5
Induction fold (log2)

Figure 33 (previous page): Identification and analysis of *hydroxycinnamoyltransferases* (*HCT*s). Phylogenetic tree (left) displays relationship between identified *Bd*HCTs and HCTs from other grass species. Proteins marked with asterisks were used as BLAST templates in the search of homologs in Brachypodium. Protein sequence similarity tree was constructed by neighbor-joining distance. Ubiquitin-conjugating enzyme 18 (UBC18) protein sequence from Brachypodium was used as an outgroup. Clades of protein sequences sharing at least 65% of identity are annotated with roman numbers. Heat map (right) indicates induction fold of *HCT* expression in Brachypodium leaves 12 h, 24 h, and 36 h post-inoculation (hpi) with *P. nodorum* spores. Induction fold was calculated as ratio between relative gene expressions measured in inoculated and non-inoculated leaves at respective time points after inoculation. Presented results are means ± SD from three independent experiments with three biological replicates in each (n = 9). As: *A. sativa*; Bradi: Brachypodium; GRMZM: *Z. mays*; HORVU: *H. vulgare*; Os: *O. sativa*.

All HCTs catalyzing HCAA formation belong to BAHD acyltransferase family whose members possess two characteristic conserved amino acid domains. Using this feature, we verified if all the identified putative *Bd*HCTs belong to this superfamily, despite the heterogeneity reflected by low percentages of sequence identity. To this purpose, we aligned all sequences composing the phylogenetic tree, and we searched for HXXXD(G) and DFGWG motifs (Figure 34). We found that the HXXXD(G) motif involved in substrate binding is fully conserved in all protein sequences of clades I, II, V and VI. Some proteins belonging to clades IV and VII have an alanine instead of the final glycine of the motif. However, this substitution may not have an impact on enzyme activity, as only the histidine and the aspartic acid of the HXXXD(G) motif have been found to have a role in substrate binding (244). On the contrary, the substitution of the aspartic acid by an alanine in *Bd*HCT7 sequence in clade III may indicate that this enzyme is not able to catalyze HCAA formation. The DFGWG motif which was suggested to play a structural role is fully conserved in clades V and VI. In other clades, the tryptophan from the motif is substituted with different amino acids. This substitution is present in *Os*TBTs and *Os*THTs, which both showed nonetheless *in vitro* acyltransferase activity (133), suggesting that this tryptophan residue is dispensable for HCT activity.

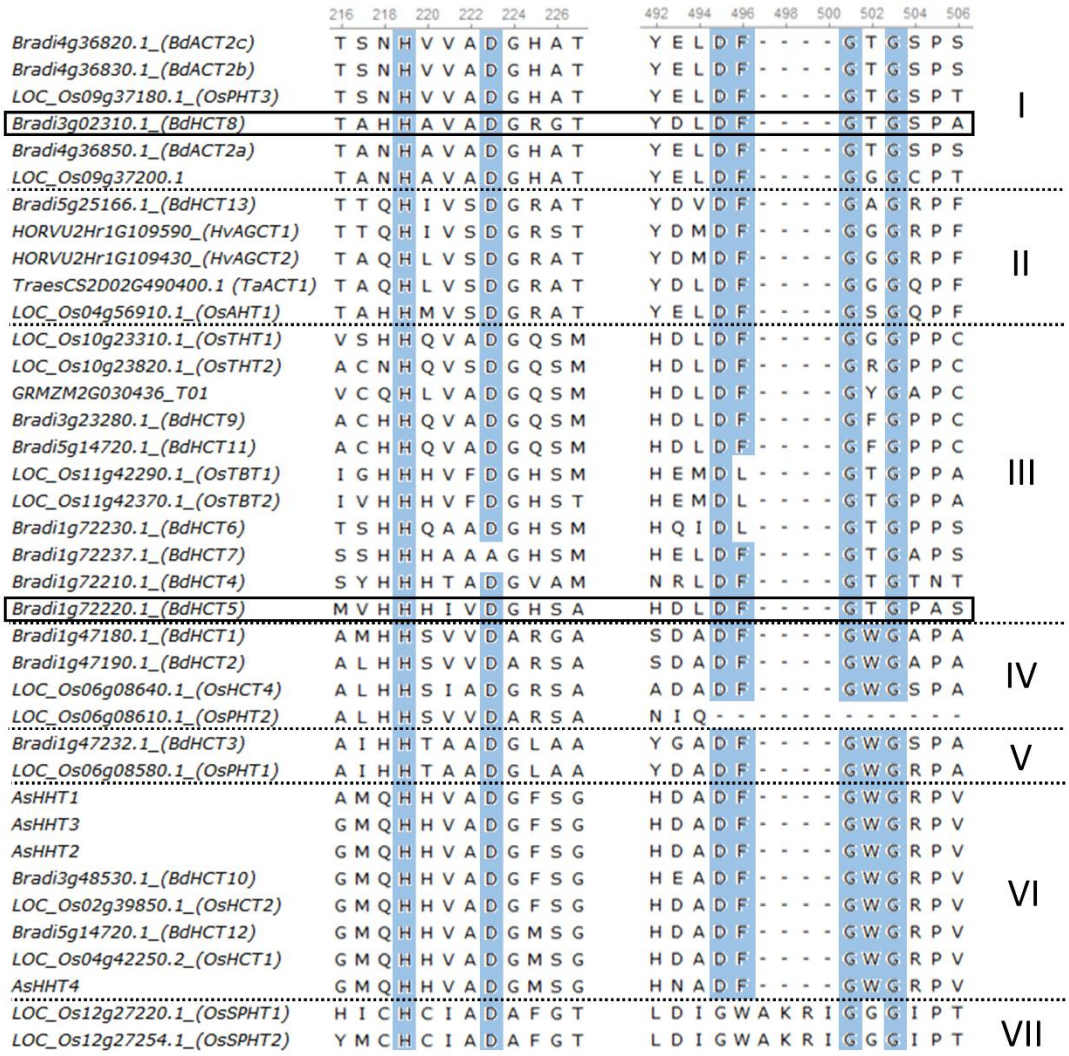

Figure 34: Alignment of selected fragments of hydroxycinnamoyltransferases (HCTs) from grasses. Amino-acid residues forming highly conserved domains of BAHD acyltransferase family, HXXXD(G) and DFGWG, are indicated in blue. Sequences of respective *BdHCT*s whose expression is induced in Brachypodium leaves upon *P. nodorum* spores inoculation are framed in black. Clades of protein sequences sharing at least 65% of identity are annotated with roman numbers. As: *A. sativa*; Bradi: Brachypodium; HORVU: *H. vulgare*; Os: *O. sativa*; Zm: *Z. mays*.

In order to determine, which of the investigated *Bd*HCTs are responsible for HCAA formation in response to pathogen recognition under our experimental conditions, we measured *P. nodorum*-triggered changes in the expression of 16 identified *BdHCT*s. Among them, only *BdHCT5*, and *BdHCT8* had their expression significantly induced upon inoculation with *P. nodorum* (Figure 33). These two genes belong respectively to

clade I and III, whose members use respectively aliphatic and aromatic amines as substrates. Expression of these genes shows different profiles (Figure 35). *BdHCT5* expression was significantly induced only at 36 hpi, while *BdHCT8* has a significantly higher expression at 12 hpi.

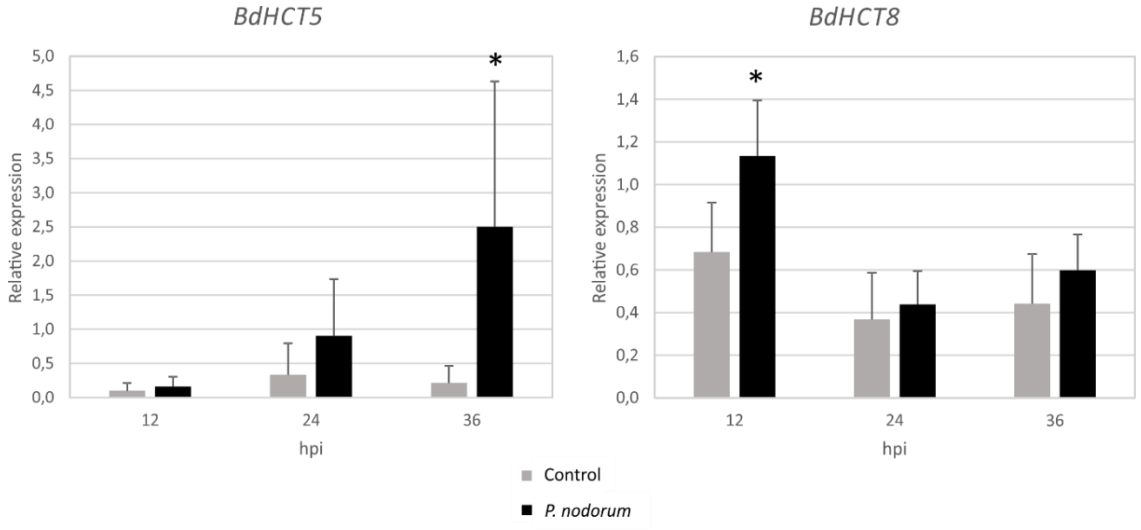

Figure 35: Expression of selected *hydroxycinnamoyltransferases* (*HCT*s) in Brachypodium leaves upon inoculation with *P. nodorum* spores at 12 h, 24 h, and 36 h post-inoculation (hpi). Non-inoculated leaves were analyzed as controls at respective time points. Presented results are means ± SD from three independent experiments with three biological replicates in each (n = 9). Values marked with asterisks are significantly different from respective controls (Student's t-test; $P < 0.01$).

Discussion

1 Brachypodium exemplifies metabolic diversity of grasses

Our unbiased UPLC-MS analysis led to the selection of 887 signals whose intensities significantly differed between samples from *P. nodorum* inoculated and non-inoculated leaves. Majority of these signals (~85%) had increased abundance in samples from infected tissue as compared with the respective controls. This indicates that the immune response is associated rather with biosynthesis than with catabolism of compounds. Among DAMs represented by these signals, we identified 27 metabolites classified as 13 tryptophan derivatives, three saponins, one hydroxyphenyllactic acid, one polyamine and 13 phenylpropanoids, including HCAAs derived from putrescine (2 metabolites) or serotonin (4 metabolites; Table 7). In addition to the identification of these metabolites, we found that certain genes encoding enzymes involved in the biosynthesis of some of these compounds had their expression induced upon inoculation with *P. nodorum* (Figure 29, 32, and 35). Collectively, these results indicate that similarly as in selected grass species serotonin, phenylpropanoid, saponin, and HCAA biosyntheses are activated during Brachypodium immune response (Figure 3 & 36).

Activation of serotonin biosynthetic pathway led to the increased accumulation of tryptamine, serotonin, together with its 11 derivatives (Figure 24 &Figure 23). Among these, to our best knowledge, serotonin-2-carbonitrile, serotonin–IAA, and *O*-threonyl-CafSer were so far not reported in any plant species. In line with the increased accumulation of all these tryptophan-derivatives, expression of *BdTDC*s, *BdT5H*, and *BdHCT*s, that are genes coding for enzymes responsible for the biosynthesis of serotonin and some of its derivatives, was induced upon pathogen inoculation (Figure 29 & 35).

Serotonin was also reported as phytoalexin rice, barley, wheat and foxtail millet (58-60). In rice, activation of serotonin biosynthetic pathway during the immune response was additionally corroborated with *B. oryzae*-triggered expression of *OsTDC1* (58). Moreover, some of serotonin derivatives identified in our study as DAMs were also identified as phytoalexins in other grass species. 5,5′-dihydroxy-2,4′-bitryptamine was found in rice, barley, and foxtail millet (59), while CouSer and FerSer, were identified in rice and bamboo (120, 121), the second one being also present in wheat (60).

Additionally, 3-(2-aminoethyl)-3-hydroxyindolin-2-one was produced in rice, barley, and foxtail millet upon pathogen inoculation (59), and FerTry was identified as phytoalexin in wheat (60) and rice (58). However, we did not identify these two compounds as DAMs in Brachypodium leaves inoculated with *P. nodorum*. Taken together, these results suggest that although serotonin is produced during the immune response in rice, barley, wheat, foxtail millet, bamboo, and Brachypodium these species may have capacity to produce different serotonin and tryptamine derivatives.

Overall, pathogen-induced biosynthesis of serotonin and its derivatives has been so far reported only in the five mentioned grass species, which are scattered among the subclades of the Poaceae phylogenetic tree (Figure 3). This suggests that serotonin biosynthetic pathway had been already present in a common grass ancestor and possibly lost during the evolution in certain species. Of course, many of grass species have been so far not investigated carefully for the presence of serotonin derivatives, for this reason we may assume that this pathway is more common in grasses that can be currently concluded based on the literature (Figure 3). In addition, our identification of 11 serotonin derivatives among DAMs clearly indicates that serotonin metabolic pathway is more complex than suggested based on the published results.

Among serotonin derived DAMs, we identified four HCAAs, FerSer, CouSer, CafSer, and *O*-threonyl-CafSer (Table 7). FerSer and CouSer accumulation have been already reported to be induced upon pathogen inoculation in Brachypodium (61), and, as mentioned above, in rice (58, 121), and bamboo (120). In addition to the HCAAs derived from serotonin, we identified putrescine-derived HCAAs as DAMs. Two representatives of this class of amides, CouPut and FerPut, were also found to accumulate during the immune response respectively in wheat (243), and rice (121). In our case, FerPut accumulation levels in infected leaves were lower than in the respective control at 72 hpi. Conversely, DiFerPut had its accumulation enhanced at all time points investigated (Figure 23), suggesting pathogen-triggered conversion of FerPut into DiFerPut.

In accordance with the reported pathogen-triggered changes in *HCT* expression in barley (138) and oat (140), the observed enhanced HCAA accumulation in Brachypodium leaves (Figure 23) correlated with elevated expression of two *BdHCT*s (Figure 35). Notably, these are different genes than *BdACT2b* and *BdACT2c* that had their expression induced in Brachypodium leaf sheaths upon inoculation with *F. pseudograminearum* (136). This

suggests that multiple *Bd*HCT isoforms can be linked with HCAA biosynthesis and the immune response in this species.

In addition to HCAAs derived from serotonin or putrescine, such amides can be produced upon pathogen inoculation from agmatine in barley (123) or from anthranilic acid in oat (125, 127, 128). Of note, HCAA biosynthesis was also induced during the immune response in dicotyledonous species. For instance, HCAAs derived either from agmatine or putrescine were reported in Arabidopsis (245), and HCAs conjugated with noradrenaline or tyramine were identified in potato and onion respectively (47, 246). Collectively, this indicates that both aliphatic and aromatic HCAAs are ubiquitous in plant kingdom, however, the occurrence of serotonin-derived HCAAs seems to be restricted to grasses.

Pathogen triggered biosynthesis of DiFerPut may point at enhanced polyamine biosynthesis especially that polyamines were identified as DAMs during immune responses in barley (137, 167, 168) and wheat (169). However, in our experiments, increase in the accumulation of polyamines upon *P. nodorum* inoculation was either moderate (spermidine) or not significant at all time points (putrescine; Figure 24), Moreover, we did not observe pathogen-triggered changes in the expression of *BdODC1* and *BdODC3* (Figure 25), unlike previously reported upon leaf sheath inoculation with *F. pseudograminearum* (136). However, as polyamines are produced constitutively we can assume that under certain conditions available pools of these compounds are sufficient for efficient biosynthesis of FerPut and DiFerPut.

Apart from amines, formation of HCAAs requires availability of HCAs. We identified ferulic acid, with three of its derivatives, as well as a sinapic acid derivative that accumulated upon *P. nodorum* recognition (Table 7). In addition to these HCAs, we identified among DAMs two additional phenylpropanoids, 5-methylcoumarin and di-*O*-methylquercetin (Table 7). The latter one represents flavonoids, compounds present in all plant species, but at least in grasses so far reported to participate in immunity only in maize (122), rice (51), sorghum (147, 148), and sugarcane (149) (Figure 3). Our finding indicates that Brachypodium is also among Poaceae species accumulating flavonoids in response to pathogen attack. However, quercetin represents different class of flavonoids than sakuranetin or 3-deoxyanthocyanidins, which are flavonoids linked with immunity

in rice, blackcurrant, sorghum, maize, and sugarcane respectively (Figure 9) (51, 53, 122, 147-149).

Opposite with serotonin, phenylpropanoid, HCAA, and saponin biosynthesis, we did not identify as DAMs products of other biosynthetic pathways, which lead to defense-related compounds reported in other grass species. For instance, tyramine was found to increase its accumulation in barley leaves inoculated with *B. sorokiniana* (59). However, we neither observed changes in tyramine amounts (Figure 24), nor in *BdTYDC* expression following pathogen inoculation (Figure 26), which indicates that tyramine biosynthetic pathway is not activated in Brachypodium upon pathogen recognition. Our analysis did not also reveal presence of gramine, a tryptophan-derived phytoanticipin, which has been identified in barley, reed canary grass, and giant cane (76, 77) (Figure 3). In barley, gramine biosynthesis depends on a single NMT (80), and as indicated by our analysis the closest homolog in Brachypodium (Bradi2g02380.1) shares only 41% of identity with this barley enzyme. This suggests that Brachypodium does not possess the key enzyme required for gramine biosynthesis. Along the same line, we did not detect BXs that are phytoanticipins ubiquitous in grass species (Figure 3). However, phylogenetic analysis of *Bx*s in different grasses showed that the closest Brachypodium homologs were phylogenetically distant from functional *Bx*s from maize, *H. lechleri* and wheat (92). Therefore, lack of BXs in our analysis is consistent with the proposed absence of the respective biosynthetic pathway in Brachypodium. Considering the fact that the ability to biosynthesize BXs seems to be an ancient feature in grasses (92), Brachypodium must have lost it during the evolution.

Our results did not point at enhanced accumulation of simple terpenoids in infected Brachypodium leaves. These compounds are ubiquitous in plant kingdom, but at least in grasses different terpenoid phytoalexins were identified only in rice and maize (176). This may suggest that in the Poaceae family capacity to couple different branches of terpenoid biosynthetic pathway with the immune response evolved independently in particular species, but not in Brachypodium.

Discussing the induction of certain biosynthetic pathways we have to keep in mind that our metabolic analyses were not complete due to several experimental and analytical limitations. For instance, as we only chose for structural identification signals that were differentially abundant between samples from inoculated and non-inoculated leaves, we

could overlook some phytoanticipins, which we constitutively present and did not change significantly their accumulation during the immune response. From the compounds known in grasses this may eventually concern cyanogenic glucosides. Moreover, because of time constraints, we focused on the identification of DAMs represented by 75 signals common to the three studied time points from which we managed to identify 22 compounds, leaving in total 53 unidentified compounds (Table 7 & Figure 22). Furthermore, we looked for FerPut and CafSer, as they are precursors of some identified DAMs, and we also found their accumulation affected with the infection, however, not at all three time points. In addition to this, the chosen analytical method, equipment sensitivity and sample preparation restricted our analysis to compounds accumulating within the range of detection and compatible with our extraction method. For example, non-polar metabolites, like certain terpenoids, or highly polar compounds, like polyamines, are either barely detectable or not detectable at all using UPLC-MS.

Overall, our analysis combined with the published results allows highlighting similarities and divergences in defensive metabolites between closely related grass species. The individual bouquets of such compounds result from the modifications or losses of conserved defense-related metabolic pathways, or from the evolution of new metabolic branches of conserved pathways that are by default not linked with immunity. For instance, BXs and serotonin biosynthesis seem to represent relatively ancient in grasses defensive metabolic pathways that have been lost in some species in the course of evolution. In addition, serotonin biosynthesis and metabolism evolved branches leading to species or clade-specific end products, including serotonin-2-carbonitrile, 3-(2-aminoethyl)-3-hydroxyindolin-2-one and possibly some of the serotonin derivatives that we were not able to identify completely. On the other hand, some grass species enrolled into their immunity newly evolved sub-branches of the flavonoid or terpenoid pathways, which are both ubiquitous in the plant kingdom, but their end products fulfill different functions that are frequently not linked with immunity. In any case, despite this diversity Brachypodium shares at least some of its defensive metabolic pathways with cereal crops including rice, wheat, and barley. For this reason, investigation of these pathways in Brachypodium may deliver results that could be useful in crop breeding.

2 Kinetics of Brachypodium metabolomic and transcriptomic response to pathogen attack

As indicated by our UPLC-MS analysis, recognition of *P. nodorum* triggered a clear change at the metabolic level in Brachypodium leaves already 24 hpi (Figure 21). Around 200 signals representing DAMs were detected at 24 hpi, and we found close to 300 additional DAM-related signals at 48 hpi. The increase in the total number of DAMs between 48 and 72 hpi was clearly lower (~150 signals) indicating that the rate of induction of metabolite biosynthesis started to slowly decrease between these two later time points. This, in turn, suggested that after 72 hpi the number of DAMs is likely to stabilize and/or decrease. In contrast, among DAM-related signals we found close to 50 linked with metabolites whose accumulation was affected exclusively at 24 hpi, around 150 unique for 48 hpi, and around 350 specific for 72 hpi (Figure 22). This suggests that even if the overall increase in the number of new DAMs decreased after 48 hpi, the total number of DAMs specific to certain time points increased with time.

The observed metabolic changes were preceded by induced expression of *BdHCT8* (Figure 35), and of genes coding for entry-point enzymes of serotonin (*BdTDCs*) and phenylpropanoid (*BdPALs*) biosynthetic pathways at 12 hpi (Figure 29 & 32). As observed 24 hpi this was followed by the induced expression of *BdT5H* and *BdCOMT*, which encode downstream enzymes in both pathways respectively. At the same time point we observed enhanced accumulation of tryptamine, DiFerPut, and serotonin and its derivatives, with the only exception of FerSer and CafSer(Figure 24, 29, 32, & 23). *BdTDC* and *BdT5H* expression levels were not further significantly changing after 24 hpi, while tryptamine, serotonin, and serotonin-2-carbonitrile accumulation continued to increase at 48 and 72 hpi. Induction of *BdCOMT* and *BdPAL* expression weakened between 24 and 36 hpi (Figure 32) while *BdHCT5* was the only among analyzed genes found to have induced expression starting at 36 hpi (Figure 35).

Our results fit with the reports on the kinetics of pathogen-triggered serotonin accumulation in other grasses. For instance, in rice leaves, *OsTDC1* expression was induced 12 hpi upon inoculation with *B. oryzae*, and tryptamine, serotonin, and serotonin derived HCAAs accumulation was enhanced 24 hpi (58). In barley leaves inoculated with *B. sorokiniana*, serotonin and 5,5′-dihydroxy-2,4′-bitryptamine were found to

differentially accumulate 24 hpi (59). In wheat leaves, tryptamine and serotonin had induced accumulation 48 h after treatment (60), however, in this case, biosynthesis was not triggered with infection, but with a fungal toxin.

In addition to the *P. nodorum* triggered changes, our gene expression analysis revealed also some temporal fluctuations in transcript amounts in the control samples. This could be observed for *BdCOMT*, *BdPAL4*, and *BdPAL5* whose expression is lower at 24 hpi than at 12 and 36 hpi (Figure 32). Because samples for gene expression analysis were collected in 12 h intervals, it is possible that circadian clock had an impact on the expression of these genes as it was shown in Arabidopsis (247). Moreover, it should be noted that phenylpropanoid and polyamine biosynthetic pathways are linked with the response to wounding (106, 248). As we used detached leaves in our experiments the observed patterns of *BdPAL* and *BdCOMT* expression in control leaves could be also affected by wounding. This abiotic stress could also contribute to the relatively high amounts of putrescine in control leaves 72 hpi as compared with other time points (Figure 24).

Altogether, our results indicate that *P. nodorum* recognition activated in Brachypodium transcription of several of the investigated genes linked with specialized metabolism at least 12 hpi. However, expression levels of these genes, with the only exception of *BdHCT5*, stopped to increase from 24 hpi (Figure 29, 32, & 35). This could reflect the fact that according to our analysis (15 & 17), fungal development was stopped at the same or even earlier time point. Despite the lack of continuous induction of gene transcription, the number of DAMs, as well as their accumulation levels in plant tissue, constantly increased between 24 and 72 hpi (Figure 21, 24,& 23). This suggests that gene expression levels reached at 24 hpi sufficed to support enhanced biosynthesis of metabolites up to 72 hpi. However, as some of the signals classified as DAMs may represent products of biosynthetic pathways that we did not investigate we cannot exclude that such pathways were triggered at a later time point, similarly as transcription of *BdHCT5*. Independently from the nature of the induced biosynthetic pathways and temporal patterns of their induction, production of specialized metabolites was not the only defense response that was still maintained, despite the restriction of pathogen development, in the analyzed leaves. The number and size of necrotic lesions, which indicate HR, also increased between 48 and 72 hpi indicating that the downstream mechanisms of Brachypodium immune response are in general not attenuated directly after defeating the pathogen.

3 Pathogen triggered gene expression can be affected by tissue-specificity

Results obtained during this study are not completely consistent with published results on Brachypodium metabolic response to the infection. For instance, we observed induced expression of *BdTDC3-7* in Brachypodium leaves inoculation with *P. nodorum* (Figure 29). Transcription of the same *TDC*s was also induced in Brachypodium spikes inoculated with *F. graminearum* (61). However, in Brachypodium leaf sheaths inoculated with *F. pseudograminearum*, only *BdTDC4* and *BdTDC6* expression was induced (31). The same pathogen was capable to trigger transcription of *BdODC1*, *BdODC3*, *BdACT2b,* and *BdACT2c* in leaf sheaths, which was not observed in our case (Figure 25) (136). *BdODC1*, *BdACT2b*, and *BdACT2c* expression was also triggered in infected spikes together with the expression of *BdHCT9* and *BdHCT13* whose transcription did not change significantly in our experiments. Conversely, these earlier studies do not report any pathogen triggered changes in the expression of *BdHCT8*. In our study, we observed induced expression of *BdPAL2*, and *BdPAL4-6* (Figure 32). Among these genes, only *BdPAL6* had induced expression in spikes inoculated with *F. graminearum*, together with *BdPAL3* (61).

All these observed discrepancies could result from different pathogens, different Brachypodium ecotypes and/or different tissues investigated in the respective studies. It has been reported in some plant species that certain isoforms of particular enzymes can be tissue specific. For example, in *Ferula assafoetida* various orthologs of *TPS* required for terpenoid biosynthesis, as well as of *PAL* and other genes involved in phenylpropanoid biosynthesis, were differentially expressed in flower, leaf, root, and stem (249).

Among the eight *BdPALs*, *BdPTAL1*, and *BdPAL2* were reported as the isoforms primarily expressed in roots, stems, leaves, and spikelets, while the remaining *BdPAL*s were constitutively expressed at low levels (108). Among these two genes, only *BdPAL2* expression was induced in response to infection in our study (Figure 32), but not in pathogen-inoculated spikes (61). This suggests that *BdPTAL1* is not linked with defense response, while *BdPAL2* has this function in leaves, but not in spikes. On the other hand,

BdPAL3-6, which are not significantly contributing to the constitutive pools of PAL (108) may be specialized in immunity, with *BdPAL3* and *BdPAL4-5* being specific to the response in spikes and leaves respectively. Contrary to *BdPAL*s, the expression of the same *TDC* isoforms were induced in both leaves and spikes, and no other isoform was transcriptionally activated during the immune response in leaf sheaths. Therefore, it indicates that pathogen triggered *BdTDC*s expression is not tissue specific. Tissue-specific pattern of *BdHCT*s during immune response suggests that *BdHCT5* is ubiquitously expressed during the immune response in leaves and spikes, while *BdACT2b* and *BdACT2c* expression is induced in leaf sheaths and spikes. On the other hand, changes in *BdHCT9* and *BdHCT13* expression are specific to spikes while *BdHCT8* is a leaf-specific isoform.

Finally, it should be noted that in the studies mentioned above gene expression was analyzed 72 hpi for leaf sheath (31), and 96 hpi for spikes (61). It is possible that expression of some of the genes reported in these studies, but not in our case, is induced specifically only at later interaction stages that we did not investigate. However, as we did not observe any pathogen development starting from 24 hpi (Figure 17) our experimental setup is not optimal to address this question.

4 Involvement of particular enzyme isoforms in immunity is frequently conserved between closely related plant species.

Analysis of TDC, PAL, and HCT phylogenetic relationship allowed us to investigate the link between protein homology and function in immunity, in Brachypodium, and among grass species. For instance, in the TDC phylogenetic tree we noted a subclade including exclusively Brachypodium TDCs (*Bd*TDC3-6) that share very high sequence identity (>93 %; Figure 26). Genes encoding all these proteins had their expression induced during the immune response (Figure 29) (61). Moreover, *BdTDC3-6* localize next to each other on chromosome III (Figure 28) and *BdTDC7* whose expression was also induced upon pathogen recognition, localizes five genes downstream of *BdTDC6.* Interestingly, out of the four genes localized between *BdTDC6* and *BdTDC7* one encodes a 77 amino acid

peptide homologous with a TDC fragment. Overall, this indicates that *TDC*s present in this region of chromosome III originate from relatively recent and complex duplications of an ancestor gene. In addition, the fact that all of these five genes have similar expression patterns upon pathogen inoculation (Figure 29) suggests that the pathogen-responsive regulatory elements in their promoters remained relatively conserved.

Similarly to *Bd*TDC3-6, *Bd*PAL3-7 form a Brachypodium-specific subclade sharing high sequence identity (>90 %; Figure 31). However, among the genes encoding these five closely related enzymes, only *BdPAL3-6*, but not *BdPAL7*, have been found to increase their expression upon pathogen inoculation (Figure 32) (61). In addition, among these genes only *BdPAL3* and *BdPAL4* have adjacent localization in Brachypodium genome on chromosome III (Figure 30). Strikingly, they localize next to *BdPTAL1* and *BdPAL2*, which encode enzymes that are neither highly homologous with each other nor with *Bd*PAL3-4 (Figure 31). Particularly *Bd*PAL2, which according to our results is involved in immunity, is phylogenetically distant from all other *Bd*PALs, including *Bd*PAL3-6 (Figure 31). These observations indicate that some, but not all of *Bd*PALs involved in the pathogen-triggered phenylpropanoid biosynthesis are closely phylogenetically related.

In contrast to *Bd*TDC3-6 and *Bd*PAL3-7, Brachypodium-specific *Bd*HCT4-7 subclade shares relatively low sequence identity (>50 %) despite the fact that the four genes encoding these enzymes are localized next to each other on chromosome I. In addition, among them only *BdHCT5* expression was induced upon pathogen recognition (Figure 35). Opposite with *Bd*HCT4-7 subclade, clade I of the HCT phylogenetic tree contains four *Bd*HCTs (*Bd*ACT2a-c & *Bd*HCT8) that share higher sequence identity (>64%) and are all involved in immunity (Figure 35) (61, 136). *Bd*HCT13 has been shown to participate in defense response in spikes (61), however, this enzyme is not closely related to any other *Bd*HCTs. Overall, this indicates that similarly to *Bd*PALs, closely related *Bd*HCTs may share function in immunity, but there are some exceptions from this rule.

During the investigation of the generated phylogenetic trees, we tried also to check if the response of particular Brachypodium isoforms to the infection fits with the reported expression of putative orthologs from other grass species. For instance in rice, *OsTDC1* transcript abundance increased upon inoculation with *B. oryzae* (58). This gene is the closest rice homolog of the *BdTDC3-7* that had their expression induced in response to infection (Figure 26 & 29). This suggests that the subclade including *Os*TDC1 and

*Bd*TDC3-7 groups enzymes with function in immunity. Of note, this clade contains also one putative TDC from sorghum, and two putative TDCs from barley. Serotonin was so far reported only in trace amounts in sorghum (250), but has been found to accumulate in elevated amounts upon pathogen inoculation in barley (59). Therefore, the two barley TDCs homologous to *Bd*TDC3-7 are good candidates to investigate pathogen-inducible serotonin biosynthesis in this species.

Similarly to *Bd*PALs, proteins encoded by *OsPAL1-7* whose expression was induced upon pathogen inoculation (119), did not group in any subclade of the generated phylogenetic tree (Figure 31). However, among them, *Os*PAL2 and *Os*PAL7 are putative orthologs of *Bd*PAL2 and *Bd*PAL3-6, respectively, that are all also involved in immunity (Figure 31) (61). In contrast, *Os*PAL1 is phylogenetically closely related to *Bd*PTAL1, which is not linked with pathogen-inducible defense (Figure 31 & 32). Taken together, these results suggest that closely phylogenetically related PALs from different grass species may share their role in immunity but function of some isoforms may also have diverged independently between species.

Among the investigated grass *HCT*s, *HvACT1* and *HvACT2* from barley (138), and *AsHHT1-4* from oat (139) were reported to have induced expression in response to the infection. *Hv*ACT1-2 belong to clade II of the generated HCT phylogenetic tree, which also includes *Bd*HCT13 (Figure 14). This relationship combined with the reported induced expression of *BdHCT13* in response to pathogen inoculation in spikes (61) suggests a shared function in immunity of enzymes from clade II. In clade I, the previously mentioned subclade containing *Bd*ACT2a-c and *Bd*HCT8, also includes *Os*PHT3 and LOC_Os09g37200 (Figure 33) suggesting that these two rice HCTs may also play a role in immunity. Contrary, *As*HHT1-4 belong to clade VI, in which no *Bd*HCTs were observed to have their gene expression induced upon inoculation (Figure 33).

Taken together, these observations indicate that sequence homology can be frequently useful in predicting function in immunity for putative gene orthologues from closely related species. However, we observed a more tight correlation between sequence homology and conserved function in immunity for TDCs than for PALs, and HCTs. This difference can be partially explained by comparing the diversity of functions of products of phenylpropanoid and serotonin biosynthetic pathways. Phenylpropanoid biosynthesis

is ubiquitous in plant kingdom, and apart from immunity involved in many physiological processes, for instance composition of cell wall structural polymers, response to abiotic stress, or participation to beneficial interspecies interactions (251). Among phenylpropanoids, HCAAs have been reported to participate in growth, senescence, reproduction, and response to biotic and abiotic stress (252). This in turn suggests a high number of evolutionary pressures that resulted in complex functional diversification of PAL and HCT isoforms. In contrast, serotonin biosynthetic pathway has been reported to be involved in fewer physiological processes, namely immune response, growth, and reproduction (57). In such a case, functional diversification among TDCs is lower, which makes the homology-based prediction of physiological function easier.

5 AADC and HCT substrate specificity is shared between closely related enzymes

Our phylogenetic analysis of the 24 grass AADCs revealed two separate clades of these proteins (Figure 26). The enzymes from one of these subclades have a conserved glycine, which is a hallmark of TDCs (64), while the second subclade grouped enzymes that have serine or threonine at the same position, which are residues characteristic for TYDCs (Figure 27). This indicates that our phylogenetic analysis clearly separated these two closely-related AADC types with different substrate preference. Similarly as in the case of AADCs phylogenetic analysis of HCTs revealed subclades of more closely related enzymes, in this case we observed seven clades of enzymes sharing more than 65% of amino acid sequence identity (Figure 33). Reported so far results of *in vitro* assays with heterologously expressed plant HCTs revealed that these enzymes accept preferentially either aliphatic or aromatic amines as substrates (129). We observed that each clade of our phylogenetic tree of grass HCTs included representatives of only one of these two HCT types (Table 8). Based on this we assume that, similar to the two subclades in the AADC phylogenetic tree, particular subclades of HCTs include enzymes with the same substrate specificity. Therefore, we propose that *Bd*HCT8, belonging to the clade I of generated HCT tree, catalyzes the formation of HCAAs derived from aliphatic amines, including FerPut and DiFerPut. On the other hand, *Bd*HCT5, belonging to clade III, may

be involved in the formation of HCAAs derived from aromatic amines, including CouSer, FerSer, CafSer, and *O*-threonyl-CafSer. These assumptions are supported by results obtained during our gene expression and metabolomic analysis. As discussed above, kinetics of changes in *BdHCT8* expression correlate with DiFerPut accumulation, while temporal *BdHCT5* expression pattern fits with the changes in FerSer accumulation (Figure 23 & 35). Finally, as *Bd*HCT13, which was linked with immune response in spikes (61), belongs to clade II of the HCT phylogenetic tree, we propose that this HCT is involved in the formation of aliphatic-derived HCAAs, similarly as *Hv*ACT1-2 (138) (Table 8).

Table 8: Representative enzymes of each clade of hydroxycinnamoyltransferase (HCT) phylogenetic tree. Substrates highlighted in orange are aliphatic amines, while substrates highlighted in blue are aromatic amines. ACT: agmatine coumaroyltransferase; AHT: agmatine hydroxycinnamoyl transferase; HHT: hydroxycinnamoyl-CoA:hydroxyanthranilate HCT; PHT: putrescine hydroxycinnamoyltransferase; TBT: tryptamine benzoyl transferase; SPHT: spermidine hydroxycinnamoyl transferase.

Clade	Investigated HCTs	Accepted substrates
I	*Bd*ACT2a-c (136) LOC_Os09g37200.1 (134) *Os*PHT3 (133)	Agmatine, cadaverine, & putrescine Agmatine & putrescine Putrescine
II	*Hv*ACT1-2 (138) *Os*AHT1 (133) *Ta*ACT1 (243)	Agmatine Agmatine Agmatine & putrescine
III	*Os*TBT1-2 *Os*THT1-2 (133)	Serotonin, tryptamine, & tyramine Tryptamine
IV	*Os*PHT2 (133)	Putrescine
V	*Os*PHT1 (133)	Putrescine
VI	*As*HHT1 (139, 228)	Anthranilate
VII	*Os*SPHT1-2 (132)	Spermidine

6 Some of the identified Brachypodium DAMs have assigned roles in immunity

In our analysis we observed 887 MS signals with significantly different abundance in samples from control and pathogen-inoculated Brachypodium leaves (Figure 22). Among DAMs represented by these signals, we expected to find metabolites with defensive functions produced by the plant in response to pathogen recognition. Apart from such compounds, MS signals assigned as DAMs may represent metabolites of other origin or function. For instance, some DAMs may be produced by *P. nodorum*, or formed during metabolization of plant compounds by the pathogen. However, limited pathogen development observed in our experiments (Figure 17) suggests very low fungal biomass, which in turn would make detection of these metabolites during our analysis not very likely. In addition, pathway intermediates that do not have any direct function in defense response, may differentially accumulate in pathogen-inoculated leaves. Examples of such DAMs could be tryptamine, which is the precursor of serotonin and its derivatives, or ferulic acid, which participate in the formation of the respective HCAAs and other partially identified derivatives. Furthermore, due to their higher accumulation such intermediates or precursors of activated biosynthetic pathways can be fed to branch pathways that are not of significance for immunity. Finally, the observed HR-triggered cell death results in the breakdown of cellular components leading to the formation of catabolites not present in living cells, and such compounds could be also counted as DAMs. Overall, we expect that only a fraction of the 887 MS signals corresponds to compounds contributing to the restriction of pathogen growth.

During this study we did not directly investigate roles in immunity of identified DAMs, however, possible functions of some of these compounds have been already studied in other grass species. Based on this we may assume that these metabolites can act as antibiotics (46), cell-wall structure components (47) or ROS scavengers (253). The identified DAMs that are directly toxic to the pathogen may include di-*O*-methylquercetin, hydroxyphenyllactic acid, saponins, serotonin, 5,5′-dihydroxy-2,4′-bitryptamine, serotonin-2-carbonitrile, CouSer, FerSer, as well as additional not completely identified serotonin derivatives (Table 8) (59-61, 121, 197, 254, 255). Of note, among these compounds, 5,5′-dihydroxy-2,4′-bitryptamine inhibited *in vitro* fungal

growth five times more efficiently than serotonin (59). Similarly, antifungal activity of 3-(2-aminoethyl)-3-hydroxyindolin-2-one, not identified as DAM in our study, was three times higher than the activity of serotonin (59) suggesting that more complex serotonin or tryptamine derivatives possess increased biological activity. Along this line, we may assume that identified in our study serotonin-2-carbonitrile acid has higher antifungal properties than serotonin. On the other hand, lower antifungal activity of serotonin may be counterbalanced by the high concentration of this metabolite we measured in leaves as compared with other compounds we were able to quantify (Figure 24). Constitutive pool of serotonin may also allow the rapid biosynthesis of its derivatives in response to pathogen attack. Additionally, it has been proposed that conversion of serotonin to 5,5′-dihydroxy-2,4′-bitryptamine restricts oxidative damage in cells adjacent to the infected cells by scavenging ROS particles (209). Altogether, this indicates that serotonin may fulfill multiple functions in immunity. Similarly as serotonin, HCAAs play also different defensive roles. It has been suggested that, in addition to their antifungal activity, these compounds hamper pathogen colonization by being covalently attached to the suberin deposited on the cell wall to reduce its digestibility by fungal enzymes (124, 141, 142). Overall, as antimicrobial properties are frequently reported for end products of plant metabolic pathways that are induced in response to infection, we may assume that at least some of the DAMs that have been not yet identified possess such activity. Similarly, we may expect that among DAMs we can still identify additional HCA-derivatives that can contribute to cell wall reinforcement.

In addition to the roles mentioned above, defense-related metabolites may fulfill other functions in immunity. For instance, experimental evidence suggests that in maize DIMBOA acts as a signaling molecule to trigger callose deposition (103, 210). Of note, this compound has been reported to have antifungal activity (103), indicating that, similarly to serotonin and some HCAAs, it may fulfill have multiple roles in plant immunity. Likewise, we can expect that some of the identified or yet unidentified DAMs observed after leaf inoculation with *P. nodorum*, may have a signaling function, either as a unique role or in addition to other defense-related functions.

7 Outlook

During this study we identified only 24 metabolites among 887 signals representing DAMs (Figure 22). Therefore, further processing of obtained LC/MS data combined with additional LC/MS/MS analysis and spectral library searches may support identification of additional compounds. In addition, structures proposed for 5-methylcoumarin, di-*O*-methylquercetin, saponins, and serotonin derivatives are preliminary and therefore need additional validation. If feasible, chemical synthesis of respective compounds and their subsequent LC/MS analysis could support our structural predictions. Alternatively, these compounds could be purified to validate their structures by Nuclear Magnetic Resonance (NMR) analyses. Identification of additional DAMs may either give a more comprehensive picture of biosynthetic pathways already investigated in this study, or indicate the involvement of other biosynthetic pathways in Brachypodium immune response.

Apart from DAMs, additional genes encoding enzymes involved in metabolic reprogramming need to be identified. During our investigations, we used only targeted analysis of a biased selection of genes. To improve this, untargeted approach, for instance deep RNA sequencing (RNA-Seq), should be performed in order to identify genes whose expression is induced upon pathogen inoculation. Among such genes, those encoding metabolic enzymes should be selected and investigated further.

Additional experiments are also necessary to assess biosynthetic activity of enzymes encoded by the identified genes, their participation to metabolic pathways, and function in immunity. To address the enzyme activity, we may investigate substrate specificity by enzymatic assays of heterologously expressed proteins. With this approach we could for instance validate substrate specificity of *Bd*HCTs that was proposed based on our phylogenetic analysis. Contribution of enzymes encoded by investigated genes to certain pathways can be additionally validated using mutant lines with defect in genes of interest. Such mutants can be nowadays obtained using modern genome editing technologies, for instance Clustered Regularly Interspaced Short Palindromic Repeats associated protein 9 (CRISPR-Cas9) system, which not only provides accurate targeted mutations, but has also been reported to allow removing genomic regions of up to 245 kb in rice (256). Subsequent comparison of metabolic profiles, between generated mutant lines and wild

type line can reveal if particular gene indeed encodes enzyme required for biosynthesis of certain metabolites. Additionally, mutant lines may also be used to address the contribution to immunity of enzymes, and subsequently of their products, by comparing susceptibility between wild type line and generated mutant plants.

Serotonin biosynthetic pathway is an example of metabolic pathway which can be further characterized using mutant lines. Actually, this pathway has already been investigated using *sl* rice mutant line lacking a functional T5H (71). However, this line exhibits spontaneous formation of necrotic lesions, probably due to tryptamine over-accumulation (72), and this unwanted pleiotropic effect can mask the immune response. Therefore, it is worth to generate Brachypodium *tdc* line, which should not accumulate tryptamine, and therefore not exhibit this pleiotropic effect. *tdc* mutant may be obtained by removing the chromosome III fragment containing four adjacent *BdTDC*s whose expression was induced upon pathogen recognition. A *t5h* mutant line may also be generated in Brachypodium to compare with the observation reported in rice, and investigate the specific contribution of serotonin and its derivative to Brachypodium immunity. Additionally, generation of *hct* mutant lines may indicate the function of certain *Bd*HCT isoforms in immunity, and their role in the biosynthesis of particular HCAAs.

Overall, with the above mentioned experiments we aim to further characterize pathways reported in this study as well as identify additional metabolic pathways linked with Brachypodium immunity. This in turn will allow obtaining a comprehensive picture of specialized metabolic pathways participating in the defense response of this species. In parallel, the different roles that end products of these pathways play in immunity should be investigated using reverse genetic approach. The knowledge obtained during these studies can be transferred into other grass species activating the same biosynthetic pathways in response to pathogen attack, for instance to assist breeding lines of species of agronomical relevance with improved resistance towards pathogens.

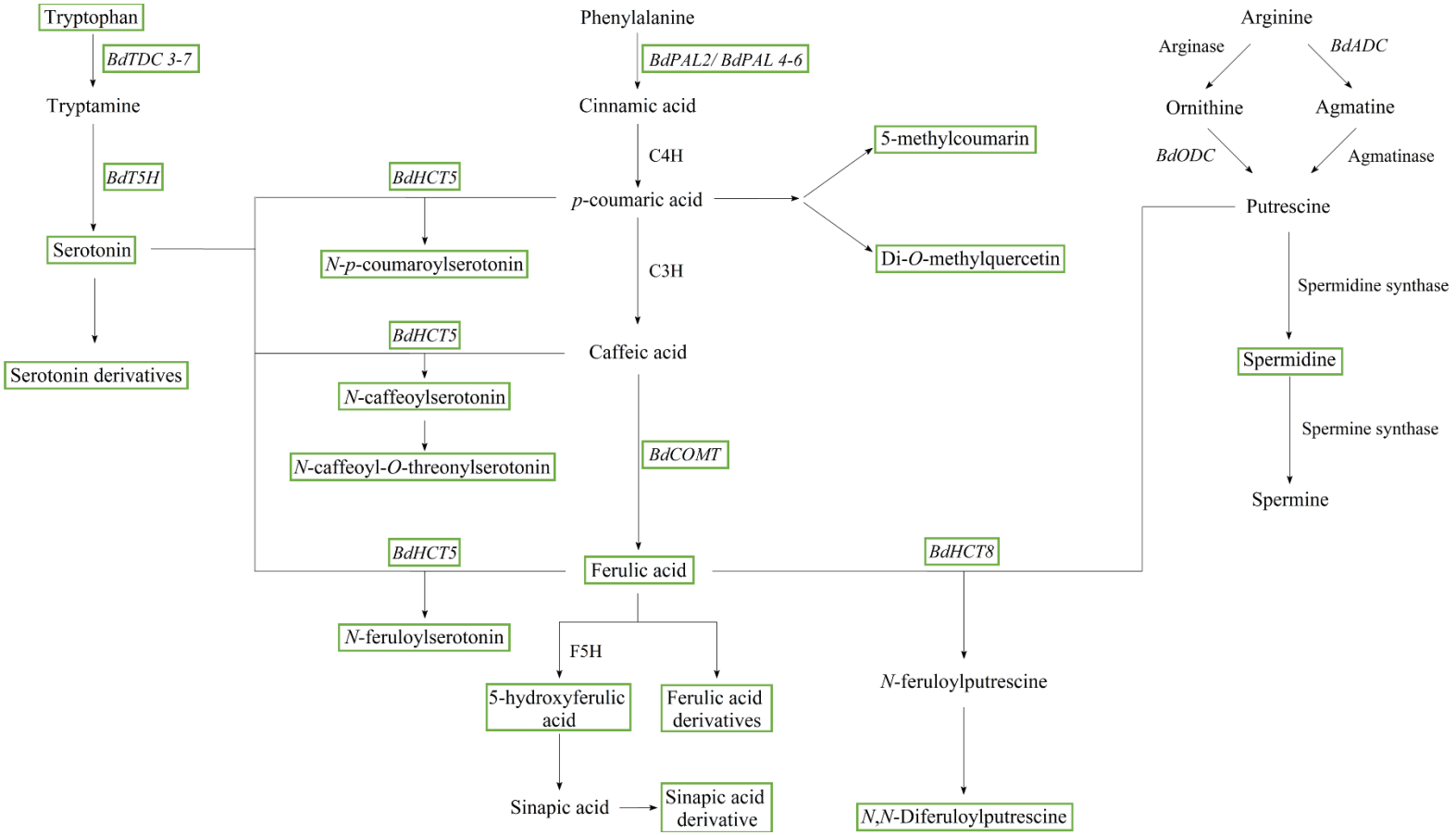

Figure 36: Model of metabolic pathways induced in response to inoculation with *P. nodorum* spores. C3H: *p*-coumarate 3-hydroxylase; C4H: 4-cinnamic acid hydroxylase; COMT: Caffeic acid O methyltransferase; F5H: Ferulate 5-hydroxylase; HCT: Hydroxycinnamoyl transferase; PAL: Phenylalanine ammonia lyase; T5H: Tryptamine 5 hydroxylase; TDC: Tryptophan decarboxylase. Compounds accumulating in higher amounts and enzymes whose gene expression is induced upon inoculation with *P. nodorum* spores are framed in green.

Conclusions

1. Inoculation of Brachypodium leaves with *P. nodorum* lead to a major metabolic reprogramming, reflected by almost 900 MS signals whose intensities significantly differed between samples extracted from inoculated and non-inoculated leaves.

2. Despite the restriction of pathogen growth at very early stages of its development Brachypodium immune response persists as shown by the continuous metabolic reprogramming and HR.

3. DAM identification supported with gene expression analysis revealed that serotonin, phenylpropanoid, and HCAA biosynthetic pathways are activated in Brachypodium leaves upon pathogen inoculation, similarly as in barley, rice, and wheat.

4. Serotonin biosynthetic pathway likely originates from an ancestor common to Poaceae and is more complex than previously thought, as shown by the 11 serotonin-derived compounds we identified in this study.

5. Our bioinformatic analysis revealed that *BdAADC*s and *BdHCT*s gene families include members additional to those that have been so far reported. These novel members include four *BdAADC*s, and 10 *BdHCT*s.

6. Presence of specific conserved amino acid residues allowed us to classify 11 *Bd*AADCs as seven *Bd*TDCs and four *Bd*TDYCs.

7. As indicated by phylogenetic analysis, function in immunity of TDCs, PALs, and HCTs from different grass species can be frequently predicted based on their homology with known defense-related isoforms.

8. Our phylogenetic analyses combined with the reported results of enzymatic assays indicated that substrate preference of HCTs can be predicted from their localization in particular phylogenetic subclades of the generated phylogenetic tree. Particularly, we propose that *Bd*HCT5 and *Bd*HCT8, which are involved in the response to *P. nodorum*, use aromatic and aliphatic amines as substrates, respectively.

9. Metabolic pathways triggered during Brachypodium immune response are relatively conserved among Poeaceae indicating that this species is a good model plant to investigate metabolites that are involved in immunity in other grass species.

10. Further metabolomic and transcriptomic analysis combined with reverse genetics approaches are necessary to decipher pathogen-triggered metabolic reprograming in Brachypodium and to effectively use knowledge obtained in this species to breed crop plants with improved production of defensive metabolites.

Abstract

Brachypodium distachyon has been proposed as a model species of Poaceae, commonly called grasses, which constitute the most agronomically important plant family. Grasses, like all plant species, are constantly attacked by pathogenic microorganisms that cause major worldwide crop losses. In order to defend themselves against pathogens, plants developed a complex immune response that, among other mechanisms, leads to the production of specialized metabolites that contribute to restriction of pathogen growth. In this doctoral project, we aimed to characterize metabolic pathways triggered during the response of Brachypodium to the infection with the necrotrophic fungal pathogen *Parastagonospora nodorum*.

Unbiased Ultra Performance Liquid Chromatography analysis combined with Mass Spectrometry revealed major infection-triggered metabolomic changes in leaves, with 887 signals differing in their intensities between samples obtained from pathogen-inoculated and non-inoculated leaves. Further analyses indicated that serotonin and its 11 derivatives, including four hydroxycinnamic acid amides, accumulated in higher amounts in leaves after pathogen inoculation. In addition, a conjugate of putrescine with ferulic acid, and seven phenylpropanoids were also found to enhance its amount after pathogen recognition. Quantitative reverse transcription polymerase chain reaction analysis showed that genes encoding enzymes involved in the biosynthesis of these compounds had their expression induced in response to pathogen attack. These included *tryptophan decarboxylases* (*TDC*s), *tryptamine 5-hydroxylase*, *phenylalanine ammonia-lyases* (*PAL*s), *caffeic acid O-methyltransferase*, and *hydroxycinnamoyl transferases* (*HCT*s). Phylogenetic analyses of reported grass TDCs, PALs, and HCTs indicated that some closely related enzymes of these families share function in immunity. Taken together, these results suggest the involvement of tryptophan, phenylpropanoid, and polyamine metabolic pathways in immune response in Brachypodium. Since these defense-related metabolic pathways have been reported in other grass species, it supports the choice of Brachypodium to characterize biosynthetic pathways involved in immunity of Poaceae plants. Acquired during this study knowledge can be used to improve defense in grass species of agronomical relevance.

Streszczenie

Brachypodium distachyon stanowi roślinę modelową dla roślin z rodzaju Poaceace, zwanych potocznie trawami, które stanowią jedną z najważniejszych grup roślin uprawnych. Trawy, podobnie jak inne gatunki roślin, są nieustannie atakowane przez mikroorganizmy patogenne, co powoduje znaczne straty plonów. Aby bronić się przed patogenami, rośliny rozwinęły szereg mechanizmów odpornościowych, obejmujących między innymi biosyntezę metabolitów, ograniczających wzrost patogenów. Celem przedłożonej pracy doktorskiej była charakterystyka szlaków metabolicznych indukowanych podczas infekcji Brachypodium przez nekrotroficznego patogena grzybowego *Parastagonospora nodorum*.

Ultrasprawna chromatografia cieczowa w połączeniu z spektometrią mas wykazała istotne zmiany w metabolomie infekowanych liści. Analizy te wykazały obecność 887 sygnałów o zróżnicowanej intensywności pomiędzy próbkami uzyskanymi z liści roślin kontrolnych i inokulowanych patogenem. Dalsze analizy pozwoliły na identyfikację wśród tych sygnałów serotoniny i jej 11 pochodnych, w tym czterech amidów kwasu hydroksycynamonowego. Ponadto w próbach z zainfekowanych liści stwierdzono również zwiększone ilości siedmiu fenylopropanoidów, trzech saponin oraz amidu putrescyny i kwasu ferulowego. Przeprowadzone analizy ilościowe metodą reakcji łańcuchowej polimerazy z odwrotną transkrypcją wykazały zwiększoną ekspresją genów kodujących enzymy biorące udział w biosyntezie tych związków po inokulacji patogenem. Należały do nich dekarboksylazy tryptofanu (TDC), 5-hydroksylaza tryptaminy, amoniakoliazy fenyloalaniny (PAL), *O*-metylotransferaza kwasu kawowego i transferazy hydroksycynamonianowe (HCT). Analizy filogenetyczne uwzgędniahjące dane literaturowe dotyczące izoform TDC, PAL ora HCT z innych gatunków traw wykazały, że funkcja w odporności jest zakonserwowana pomiędzy niektórymi blisko spokrewnionymi enzymami z tych rodzin. Podsumowując, uzyskane wyniki wskazują na udział szlaków metabolicznych tryptofanu, fenyloalaniny i poliamin w odpowiedzi immunologicznej u Brachypodium.

Ze wzgędu na fakt, iż według doniesień literaturowych te same szlaki metaboliczne mogą brać udział w odpowiedzi na infekcję na innych gatunków traw, nasze wyniki uzasadniają wybór Brachypodium jako modelu do badań funkcji wyspecjalizowanych metabolitów w odporności roślin z rodziny Poaceae na infekcję. Wiedza zdobyta podczas realizacji

niniejszej pracy doktorskiej może być w przyszłości wykorzystana do poprawy odporności ważnych roślin uprawnych na patogeny grzybowe.

Bibliography

1. Şerban P, Wilson JRU, Vamosi JC, & Richardson DM (2008) Plant diversity in the human diet: weak phylogenetic signal indicates breadth. *Bioscience* 58(2):151-159.
2. Awika JM (2011) Major cereal grains production and use around the world. *Advances in Cereal Science: Implications to Food Processing and Health Promotion,* ACS Symposium Series, eds Awika JM, Piironen V, & Bean S (American Chemical Society), Vol 1089, pp 1-13.
3. McMichael AJ, Powles JW, Butler CD, & Uauy R (2007) Food, livestock production, energy, climate change, and health. *The Lancet* 370(9594):1253-1263.
4. Muller A, *et al.* (2017) Strategies for feeding the world more sustainably with organic agriculture. *Nat. Commun.* 8(1):1290.
5. Brutnell TP, Bennetzen JL, & Vogel JP (2015) *Brachypodium distachyon* and *Setaria viridis*: model genetic systems for the grasses. *Annu. Rev. Plant Biol.* 66:465-485.
6. Brkljacic J, *et al.* (2011) Brachypodium as a model for the grasses: today and the future. *Plant Physiol.* 157(1):3-13.
7. Catalan P, López-Álvarez D, Díaz-Pérez A, Sancho R, & López-Herránz ML (2016) Phylogeny and evolution of the genus *Brachypodium*. *Genetics and Genomics of Brachypodium*, ed Vogel JP (Springer International Publishing, Cham), pp 9-38.
8. Saarela JM, Burke SV, Wysocki WP, & Barrett MD (2018) A 250 plastome phylogeny of the grass family (Poaceae): topological support under different data partitions. *PeerJ* 6:e4299.
9. Teisher JK, McKain MR, Schaal BA, & Kellogg EA (2017) Polyphyly of Arundinoideae (Poaceae) and evolution of the twisted geniculate lemma awn. *Ann. Bot.* 120(5):725-738.
10. Mason-Gamer RJ, Orme NL, & Anderson CM (2002) Phylogenetic analysis of North American Elymus and the monogenomic Triticeae (Poaceae) using three chloroplast DNA data sets. *Genome* 45(6):991-1002.
11. Arthan W, *et al.* (2017) Phylogenomics of andropogoneae (Panicoideae: Poaceae) of mainland southeast asia. *Syst. Bot.* 42(3):418-431.
12. Vogel JP, *et al.* (2010) Genome sequencing and analysis of the model grass *Brachypodium distachyon*. *Nature* 463(7282):763-768.
13. Phytozome (2017) *Brachypodium distachyon* v3.1 (Purple false brome).

14. Mayer KFX, *et al.* (2012) A physical, genetic and functional sequence assembly of the barley genome. *Nature* 491:711.
15. Appels R, *et al.* (2018) Shifting the limits in wheat research and breeding using a fully annotated reference genome. *Science* 361(6403):eaar7191.
16. Gottlieb A, *et al.* (2013) Insular organization of gene space in grass genomes. *PLOS One* 8(1):e54101.
17. Bragg JN, Anderton A, Nieu R, & Vogel JP (2015) *Brachypodium distachyon*. *Agrobacterium Protocols: Volume 1*, ed Wang K (Springer New York), pp 17-33.
18. Moore D, Robson GD, & Trinci APJ (2011) *21st Century Guidebook to Fungi* (Cambridge University Press, Cambridge).
19. Savary S, Ficke A, Aubertot J-N, & Hollier C (2012) Crop losses due to diseases and their implications for global food production losses and food security. *Food Security* 4(4):519-537.
20. Kaku H, *et al.* (2006) Plant cells recognize chitin fragments for defense signaling through a plasma membrane receptor. *Proc. Natl. Acad. Sci. USA* 103(29):11086-11091.
21. Liebrand TWH, *et al.* (2013) Receptor-like kinase SOBIR1/EVR interacts with receptor-like proteins in plant immunity against fungal infection. *Proc. Natl. Acad. Sci. USA* 110(24):10010-10015.
22. Pitzschke A, Schikora A, & Hirt H (2009) MAPK cascade signalling networks in plant defence. *Curr. Opin. Plant Biol.* 12(4):421-426.
23. Jones JDG & Dangl JL (2006) The plant immune system. *Nature* 444(7117):323-329.
24. Dodds PN & Rathjen JP (2010) Plant immunity: towards an integrated view of plant-pathogen interactions. *Nat. Rev. Genet.* 11(8):539-548.
25. Elmore JM, Lin ZJ, & Coaker G (2011) Plant NB-LRR signaling: upstreams and downstreams. *Curr. Opin. Plant Biol.* 14(4):365-371.
26. Underwood W (2012) The plant cell wall: a dynamic barrier against pathogen invasion. *Front Plant Sci* 3:85.
27. Smith AH, Gill WM, Pinkard EA, & Mohammed CL (2007) Anatomical and histochemical defence responses induced in juvenile leaves of *Eucalyptus globulus* and *Eucalyptus nitens* by *Mycosphaerella* infection. *For. Pathol.* 37(6):361-373.
28. Wojtaszek P (1997) Oxidative burst: an early plant response to pathogen infection. *Biochem. J.* 322 (Pt 3):681-692.

29. Torres MA, Jones JDG, & Dangl JL (2006) Reactive oxygen species signaling in response to pathogens. *Plant Physiol.* 141(2):373.
30. Fitzgerald TL, *et al.* (2015) Brachypodium as an emerging model for cereal-pathogen interactions. *Ann. Bot.* 115(5):717-731.
31. Powell JJ, *et al.* (2017) Transcriptome analysis of Brachypodium during fungal pathogen infection reveals both shared and distinct defense responses with wheat. *Sci. Rep.* 7(1):17212.
32. Parker D, *et al.* (2009) Metabolomic analysis reveals a common pattern of metabolic re-programming during invasion of three host plant species by *Magnaporthe grisea*. *Plant J.* 59(5):723-737.
33. Gill US, Uppalapati SR, Nakashima J, & Mysore KS (2015) Characterization of *Brachypodium distachyon* as a nonhost model against switchgrass rust pathogen *Puccinia emaculata*. *BMC Plant Biol.* 15(1):113.
34. Sandoya GV & Buanafina MMdO (2014) Differential responses of *Brachypodium distachyon* genotypes to insect and fungal pathogens. *Physiol. Mol. Plant Pathol.* 85:53-64.
35. O'Driscoll A, Doohan F, & Mullins E (2015) Exploring the utility of *Brachypodium distachyon* as a model pathosystem for the wheat pathogen *Zymoseptoria tritici*. *BMC Res Notes* 8:132.
36. Hartmann T (2007) From waste products to ecochemicals: fifty years research of plant secondary metabolism. *Phytochemistry* 68(22):2831-2846.
37. De Luca V & St Pierre B (2000) The cell and developmental biology of alkaloid biosynthesis. *Trends Plant Sci.* 5(4):168-173.
38. Weng J-K, Philippe R, & Noel J (2012) The rise of chemodiversity in plants. *Science* 336(6089):1667-1670.
39. Kössel A (1891) Über die chemische zusammensetzung der zelle. *Archiv für Physiologie*:181-186.
40. Ramakrishna A & Ravishankar GA (2011) Influence of abiotic stress signals on secondary metabolites in plants. *Plant Signal Behav* 6(11):1720-1731.
41. Hadacek F, Bachmann G, Engelmeier D, & Chobot V (2011) Hormesis and a chemical raison d'être for secondary plant metabolites. *Dose-Response* 9(1):79-116.
42. Falcone Ferreyra ML, Rius SP, & Casati P (2012) Flavonoids: biosynthesis, biological functions, and biotechnological applications. *Front Plant Sci* 3:222.
43. Yuan Z-L, Dai C-C, & Chen L-q (2007) Regulation and accumulation of secondary metabolites in plant-fungus symbiotic system. *Afr. J. Biotechnol.* 6(11).

44. Gols R (2014) Direct and indirect chemical defences against insects in a multitrophic framework. *Plant, Cell Environ.* 37(8):1741-1752.
45. Li Z-H, Wang Q, Ruan X, Pan C-D, & Jiang D-A (2010) Phenolics and plant allelopathy. *Molecules* 15(12):8933.
46. Piasecka A, Jedrzejczak-Rey N, & Bednarek P (2015) Secondary metabolites in plant innate immunity: conserved function of divergent chemicals. *New Phytol.* 206(3):948-964.
47. McLusky SR, *et al.* (1999) Cell wall alterations and localized accumulation of feruloyl-3′-methoxytyramine in onion epidermis at sites of attempted penetration by *Botrytis allii* are associated with actin polarisation, peroxidase activity and suppression of flavonoid biosynthesis. *Plant J.* 17(5):523-534.
48. Chang X, Heene E, Qiao F, & Nick P (2011) The phytoalexin resveratrol regulates the initiation of hypersensitive cell death in *Vitis* cell. *PLOS One* 6(10):e26405.
49. Bednarek P & Schulze-Lefert P (2009) Role of plant secondary metabolites at the host-pathogen interface. *Molecular Aspects of Plant Disease Resistance*, ed Parker J (Wiley-Blackwell), Vol 34, pp 220-260.
50. VanEtten HD, Mansfield JW, Bailey JA, & Farmer EE (1994) Two classes of plant antibiotics: phytoalexins versus "phytoanticipins". *Plant Cell* 6(9):1191-1192.
51. Hasegawa M, *et al.* (2014) Analysis on blast fungus-responsive characters of a flavonoid phytoalexin sakuranetin; accumulation in infected rice leaves, antifungal activity and detoxification by fungus. *Molecules* 19(8):11404.
52. Li W, *et al.* (2013) *Oscyp71Z2* involves diterpenoid phytoalexin biosynthesis that contributes to bacterial blight resistance in rice. *Plant Sci.* 207:98-107.
53. Atkinson P & Blakeman JP (1982) Seasonal occurrence of an antimicrobial flavanone, sakuranetin, associated with glands on leaves of *Ribes nigrum*. *New Phytol.* 92(1):63-74.
54. Cartwright DW, Langcake P, Pryce RJ, Leworthy DP, & Ride JP (1981) Isolation and characterization of two phytoalexins from rice as momilactones A and B. *Phytochemistry* 20(3):535-537.
55. Kato T, *et al.* (1973) Momilactones, growth inhibitors from rice, *Oryza sativa* L. *Tetrahedron Lett.* 14(39):3861-3864.
56. Tsuji J, Jackson EP, Gage DA, Hammerschmidt R, & Somerville SC (1992) Phytoalexin accumulation in *Arabidopsis thaliana* during the hypersensitive reaction to *Pseudomonas syringae* pv *syringae*. *Plant Physiol.* 98(4):1304.
57. Erland LA, Turi CE, & Saxena PK (2016) Serotonin: an ancient molecule and an important regulator of plant processes. *Biotechnol. Adv.* 34(8):1347-1361.

58. Ishihara A, *et al.* (2008) The tryptophan pathway is involved in the defense responses of rice against pathogenic infection via serotonin production. *Plant J.* 54(3):481-495.
59. Ishihara A, *et al.* (2017) Induced accumulation of tyramine, serotonin, and related amines in response to *Bipolaris sorokiniana* infection in barley. *Biosci., Biotechnol., Biochem.* 81(6):1090-1098.
60. Du Fall LA & Solomon PS (2013) The necrotrophic effector SnToxA induces the synthesis of a novel phytoalexin in wheat. *New Phytol.* 200(1):185-200.
61. Pasquet JC, *et al.* (2014) Differential gene expression and metabolomic analyses of *Brachypodium distachyon* infected by deoxynivalenol producing and non-producing strains of *Fusarium graminearum*. *BMC Genomics* 15:629.
62. Blattner FR (2004) Phylogenetic analysis of *Hordeum* (Poaceae) as inferred by nuclear rDNA ITS sequences. *Mol. Phylogen. Evol.* 33(2):289-299.
63. Blattner FR (2009) Progress in phylogenetic analysis and a new infrageneric classification of the barley genus *Hordeum* (Poaceae: Triticeae). *Breed. Sci.* 59(5):471-480.
64. Torrens-Spence MP, *et al.* (2018) Structural basis for independent origins of new catalytic machineries in plant AAAD proteins. *bioRxiv*:404970.
65. Kanjanaphachoat P, *et al.* (2012) Serotonin accumulation in transgenic rice by over-expressing tryptophan decarboxylase results in a dark brown phenotype and stunted growth. *Plant Mol. Biol.* 78(6):525-543.
66. Kang S, Kang K, Lee K, & Back K (2007) Characterization of rice tryptophan decarboxylases and their direct involvement in serotonin biosynthesis in transgenic rice. *Planta* 227(1):263-272.
67. Noda S, *et al.* (2015) Evaluation of *Brachypodium distachyon* L-tyrosine decarboxylase using L-tyrosine over-producing *Saccharomyces cerevisiae*. *PLOS One* 10(5):e0125488.
68. Abu-Zaitoon YM (2014) Phylogenetic analysis of putative genes involved in the tryptophan-dependent pathway of auxin biosynthesis in rice. *Appl. Biochem. Biotechnol.* 172(5):2480-2495.
69. Mizutani M & Sato F (2011) Unusual P450 reactions in plant secondary metabolism. *Arch Biochem Biophys* 507(1):194-203.
70. Ueno M, Kihara J, Honda Y, Isota J, & Arase S (2004) DNA fragmentation in Sekiguchi lesion mutants of rice infected with *Magnaporthe grisea*. *J. Gen. Plant Pathol.* 70(6):321-328.

71. Fujiwara T, *et al.* (2010) Sekiguchi lesion gene encodes a cytochrome p450 monooxygenase that catalyzes conversion of tryptamine to serotonin in rice. *J. Biol. Chem.* 285(15):11308-11313.
72. Ueno M, Shibata H, Kihara J, Honda Y, & Arase S (2003) Increased tryptophan decarboxylase and monoamine oxidase activities induce Sekiguchi lesion formation in rice infected with *Magnaporthe grisea*. *Plant J.* 36(2):215-228.
73. Park S, Lee K, Kim YS, & Back K (2012) Tryptamine 5-hydroxylase-deficient Sekiguchi rice induces synthesis of 5-hydroxytryptophan and *N*-acetyltryptamine but decreases melatonin biosynthesis during senescence process of detached leaves. *J. Pineal Res.* 52(2):211-216.
74. Park M, Kang K, Park S, & Back K (2008) Conversion of 5-hydroxytryptophan into serotonin by tryptophan decarboxylase in plants, *Escherichia coli*, and yeast. *Biosci., Biotechnol., Biochem.* 72(9):2456-2458.
75. Park S, Byeon Y, & Back K (2013) Transcriptional suppression of tryptamine 5-hydroxylase, a terminal serotonin biosynthetic gene, induces melatonin biosynthesis in rice (*Oryza sativa* L.). *J. Pineal Res.* 55(2):131-137.
76. Ube N, *et al.* (2017) Evolutionary changes in defensive specialized metabolism in the genus *Hordeum*. *Phytochemistry* 141:1-10.
77. Kokubo Y, *et al.* (2017) Distribution of the tryptophan pathway-derived defensive secondary metabolites gramine and benzoxazinones in Poaceae. *Biosci., Biotechnol., Biochem.* 81(3):431-440.
78. Matsuo H, *et al.* (2001) Gramine increase associated with rapid and transient systemic resistance in barley seedlings induced by mechanical and biological stresses. *Plant and Cell Physiology* 42(10):1103-1111.
79. Leland TJ & Hanson AD (1985) Induction of a specific *N*-methyltransferase enzyme by long-term heat stress during barley leaf growth. *Plant Physiol.* 79(2):451.
80. Larsson KAE, Zetterlund I, Delp G, & Jonsson LMV (2006) *N*-Methyltransferase involved in gramine biosynthesis in barley: cloning and characterization. *Phytochemistry* 67(18):2002-2008.
81. Meyer J, Murray SL, & Berger DK (2016) Signals that stop the rot: regulation of secondary metabolite defences in cereals. *Physiol. Mol. Plant Pathol.* 94(Supplement C):156-166.
82. Niemeyer HM (2009) Hydroxamic acids derived from 2-hydroxy-2H-1,4-benzoxazin-3(4H)-one: key defense chemicals of cereals. *J. Agric. Food Chem.* 57(5):1677-1696.

83. Niemeyer HM (1988) Hydroxamic acids (4-hydroxy-1,4-benzoxazin-3-ones), defence chemicals in the gramineae. *Phytochemistry* 27(11):3349-3358.
84. Grün S, Frey M, & Gierl A (2005) Evolution of the indole alkaloid biosynthesis in the genus *Hordeum*: distribution of gramine and DIBOA and isolation of the benzoxazinoid biosynthesis genes from *Hordeum lechleri*. *Phytochemistry* 66(11):1264-1272.
85. Oikawa A, *et al.* (2004) Accumulation of HDMBOA-Glc is induced by biotic stresses prior to the release of MBOA in maize leaves. *Phytochemistry* 65(22):2995-3001.
86. Bücker C & Grambow HJ (1990) Alterations in 1,4-benzoxazinone levels following inoculation with stem rust in white leaves carrying various alleles for resistance and their possible role as phytoalexins in moderately resistant leaves. *Zeitschrift für Naturforschung. Section C, Biosciences* 45(11-12):1151-1155.
87. Oikawa A, Ishihara A, & Iwamura H (2002) Induction of HDMBOA-Glc accumulation and DIMBOA-Glc 4-O-methyltransferase by jasmonic acid in poaceous plants. *Phytochemistry* 61(3):331-337.
88. Frey M, *et al.* (1997) Analysis of a chemical plant defense mechanism in grasses. *Science* 277(5326):696-699.
89. Kriechbaumer V, *et al.* (2008) Characterisation of the tryptophan synthase alpha subunit in maize. *BMC Plant Biol.* 8:44-44.
90. Hamilton RH (1964) A corn mutant deficient in 2,4-dihydroxy-7-methoxy-1,4-benzoxazin-3-one with an altered tolerance of atrazine. *Weeds* 12(1):27-30.
91. Nomura T, *et al.* (2002) Molecular characterization and chromosomal localization of cytochrome P450 genes involved in the biosynthesis of cyclic hydroxamic acids in hexaploid wheat. *Mol. Genet. Genomics* 267(2):210-217.
92. Dutartre L, Hilliou F, & Feyereisen R (2012) Phylogenomics of the benzoxazinoid biosynthetic pathway of Poaceae: gene duplications and origin of the Bx cluster. *BMC Evol. Biol.* 12:64-64.
93. Von Rad U, Hüttl R, Lottspeich F, Gierl A, & Frey M (2002) Two glucosyltransferases are involved in detoxification of benzoxazinoids in maize. *Plant J.* 28(6):633-642.
94. Sue M, Nakamura C, & Nomura T (2011) Dispersed benzoxazinone gene cluster: molecular characterization and chromosomal localization of glucosyltransferase and glucosidase genes in wheat and rye. *Plant Physiol.* 157(3):985-997.

95. Jonczyk R, *et al.* (2008) Elucidation of the final reactions of DIMBOA-glucoside biosynthesis in maize: characterization of *Bx6* and *Bx7*. *Plant Physiol.* 146(3):1053.
96. Meihls LN, *et al.* (2013) Natural variation in maize aphid resistance is associated with 2,4-dihydroxy-7-methoxy-1,4-benzoxazin-3-one glucoside methyltransferase activity. *Plant Cell* 25(6):2341-2355.
97. Frey M, Schullehner K, Dick R, Fiesselmann A, & Gierl A (2009) Benzoxazinoid biosynthesis, a model for evolution of secondary metabolic pathways in plants. *Phytochemistry* 70(15):1645-1651.
98. Nomura T, *et al.* (2003) Rearrangement of the genes for the biosynthesis of benzoxazinones in the evolution of Triticeae species. *Planta* 217(5):776-782.
99. Cicek M & Esen A (2000) Expression of soluble and catalytically active plant (monocot) *β*-glucosidases in *E. coli*. *Biotechnol. Bioeng.* 63(4):392-400.
100. Sue M, Ishihara A, & Iwamura H (2000) Purification and characterization of a hydroxamic acid glucoside *β*-glucosidase from wheat (*Triticum aestivum* L.) seedlings. *Planta* 210(3):432-438.
101. Nikus J, Esen A, & Jonsson Lisbeth MV (2003) Cloning of a plastidic rye (*Secale cereale*) *β*-glucosidase cDNA and its expression in *Escherichia coli*. *Physiol. Plant.* 118(3):337-345.
102. Wilkes MA, Marshall DR, & Copeland L (1999) Hydroxamic acids in cereal roots inhibit the growth of take-all. *Soil Biol. Biochem.* 31(13):1831-1836.
103. Couture RM, Routley DG, & Dunn GM (1971) Role of cyclic hydroxamic acids in monogenic resistance of maize to *Helminthosporium-turcicum*. *Physiological Plant Pathology* 1(4):515-521.
104. Whitney NJ & Mortimore CG (1959) Isolation of the antifungal substance, 6-methoxybenzoxazolinone, from field corn (*Zea mays* L) in canada. *Nature* 184(4695):1320-1320.
105. Cambier V, Hance T, & de Hoffmann E (1999) Non-injured maize contains several 1,4-benzoxazin-3-one related compounds but only as glucoconjugates. *Phytochem. Anal.* 10(3):119-126.
106. Dixon RA & Paiva NL (1995) Stress-induced phenylpropanoid metabolism. *Plant Cell* 7(7):1085-1097.
107. Zhang X & Liu C-J (2015) Multifaceted regulations of gateway enzyme phenylalanine ammonia-lyase in the biosynthesis of phenylpropanoids. *Mol Plant.* 8(1):17-27.

108. Barros J, *et al.* (2016) Role of bifunctional ammonia-lyase in grass cell wall biosynthesis. *Nat. Plants.* 2:16050.
109. Rosler J, Krekel F, Amrhein N, & Schmid J (1997) Maize phenylalanine ammonia-lyase has tyrosine ammonia-lyase activity. *Plant Physiol.* 113(1):175.
110. Watts KT, Mijts BN, Lee PC, Manning AJ, & Schmidt-Dannert C (2006) Discovery of a substrate selectivity switch in tyrosine ammonia-lyase, a member of the aromatic amino acid lyase family. *Chemical Biology* 13(12):1317-1326.
111. Shakoor N, *et al.* (2014) A *Sorghum bicolor* expression atlas reveals dynamic genotype-specific expression profiles for vegetative tissues of grain, sweet and bioenergy sorghums. *BMC Plant Biol.* 14:35.
112. Sahu R, *et al.* (2016) Elucidation of defense-related signaling responses to spot blotch infection in bread wheat (*Triticum aestivum* L.). *Plant J.* 86(1):35-49.
113. Hsieh L-S, Ma G-J, Yang C-C, & Lee P-D (2010) Cloning, expression, site-directed mutagenesis and immunolocalization of phenylalanine ammonia-lyase in *Bambusa oldhamii*. *Phytochemistry* 71(17):1999-2009.
114. Kervinen T, *et al.* (1997) Cloning and characterization of cDNA clones encoding phenylalanine ammonia-lyase in barley. *Plant Sci.* 123(1):143-150.
115. Minami E, Ozeki Y, Matsuoka M, Koizuka N, & Tanaka Y (1989) Structure and some characterization of the gene for phenylalanine ammonia-lyase from rice plants. *Eur. J. Biochem.* 185(1):19-25.
116. Starr JL, Yang W, Yan Y, Crutcher F, & Kolomiets M (2014) Expression of phenylalanine ammonia lyase genes in maize lines differing in susceptibility to *Meloidogyne incognita*. *J. Nematol.* 46(4):360-364.
117. Routledge AP, *et al.* (2004) *Magnaporthe grisea* interactions with the model grass *Brachypodium distachyon* closely resemble those with rice (*Oryza sativa*). *Mol. Plant Pathol.* 5(4):253-265.
118. Cass CL, *et al.* (2015) Effects of *PHENYLALANINE AMMONIA LYASE* (*PAL*) knockdown on cell wall composition, biomass digestibility, and biotic and abiotic stress responses in *Brachypodium*. *J. Exp. Bot.* 66(14):4317-4335.
119. Tonnessen BW, *et al.* (2015) Rice phenylalanine ammonia-lyase gene *OsPAL4* is associated with broad spectrum disease resistance. *Plant Mol. Biol.* 87(3):273-286.
120. Tanaka E, Tanaka C, Mori N, Kuwahara Y, & Tsuda M (2003) Phenylpropanoid amides of serotonin accumulate in witches' broom diseased bamboo. *Phytochemistry* 64(5):965-969.

121. Morimoto N, *et al.* (2018) Induced phenylamide accumulation in response to pathogen infection and hormone treatment in rice (*Oryza sativa*). *Biosci., Biotechnol., Biochem.* 82(3):407-416.
122. Balmer D, de Papajewski DV, Planchamp C, Glauser G, & Mauch-Mani B (2013) Induced resistance in maize is based on organ-specific defence responses. *Plant J.* 74(2):213-225.
123. Stoessl A (1966) The antifungal factors in barley - the constitutions of hordatines A and B. *Tetrahedron Lett.* 7(21):2287-2292.
124. von Röpenack E, Parr A, & Schulze-Lefert P (1998) Structural analyses and dynamics of soluble and cell wall-bound phenolics in a broad spectrum resistance to the powdery mildew fungus in barley. *J. Biol. Chem.* 273(15):9013-9022.
125. Okazaki Y, Ishizuka A, Ishihara A, Nishioka T, & Iwamura H (2007) New dimeric compounds of avenanthramide phytoalexin in oats. *The Journal of organic chemistry* 72(10):3830-3839.
126. Wise ML, Sreenath HK, Skadsen RW, & Kaeppler HF (2009) Biosynthesis of avenanthramides in suspension cultures of oat (*Avena sativa*). *Plant Cell Tiss. Org. Cult.* 97(1):81-90.
127. Okazaki Y, Ishihara A, Nishioka T, & Iwamura H (2004) Identification of a dehydrodimer of avenanthramide phytoalexin in oats. *Tetrahedron* 60(22):4765-4771.
128. Miyagawa H, Ishihara A, Nishimoto T, Ueno T, & Mayama S (1995) Induction of avenanthramides in oat leaves inoculated with crown rust fungus, *Puccinia coronata* f. sp. *avenae*. *Biosci., Biotechnol., Biochem.* 59(12):2305-2306.
129. Petersen M (2016) Hydroxycinnamoyltransferases in plant metabolism. *Phytochem. Rev.* 15(5):699-727.
130. Unno H, *et al.* (2007) Structural and mutational studies of anthocyanin malonyltransferases establish the features of BAHD enzyme catalysis. *J. Biol. Chem.* 282(21):15812-15822.
131. D'Auria JC (2006) Acyltransferases in plants: a good time to be BAHD. *Curr. Opin. Plant Biol.* 9(3):331-340.
132. Dong X, *et al.* (2015) Spatiotemporal distribution of phenolamides and the genetics of natural variation of hydroxycinnamoyl spermidine in rice. *Mol Plant.* 8(1):111-121.
133. Peng M, *et al.* (2016) Evolutionarily distinct BAHD *N*-acyltransferases are responsible for natural variation of aromatic amine conjugates in rice. *Plant Cell* 28(7):1533-1550.

134. Tanabe K, Hojo Y, Shinya T, & Galis I (2016) Molecular evidence for biochemical diversification of phenolamide biosynthesis in rice plants. *J Integr Plant Biol* 58(11):903-913.
135. Wen W, *et al.* (2014) Metabolome-based genome-wide association study of maize kernel leads to novel biochemical insights. *Nat. Commun.* 5:3438.
136. Carere J, Powell J, Fitzgerald T, Kazan K, & Gardiner DM (2018) *BdACT2a* encodes an agmatine coumaroyl transferase required for pathogen defence in *Brachypodium distachyon*. *Physiol. Mol. Plant Pathol.* 104:69-76.
137. Cowley T & Walters DR (2002) Polyamine metabolism in barley reacting hypersensitively to the powdery mildew fungus *Blumeria graminis* f. sp *hordei*. *Plant Cell Environ.* 25(3):461-468.
138. Burhenne K, Kristensen BK, & Rasmussen SK (2003) A new class of *N*-hydroxycinnamoyltransferases: purification, cloning, and expression of a barley agmatine coumaroyltransferase (EC 2.3.1.64). *J. Biol. Chem.* 278(16):13919-13927.
139. Yang Q, *et al.* (2004) Analysis of the involvement of hydroxyanthranilate hydroxycinnamoyltransferase and caffeoyl-CoA 3-*O*-methyltransferase in phytoalexin biosynthesis in oat. *Mol. Plant-Microbe Interact.* 17(1):81-89.
140. Figueiró AdA, *et al.* (2017) RNAseq analysis reveals the role of secondary metabolism in the response of URS 21, a race-nonspecific resistant cultivar, to crown rust. *Plant Pathol.* 66(5):702-712.
141. Graça J (2010) Hydroxycinnamates in suberin formation. *Phytochem. Rev.* 9(1):85-91.
142. Clarke DD (1982) The accumulation of cinnamic acid amides in the cell walls of potato tissue as an early response to fungal attack. *Active Defense Mechanism in Plants*, ed Wood RKS (Plenum Press), pp 321-322.
143. Macoy DM, Kim W-Y, Lee SY, & Kim MG (2015) Biotic stress related functions of hydroxycinnamic acid amide in plants. *J. Plant Biol.* 58(3):156-163.
144. Park HL, *et al.* (2014) Antimicrobial activity of UV-induced phenylamides from rice leaves. *Molecules* 19(11):18139-18151.
145. Stoessl A & Unwin CH (1970) The antifungal factors in barley. V. Antifungal activity of the hordatines. *Can J Bot* 48(3):465-470.
146. Mathesius U (2018) Flavonoid functions in plants and their interactions with other organisms. *Plants (Basel)* 7(2):30.

147. Lo S-CC, De Verdier K, & Nicholson RL (1999) Accumulation of 3-deoxyanthocyanidin phytoalexins and resistance to *Colletotrichum sublineolum* in sorghum. *Physiol. Mol. Plant Pathol.* 55(5):263-273.
148. Wharton PS & Nicholson RL (2000) Temporal synthesis and radiolabelling of the sorghum 3-deoxyanthocyanidin phytoalexins and the anthocyanin, cyanidin 3-dimalonyl glucoside. *New Phytol.* 145(3):457-469.
149. Ganesh Kumar V, Viswanathan R, Malathi P, Nandakumar M, & Ramesh Sundar A (2015) Differential induction of 3-deoxyanthocyanidin phytoalexins in relation to *Colletotrichum falcatum* resistance in sugarcane. *Sugar Tech* 17(3):314-321.
150. Lue WL, Kuhn D, & Nicholson RL (1989) Chalcone synthase activity in sorghum mesocotyls inoculated with *Colletotrichum graminicola*. *Physiol. Mol. Plant Pathol.* 35(5):413-422.
151. Christensen AB, Gregersen PL, Schröder J, & Collinge DB (1998) A chalcone synthase with an unusual substrate preference is expressed in barley leaves in response to UV light and pathogen attack. *Plant Mol. Biol.* 37(5):849-857.
152. Kodama O, Miyakawa J, Akatsuka T, & Kiyosawa S (1992) Sakuranetin, a flavanone phytoalexin from ultraviolet-irradiated rice leaves. *Phytochemistry* 31(11):3807-3809.
153. Zhang L, *et al.* (2008) Three flavonoids targeting the *β*-hydroxyacyl-acyl carrier protein dehydratase from *Helicobacter pylori*: crystal structure characterization with enzymatic inhibition assay. *Protein Sci.* 17(11):1971-1978.
154. Lo SC, *et al.* (1996) Phytoalexin accumulation in sorghum: identification of a methyl ether of luteolinidin. *Physiol. Mol. Plant Pathol.* 49(1):21-31.
155. Nicholson RL, Kollipara SS, Vincent JR, Lyons PC, & Cadena-Gomez G (1987) Phytoalexin synthesis by the sorghum mesocotyl in response to infection by pathogenic and nonpathogenic fungi. *Proc. Natl. Acad. Sci. USA* 84(16):5520-5524.
156. Aida Y, Tamogami S, Kodama O, & Tsukiboshi T (1996) Synthesis of 7-methoxyapigeninidin and its fungicidal activity against *Gloeocercospora sorghi*. *Biosci., Biotechnol., Biochem.* 60(9):1495-1496.
157. Nielsen KA, *et al.* (2004) Inclusions of flavonoid 3-deoxyanthocyanidins in *Sorghum bicolor* self-organize into spherical structures. *Physiol. Mol. Plant Pathol.* 65(4):187-196.
158. Shen T, Wang X-N, & Lou H-X (2009) Natural stilbenes: an overview. *Nat. Prod. Rep.* 26(7):916-935.

159. Niesen D, Hessler C, & Seeram N (2013) Beyond resveratrol: a review of natural stilbenoids identified from 2009-2013. *J Berry Res* 3(4):181-196.
160. Powell RG, TePaske MR, Plattner RD, White JF, & Clement SL (1994) Isolation of resveratrol from *Festuca versuta* and evidence for the widespread occurrence of this stilbene in the Poaceae. *Phytochemistry* 35(2):335-338.
161. Yu CK, Shih CH, Chu IK, & Lo C (2008) Accumulation of *trans*-piceid in sorghum seedlings infected with *Colletotrichum sublineolum*. *Phytochemistry* 69(3):700-706.
162. Yu CKY, *et al.* (2005) A stilbene synthase gene (*SbSTS1*) is involved in host and nonhost defense responses in sorghum. *Plant Physiol.* 138(1):393-401.
163. Adrian M, Jeandet P, Veneau J, Weston LA, & Bessis R (1997) Biological activity of resveratrol, a stilbenic compound from grapevines, against *Botrytis cinerea*, the causal agent for gray mold. *J. Chem. Ecol.* 23(7):1689-1702.
164. Liu Z, *et al.* (2011) Overexpression of a resveratrol synthase gene (*PcRS*) from *Polygonum cuspidatum* in transgenic Arabidopsis causes the accumulation of *trans*-piceid with antifungal activity. *Plant Cell Rep.* 30(11):2027-2036.
165. Walters DR (2003) Polyamines and plant disease. *Phytochemistry* 64(1):97-107.
166. Bouchereau A, Aziz A, Larher F, & Martin-Tanguy J (1999) Polyamines and environmental challenges: recent development. *Plant Sci.* 140(2):103-125.
167. Walters D R, Wilson P. W F, & Shuttleton M A (1985) Relative changes in levels of polyamines and activities of their biosynthetic enzymes in barley infected with the powdery mildew fungus, *Erysiphe graminis* D.C. ex Merat f.sp. *hordei* Marchal. *New Phytol.* 101(4):695-705.
168. Greenland A J & Lewis D H (2006) Amines in barley laves infected by brown rust and their possible relevance to formation of 'green islands'. *New Phytol.* 96(2):283-291.
169. Gardiner DM, *et al.* (2010) Early activation of wheat polyamine biosynthesis during Fusarium head blight implicates putrescine as an inducer of trichothecene mycotoxin production. *BMC Plant Biol.* 10:289.
170. Gevrekci AÖ (2017) The roles of polyamines in microorganisms. *World J. Microbiol. Biotechnol.* 33(11):204.
171. Gleadow RM & Moller BL (2014) Cyanogenic glycosides: synthesis, physiology, and phenotypic plasticity. *Annu. Rev. Plant Biol.* 65(1):155-185.
172. Kojima M, Poulton JE, Thayer SS, & Conn EE (1979) Tissue distributions of dhurrin and of enzymes involved in its metabolism in leaves of *Sorghum bicolor*. *Plant Physiol.* 63(6):1022-1028.

173. Nielsen KA, Olsen CE, Pontoppidan K, & Moller BL (2002) Leucine-derived cyano glucosides in barley. *Plant Physiol.* 129(3):1066-1075.
174. Takos AM, *et al.* (2011) Genomic clustering of cyanogenic glucoside biosynthetic genes aids their identification in *Lotus japonicus* and suggests the repeated evolution of this chemical defence pathway. *Plant J.* 68(2):273-286.
175. Leavesley HB, Li L, Prabhakaran K, Borowitz JL, & Isom GE (2008) Interaction of cyanide and nitric oxide with cytochrome c oxidase: implications for acute cyanide toxicity. *Toxicol. Sci.* 101(1):101-111.
176. McCaskill D & Croteau R (1997) Prospects for the bioengineering of isoprenoid biosynthesis. *Biotechnology of Aroma Compounds*, Advances in Biochemical Engineering/Biotechnology, eds Berger RG, Babel W, Blanch HW, Cooney CL, Enfors S-O, Eriksson K-EL, Fiechter A, Klibanov AM, Mattiasson B, Primrose SB, *et al.* (Springer), Vol 55, pp 107-146.
177. Tholl D (2015) Biosynthesis and biological functions of terpenoids in plants. *Biotechnology of Isoprenoids*, Advances in Biochemical Engineering/Biotechnology, eds Schrader J & Bohlmann J (Springer), Vol 148, pp 63-106.
178. Yamane H (2013) Biosynthesis of phytoalexins and regulatory mechanisms of it in rice. *Biosci., Biotechnol., Biochem.* 77(6):1141-1148.
179. Koga J, *et al.* (1995) Phytocassanes A, B, C and D, novel diterpene phytoalexins from rice, *Oryza sativa* L. *Tetrahedron* 51(29):7907-7918.
180. Koga J, *et al.* (1997) Functional moiety for the antifungal activity of phytocassane E, a diterpene phytoalexin from rice. *Phytochemistry* 44(2):249-253.
181. Umemura K, *et al.* (2003) Possible role of phytocassane, rice phytoalexin, in disease resistance of rice against the blast fungus *Magnaporthe grisea*. *Biosci., Biotechnol., Biochem.* 67(4):899-902.
182. Akatsuka T, Kodama O, Sekido H, Kono Y, & Takeuchi S (1985) Novel phytoalexins (oryzalexins A, B and C) isolated from rice blast leaves infected with *Pricularia oryzae*. *Agric. Biol. Chem.* 49(6):1689-1701.
183. Schmelz EA, *et al.* (2011) Identity, regulation, and activity of inducible diterpenoid phytoalexins in maize. *Proc. Natl. Acad. Sci. USA* 108(13):5455-5460.
184. Huffaker A, *et al.* (2011) Novel acidic sesquiterpenoids constitute a dominant class of pathogen-induced phytoalexins in maize. *Plant Physiol.* 156(4):2082-2097.

185. Mafu S, *et al.* (2018) Discovery, biosynthesis and stress-related accumulation of dolabradiene-derived defenses in maize. *Plant Physiol.* 176(4):2677-2690.
186. Harris LJ, *et al.* (2005) The maize *An2* gene is induced by *Fusarium* attack and encodes an *ent*-copalyl diphosphate synthase. *Plant Mol. Biol.* 59(6):881-894.
187. Shimura K, *et al.* (2007) Identification of a biosynthetic gene cluster in rice for momilactones. *J. Biol. Chem.* 282(47):34013-34018.
188. Swaminathan S, Morrone D, Wang Q, Fulton DB, & Peters RJ (2009) CYP76M7 is an *ent*-cassadiene C11α-hydroxylase defining a second multifunctional diterpenoid biosynthetic gene cluster in rice. *Plant Cell* 21(10):3315-3325.
189. Spielmeyer W, *et al.* (2004) Isolation of gibberellin metabolic pathway genes from barley and comparative mapping in barley, wheat and rice. *Theor. Appl. Genet.* 109(4):847-855.
190. Toyomasu T, *et al.* (2009) Cloning and characterization of cDNAs encoding *ent*-copalyl diphosphate synthases in wheat: insight into the evolution of rice phytoalexin biosynthetic genes. *Biosci., Biotechnol., Biochem.* 73(3):772-775.
191. Christensen SA, *et al.* (2018) Fungal and herbivore elicitation of the novel maize sesquiterpenoid, zealexin A4, is attenuated by elevated CO2. *Planta* 247(4):863-873.
192. Osbourn AE (1996) Preformed antimicrobial compounds and plant defense against fungal attack. *Plant Cell* 8(10):1821-1831.
193. Papadopoulou K, Melton RE, Leggett M, Daniels MJ, & Osbourn AE (1999) Compromised disease resistance in saponin-deficient plants. *Proc. Natl. Acad. Sci. USA* 96(22):12923-12928.
194. Nisius A (1988) The stromacentre in *Avena* plastids: an aggregation of *β*-glucosidase responsible for the activation of oat-leaf saponins. *Planta* 173(4):474-481.
195. Pecio Ł, *et al.* (2012) Revised structures of avenacosides A and B and a new sulfated saponin from *Avena sativa* L. *Magn Reson Chem.* 50(11):755-758.
196. Qi X, *et al.* (2004) A gene cluster for secondary metabolism in oat: implications for the evolution of metabolic diversity in plants. *Proc. Natl. Acad. Sci. USA* 101(21):8233-8238.
197. Crombie WML, Crombie L, Green JB, & Lucas JA (1986) Pathogenicity of 'take-all' fungus to oats: its relationship to the concentration and detoxification of the four avenacins. *Phytochemistry* 25(9):2075-2083.

198. Inagaki Y-S, *et al.* (2013) Infection-inhibition activity of avenacin saponins against the fungal pathogens *Blumeria graminis* f. sp. *hordei*, *Bipolaris oryzae*, and *Magnaporthe oryzae*. *J. Gen. Plant Pathol.* 79(1):69-73.
199. Armah CN, *et al.* (1999) The membrane-permeabilizing effect of avenacin A-1 involves the reorganization of bilayer cholesterol. *Biophys. J.* 76(1):281-290.
200. Gus-Mayer S, Brunner H, Schneider-Poetsch HAW, & Rüdiger W (1994) Avenacosidase from oat: purification, sequence analysis and biochemical characterization of a new member of the BGA family of *β*-glucosidases. *Plant Mol. Biol.* 26(3):909-921.
201. Duan L, Liu H, Li X, Xiao J, & Wang S (2014) Multiple phytohormones and phytoalexins are involved in disease resistance to *Magnaporthe oryzae* invaded from roots in rice. *Physiol. Plant.* 152(3):486-500.
202. Ibraheem F, Gaffoor I, & Chopra S (2010) Flavonoid phytoalexin-dependent resistance to anthracnose leaf blight requires a functional *yellow seed1* in *Sorghum bicolor*. *Genetics* 184(4):915-926.
203. Haralampidis K, *et al.* (2001) A new class of oxidosqualene cyclases directs synthesis of antimicrobial phytoprotectants in monocots. *Proc. Natl. Acad. Sci. USA* 98(23):13431-13436.
204. van der Linde K, Kastner C, Kumlehn J, Kahmann R, & Doehlemann G (2011) Systemic virus-induced gene silencing allows functional characterization of maize genes during biotrophic interaction with *Ustilago maydis*. *New Phytol.* 189(2):471-483.
205. Christensen SA, *et al.* (2018) Commercial hybrids and mutant genotypes reveal complex protective roles for inducible terpenoid defenses in maize. *J. Exp. Bot.* 69(7):1693-1705.
206. Toyomasu T, *et al.* (2014) Reverse-genetic approach to verify physiological roles of rice phytoalexins: characterization of a knockdown mutant of *OsCPS4* phytoalexin biosynthetic gene in rice. *Physiol. Plant.* 150(1):55-62.
207. Nielsen KA, *et al.* (2006) Reconstitution of cyanogenesis in barley (*Hordeum vulgare* L.) and its implications for resistance against the barley powdery mildew fungus. *Planta* 223(5):1010-1023.
208. Ishihara A, *et al.* (2011) Probing the role of tryptophan-derived secondary metabolism in defense responses against *Bipolaris oryzae* infection in rice leaves by a suicide substrate of tryptophan decarboxylase. *Phytochemistry* 72(1):7-13.

209. Hayashi K, *et al.* (2016) Serotonin attenuates biotic stress and leads to lesion browning caused by a hypersensitive response to *Magnaporthe oryzae* penetration in rice. *Plant J.* 85(1):46-56.
210. Ahmad S, *et al.* (2011) Benzoxazinoid metabolites regulate innate immunity against aphids and fungi in maize. *Plant Physiol.* 157(1):317-327.
211. Garvin DF, *et al.* (2008) Development of genetic and genomic research resources for *Brachypodium distachyon*, a new model system for grass crop research. *Crop Sci.* 48(Supplement_1):S-69-S-84.
212. Hane JK, *et al.* (2007) Dothideomycete–plant interactions illuminated by genome sequencing and EST analysis of the wheat pathogen *Stagonospora nodorum*. *Plant Cell* 19(11):3347-3368.
213. Friesen TL, *et al.* (2009) Host-selective toxins produced by *Stagonospora nodorum* confer disease susceptibility in adult wheat plants under field conditions. *Theor. Appl. Genet.* 118(8):1489-1497.
214. Lin Y & Yan Y (2012) Biosynthesis of caffeic acid in *Escherichia coli* using its endogenous hydroxylase complex. *Microb. Cell Fact.* 11(1):42.
215. Pluskal T, Castillo S, Villar-Briones A, & Orešič M (2010) MZmine 2: modular framework for processing, visualizing, and analyzing mass spectrometry-based molecular profile data. *BMC Bioinform.* 11(1):395.
216. Tautenhahn R, Böttcher C, & Neumann S (2008) Highly sensitive feature detection for high resolution LC/MS. *BMC Bioinform.* 9(1):504.
217. Chong J, *et al.* (2018) MetaboAnalyst 4.0: towards more transparent and integrative metabolomics analysis. *Nucleic Acids Res.* 46(W1):W486-W494.
218. Kaever A, *et al.* (2015) MarVis-Pathway: integrative and exploratory pathway analysis of non-targeted metabolomics data. *Metabolomics* 11(3):764-777.
219. Guijas C, *et al.* (2018) METLIN: a technology platform for identifying knowns and unknowns. *Anal. Chem.* 90(5):3156-3164.
220. Kanehisa M, Goto S, Kawashima S, Okuno Y, & Hattori M (2004) The KEGG resource for deciphering the genome. *Nucleic Acids Res.* 32(suppl_1):D277-D280.
221. Karp PD, *et al.* (2017) The BioCyc collection of microbial genomes and metabolic pathways. *Brief. Bioinformatics* bbx085.
222. Kim S, *et al.* (2016) PubChem substance and compound databases. *Nucleic Acids Res.* 44(D1):D1202-D1213.

223. Afendi FM, *et al.* (2011) KNApSAcK family databases: integrated metabolite–plant species databases for multifaceted plant research. *Plant Cell Physiol.* 53(2):e1-e1.
224. Hastings J, *et al.* (2016) ChEBI in 2016: improved services and an expanding collection of metabolites. *Nucleic Acids Res.* 44(D1):D1214-D1219.
225. Little JL, Williams AJ, Pshenichnov A, & Tkachenko V (2012) Identification of "Known unknowns" utilizing accurate mass data and ChemSpider. *J. Am. Soc. Mass Spectrom.* 23(1):179-185.
226. Peremarti A, Bassie L, Zhu C, Christou P, & Capell T (2010) Molecular characterization of the *Arginine decarboxylase* gene family in rice. *Transgenic Res.* 19(5):785-797.
227. Chen W, *et al.* (2014) Genome-wide association analyses provide genetic and biochemical insights into natural variation in rice metabolism. *Nat. Genet.* 46:714.
228. Kim IA, Kim B-G, Kim M, & Ahn J-H (2012) Characterization of hydroxycinnamoyltransferase from rice and its application for biological synthesis of hydroxycinnamoyl glycerols. *Phytochemistry* 76:25-31.
229. Do PT, *et al.* (2013) Dissecting rice polyamine metabolism under controlled long-term drought stress. *PLOS One* 8(4):e60325.
230. Hong S-Y, Seo PJ, Yang M-S, Xiang F, & Park C-M (2008) Exploring valid reference genes for gene expression studies in *Brachypodium distachyon* by real-time PCR. *BMC Plant Biol.* 8:112-112.
231. Oliver RP, *et al.* (2008) Quantitative disease resistance assessment by real-time PCR using the *Stagonospora nodorum*-wheat pathosystem as a model. *Plant Pathol.* 57(3):527-532.
232. Falter C & Voigt CA (2014) Comparative cellular analysis of pathogenic fungi with a disease incidence in *Brachypodium distachyon* and *Miscanthus x giganteus*. *Bioenergy Res* 7(3):958-973.
233. Sumner LW, *et al.* (2007) Proposed minimum reporting standards for chemical analysis Chemical Analysis Working Group (CAWG) Metabolomics Standards Initiative (MSI). *Metabolomics* 3(3):211-221.
234. Piasecka A, Sawikowska A, Krajewski P, & Kachlicki P (2015) Combined mass spectrometric and chromatographic methods for in-depth analysis of phenolic secondary metabolites in barley leaves. *J. Mass Spectrom.* 50(3):513-532.
235. Kumaraswamy KG, Kushalappa AC, Choo TM, Dion Y, & Rioux S (2011) Mass spectrometry based metabolomics to identify potential biomarkers for resistance

in barley against fusarium head blight (*Fusarium graminearum*). *J. Chem. Ecol.* 37(8):846-856.

236. Ozarowski M, *et al.* (2015) Improvement in long-term memory following chronic administration of *Eryngium planum* root extract in scopolamine model: behavioral and molecular study. *Evid Based Complement Alternat Med* 2015:145140-145140.
237. Ozarowski M, *et al.* (2017) Determination of phenolic compounds and diterpenes in roots of *Salvia miltiorrhiza* and *Salvia przewalskii* by two LC-MS tools: multi-stage and high resolution tandem mass spectrometry with assessment of antioxidant capacity. *Phytochem Lett* 20:331-338.
238. Wen W, *et al.* (2015) Genetic determinants of the network of primary metabolism and their relationships to plant performance in a maize recombinant inbred line population. *Plant Cell* 27(7):1839-1856.
239. Ouyang S, *et al.* (2006) The TIGR rice genome annotation resource: improvements and new features. *Nucleic Acids Res.* 35(suppl_1):D883-D887.
240. McCormick RF, *et al.* (2018) The *Sorghum bicolor* reference genome: improved assembly, gene annotations, a transcriptome atlas, and signatures of genome organization. *Plant J.* 93(2):338-354.
241. Schnable PS, *et al.* (2009) The B73 maize genome: complexity, diversity, and dynamics. *Science* 326(5956):1112-1115.
242. Daly P, *et al.* (2018) RNAi-suppression of barley caffeic acid *O*-methyltransferase modifies lignin despite redundancy in the gene family. *Plant Biotechnol. J.*
243. Kage U, Karre S, Kushalappa AC, & McCartney C (2017) Identification and characterization of a fusarium head blight resistance gene *TaACT* in wheat QTL-2DL. *Plant Biotechnol. J.* 15(4):447-457.
244. Ma X, Koepke J, Panjikar S, Fritzsch G, & Stöckigt J (2005) Crystal structure of vinorine synthase, the first representative of the BAHD superfamily. *J. Biol. Chem.* 280(14):13576-13583.
245. Muroi A, *et al.* (2009) Accumulation of hydroxycinnamic acid amides induced by pathogen infection and identification of agmatine coumaroyltransferase in *Arabidopsis thaliana*. *Planta* 230(3):517.
246. von Roepenack-Lahaye E, *et al.* (2003) *p*-coumaroylnoradrenaline, a novel plant metabolite implicated in tomato defense against pathogens. *J. Biol. Chem.* 278(44):43373-43383.
247. Harmer SL, *et al.* (2000) Orchestrated transcription of key pathways in *Arabidopsis* by the circadian clock. *Science* 290(5499):2110-2113.

248. Perez-Amador MA, Leon J, Green PJ, & Carbonell J (2002) Induction of the arginine decarboxylase *ADC2* gene provides evidence for the involvement of polyamines in the wound response in Arabidopsis. *Plant Physiol.* 130(3):1454-1463.
249. Amini H, *et al.* (2019) Tissue-specific transcriptome analysis reveals candidate genes for terpenoid and phenylpropanoid metabolism in the medicinal plant *Ferula assafoetida*. *G3: Genes|Genomes|Genetics* 9(3):807-816.
250. Ishihara A, *et al.* (2015) Involvement of tryptophan-pathway-derived secondary metabolism in the defence responses of grasses. *Amino Acids in Higher Plants*, ed Dmello JPF (Cabi Publishing-C a B Int, Wallingford), pp 362-389.
251. Deng Y & Lu S (2017) Biosynthesis and regulation of phenylpropanoids in plants. *Crit. Rev. Plant Sci.* 36(4):257-290.
252. Macoy DM, Kim W-Y, Lee SY, & Kim MG (2015) Biosynthesis, physiology, and functions of hydroxycinnamic acid amides in plants. *Plant Biotechnology Reports* 9(5):269-278.
253. Franklin G, Conceicao LF, Kombrink E, & Dias AC (2009) Xanthone biosynthesis in *Hypericum perforatum* cells provides antioxidant and antimicrobial protection upon biotic stress. *Phytochemistry* 70(1):60-68.
254. Afifi FÜ, *et al.* (1991) Antifungal flavonoids from *Varthemia iphionoides*. *Phytother. Res.* 5(4):173-175.
255. Lavermicocca P, *et al.* (2000) Purification and characterization of novel antifungal compounds from the sourdough *Lactobacillus plantarum* Strain 21B. *Appl. Environ. Microbiol.* 66(9):4084-4090.
256. Zhou H, Liu B, Weeks DP, Spalding MH, & Yang B (2014) Large chromosomal deletions and heritable small genetic changes induced by CRISPR/Cas9 in rice. *Nucleic Acids Res.* 42(17):10903-10914.

Supplementary data

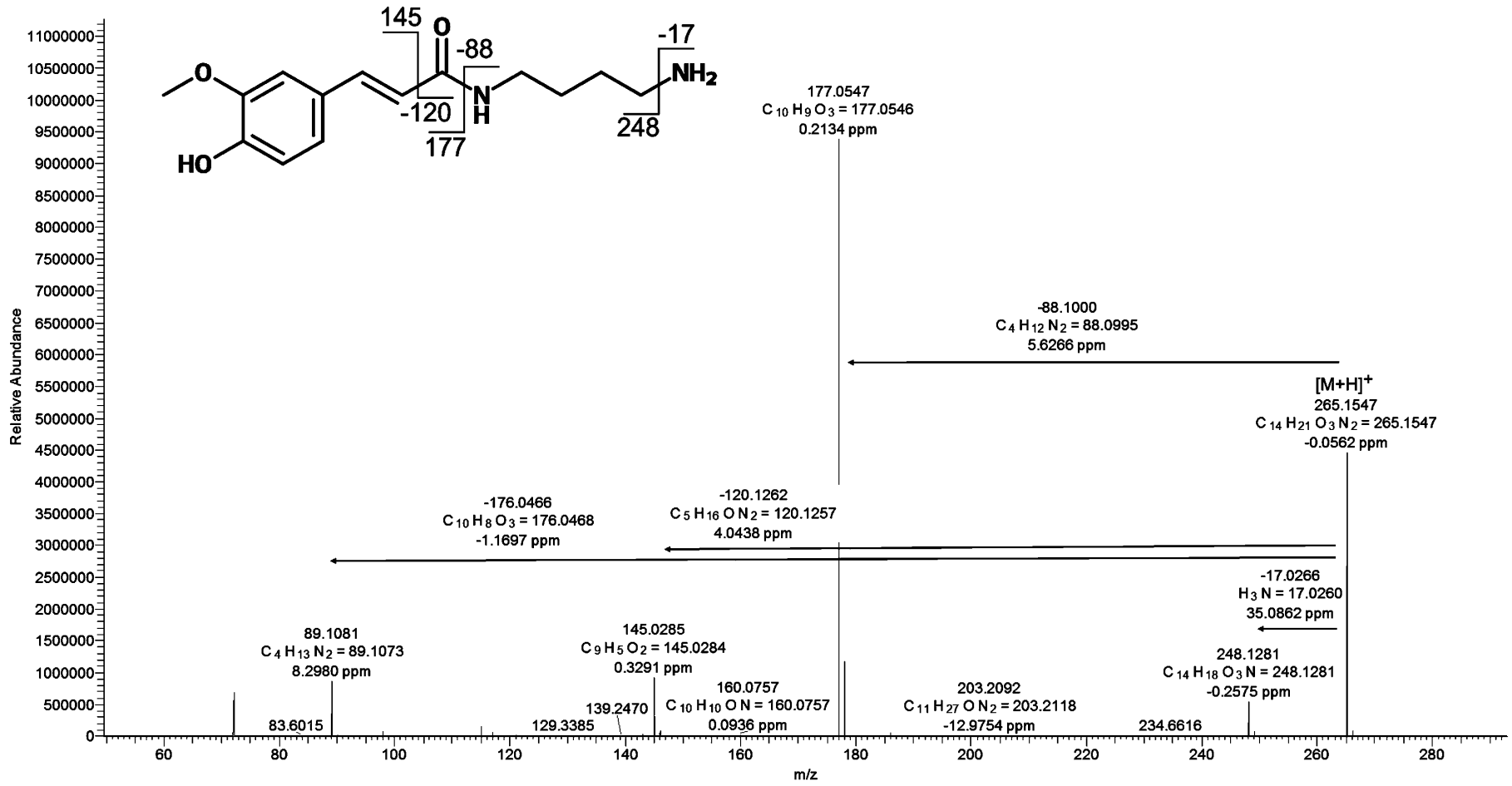

Supplementary figure 1: Mass spectra of *N*-feruloylputrescine (FerPut) in positive ionization with suggested structure and fragmentation mechanism.

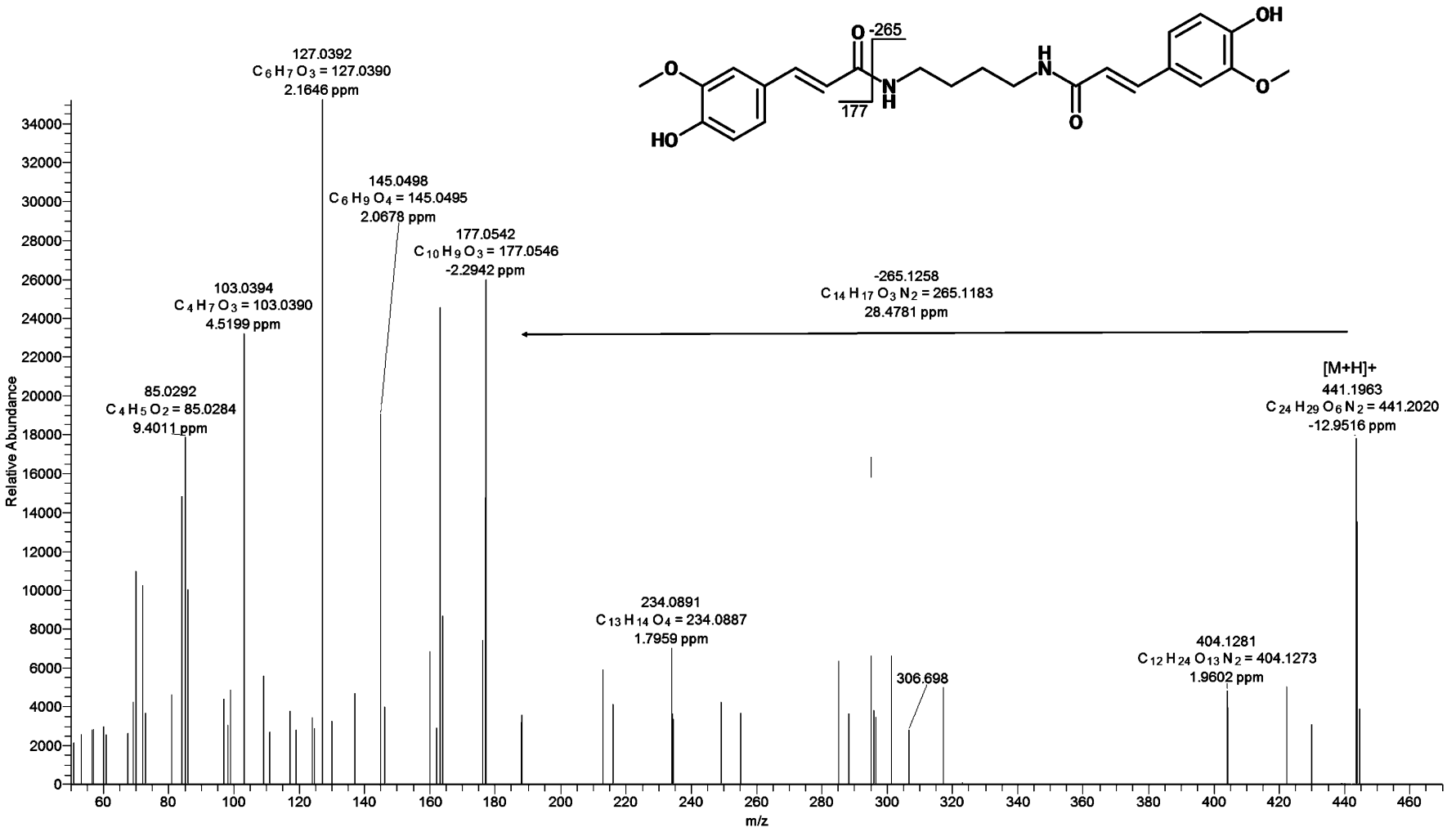

Supplementary figure 2: Mass spectra of *N*,*N*-di-feruloylputrescine (DiFerPut) in positive ionization with suggested structure and fragmentation mechanism.

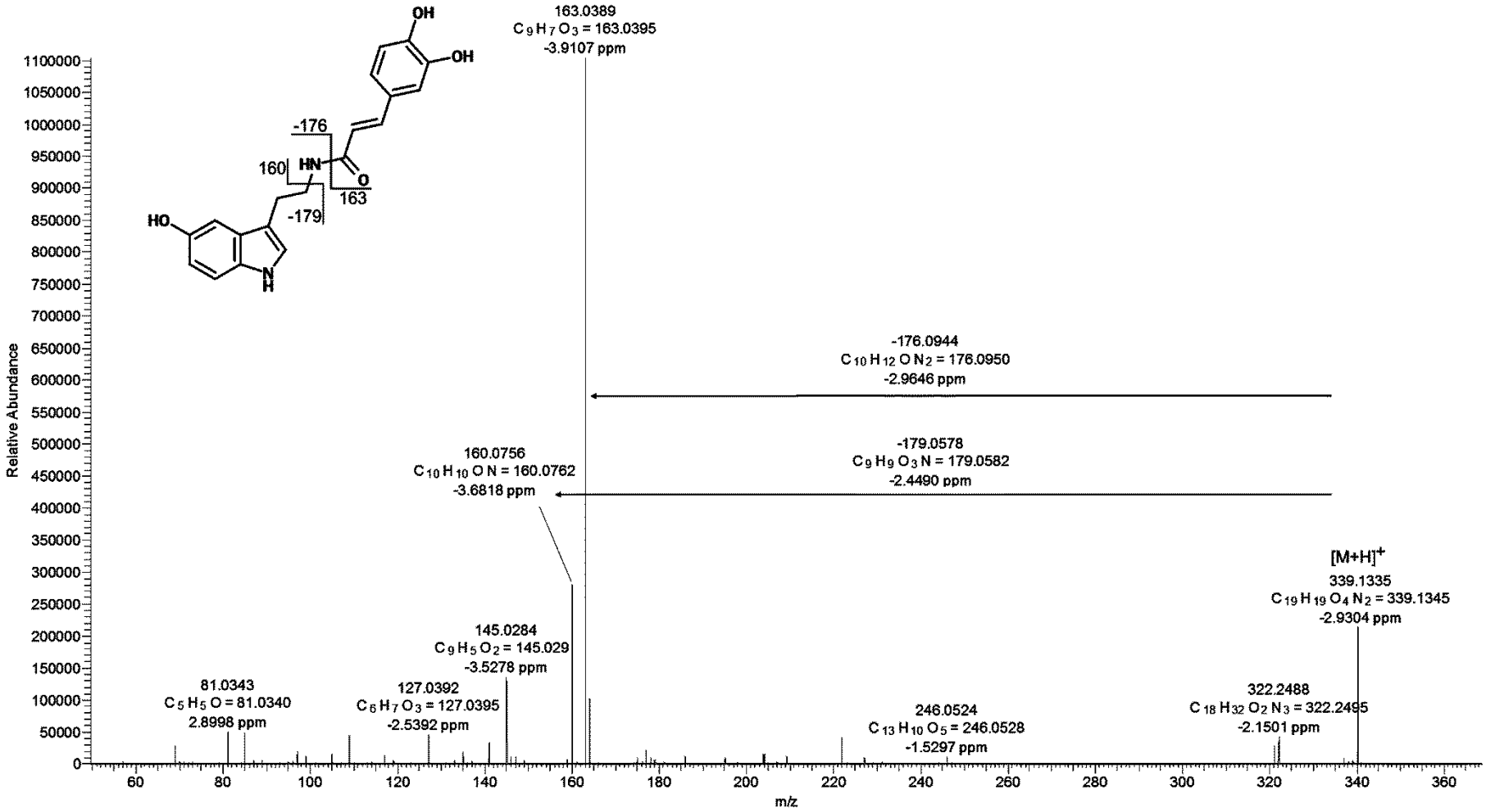

Supplementary figure 3: Mass spectra of *N*-caffeoylserotonin (CafSer) in positive ionization with suggested structure and fragmentation mechanism.

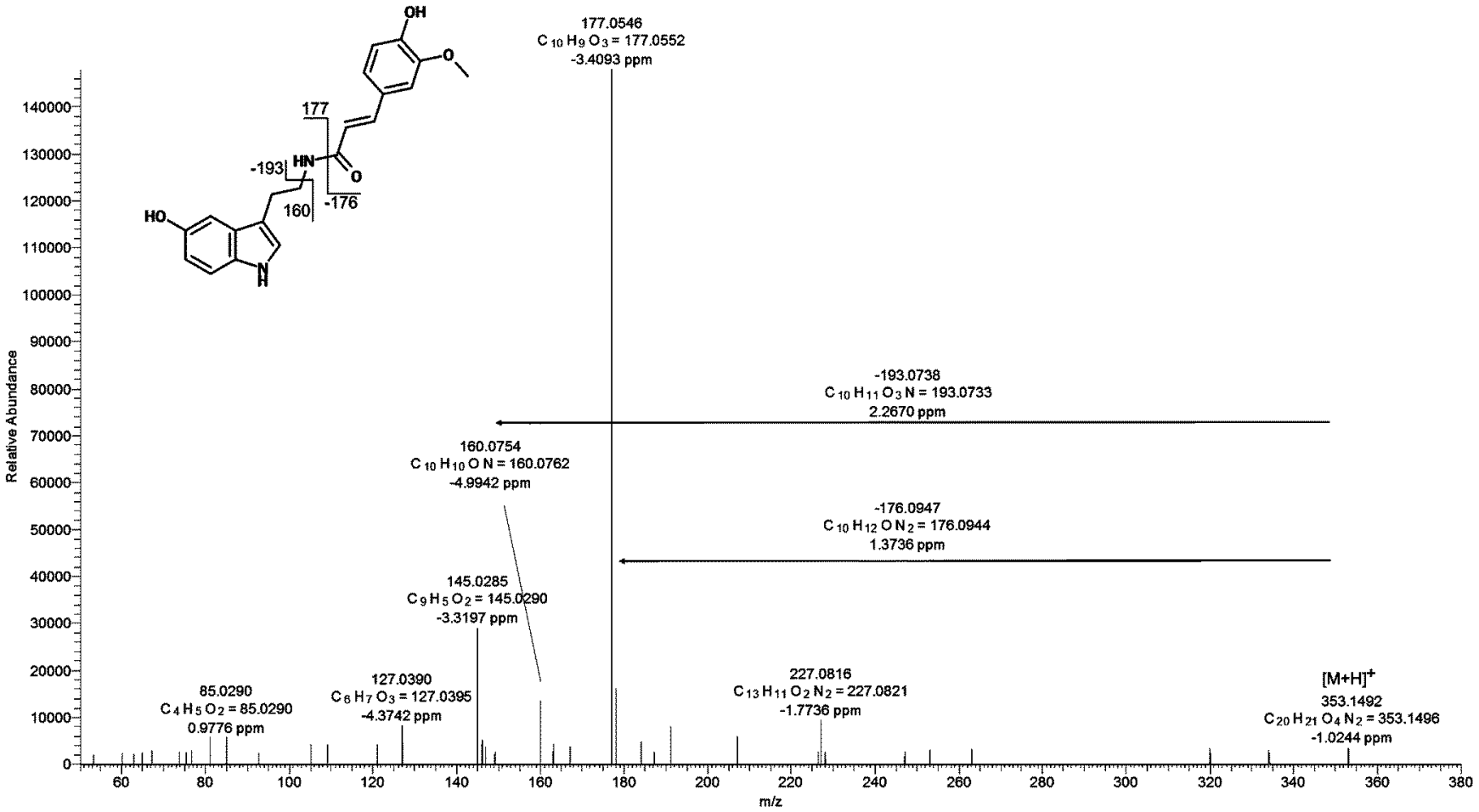

Supplementary figure 4: Mass spectra of *N*-feruloylserotonin (FerSer) in positive ionization with suggested structure and fragmentation mechanism.

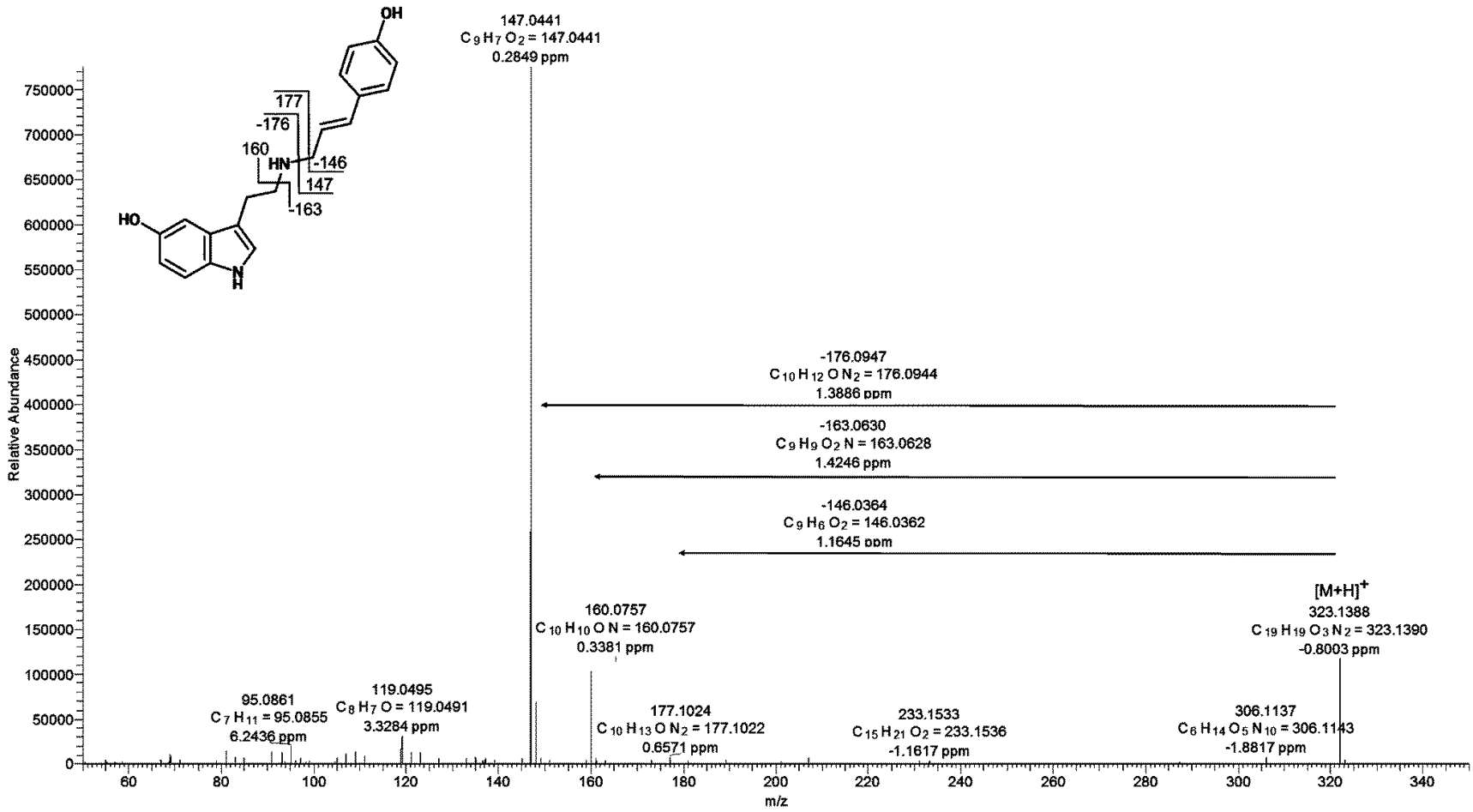

Supplementary figure 5: Mass spectra of *N-p*-coumaroylserotonin (CouSer) in positive ionization with suggested structure and fragmentation mechanism.

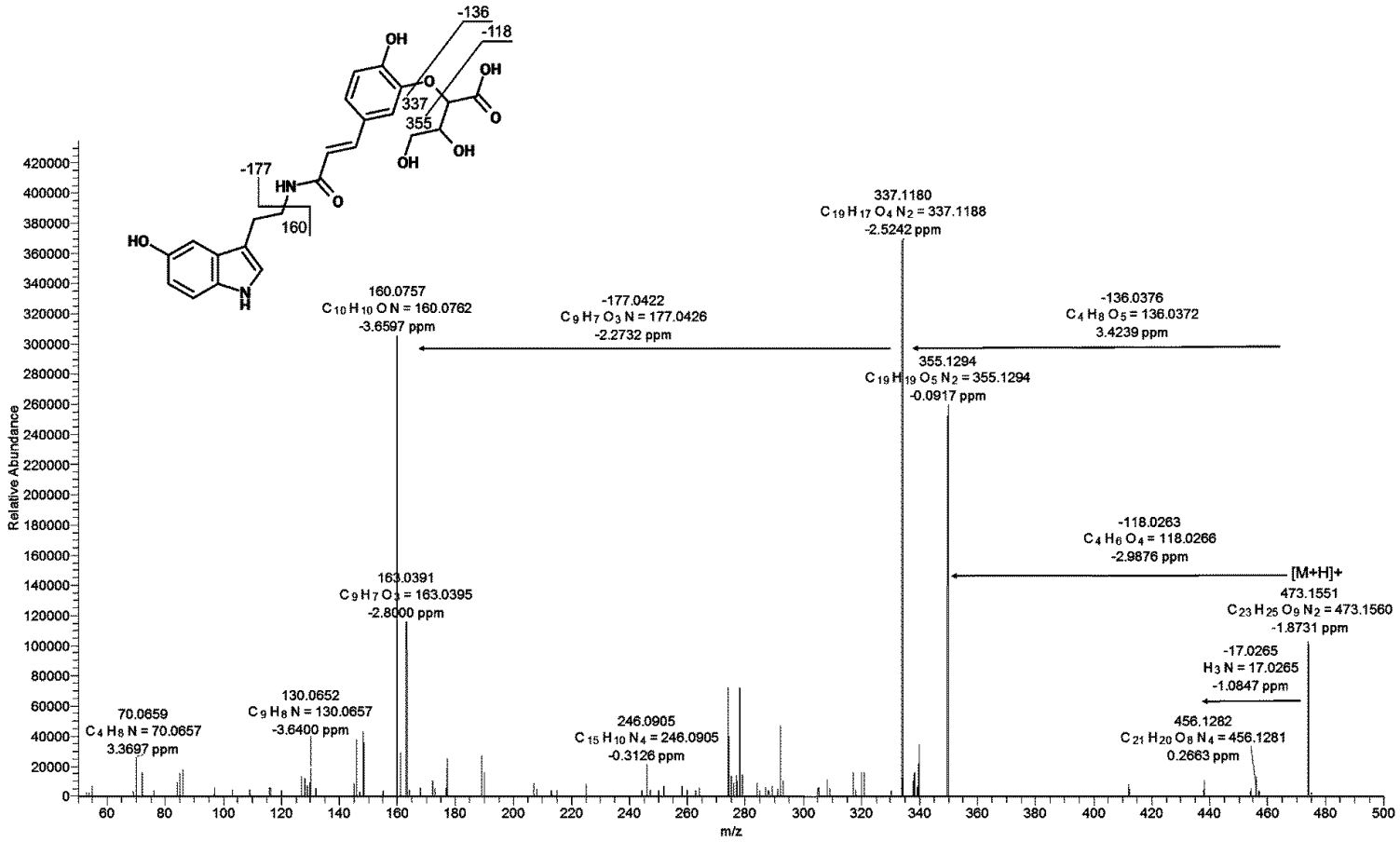

Supplementary figure 6: Mass spectra of *N*-caffeoyl-*O*-threonyl-serotonin (*O*-threonyl-CafSer) in positive ionization with suggested structure and fragmentation mechanism.

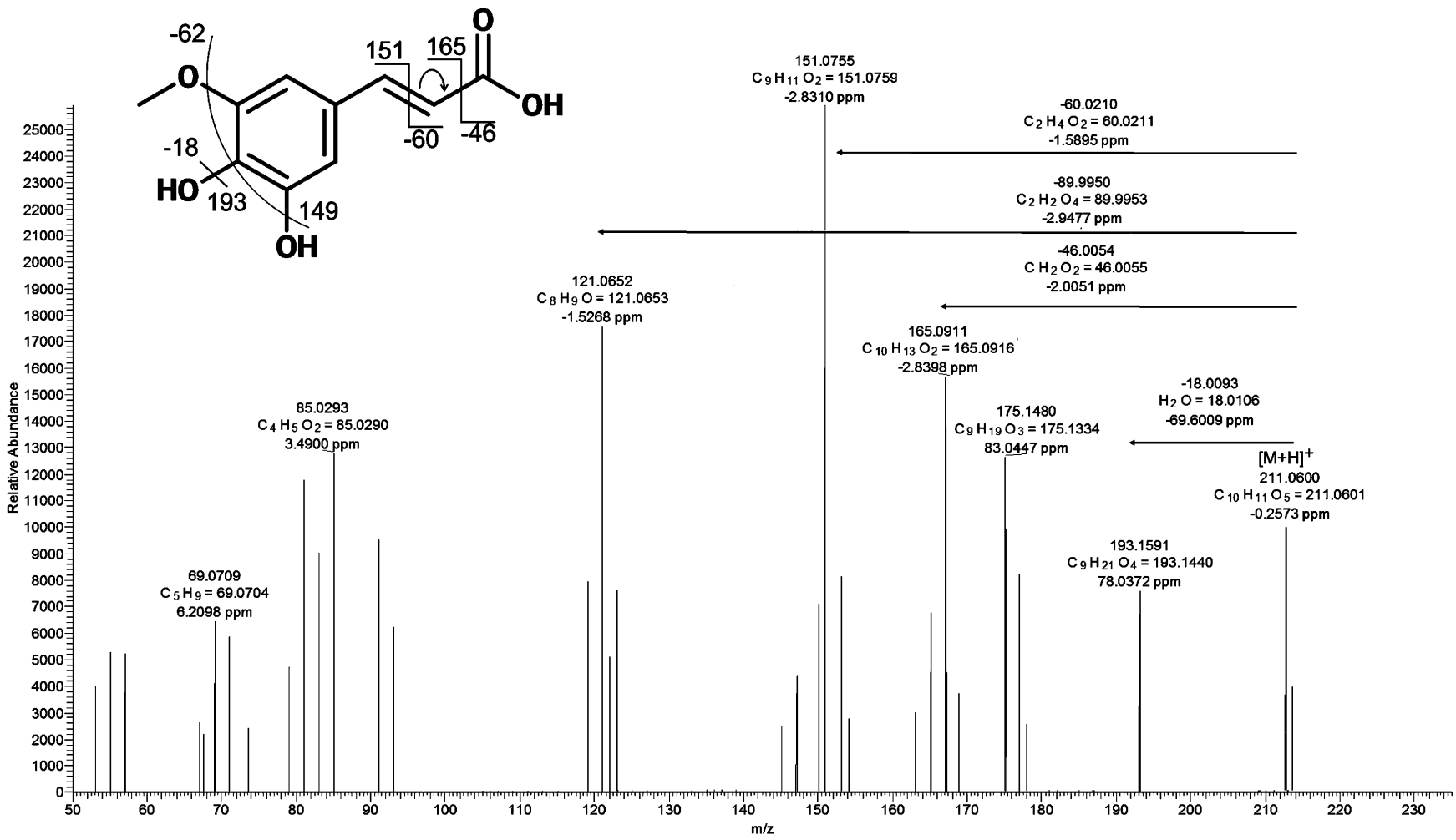

Supplementary figure 7: Mass spectra of 5-hydroxyferulic acid in positive ionization with suggested structure and fragmentation mechanism.

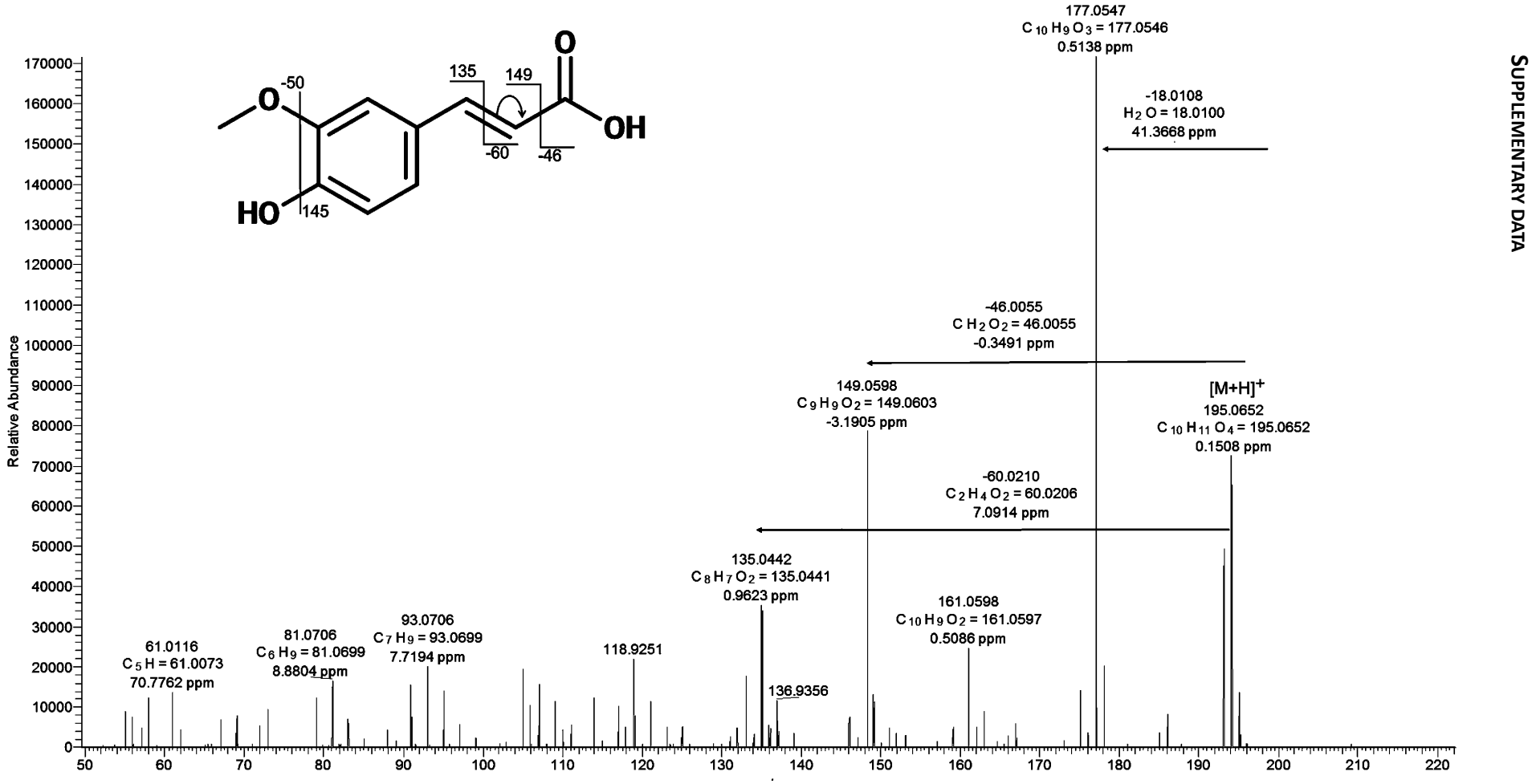

Supplementary figure 8: Mass spectra of ferulic acid in positive ionization with suggested structure and fragmentation mechanism.

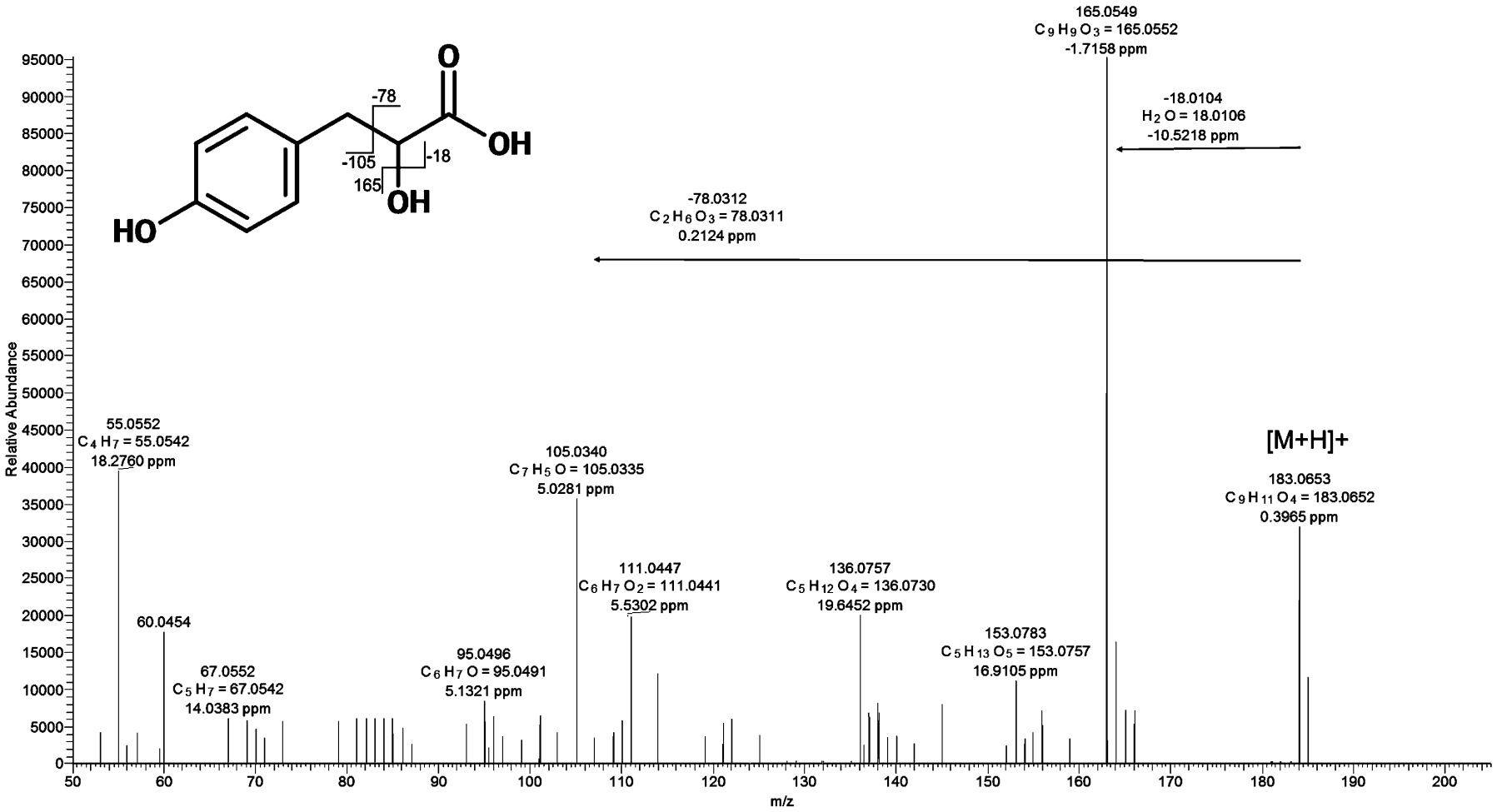

Supplementary figure 9: Mass spectra of hydroxyphenyllactic acid in positive ionization with suggested structure and fragmentation mechanism.

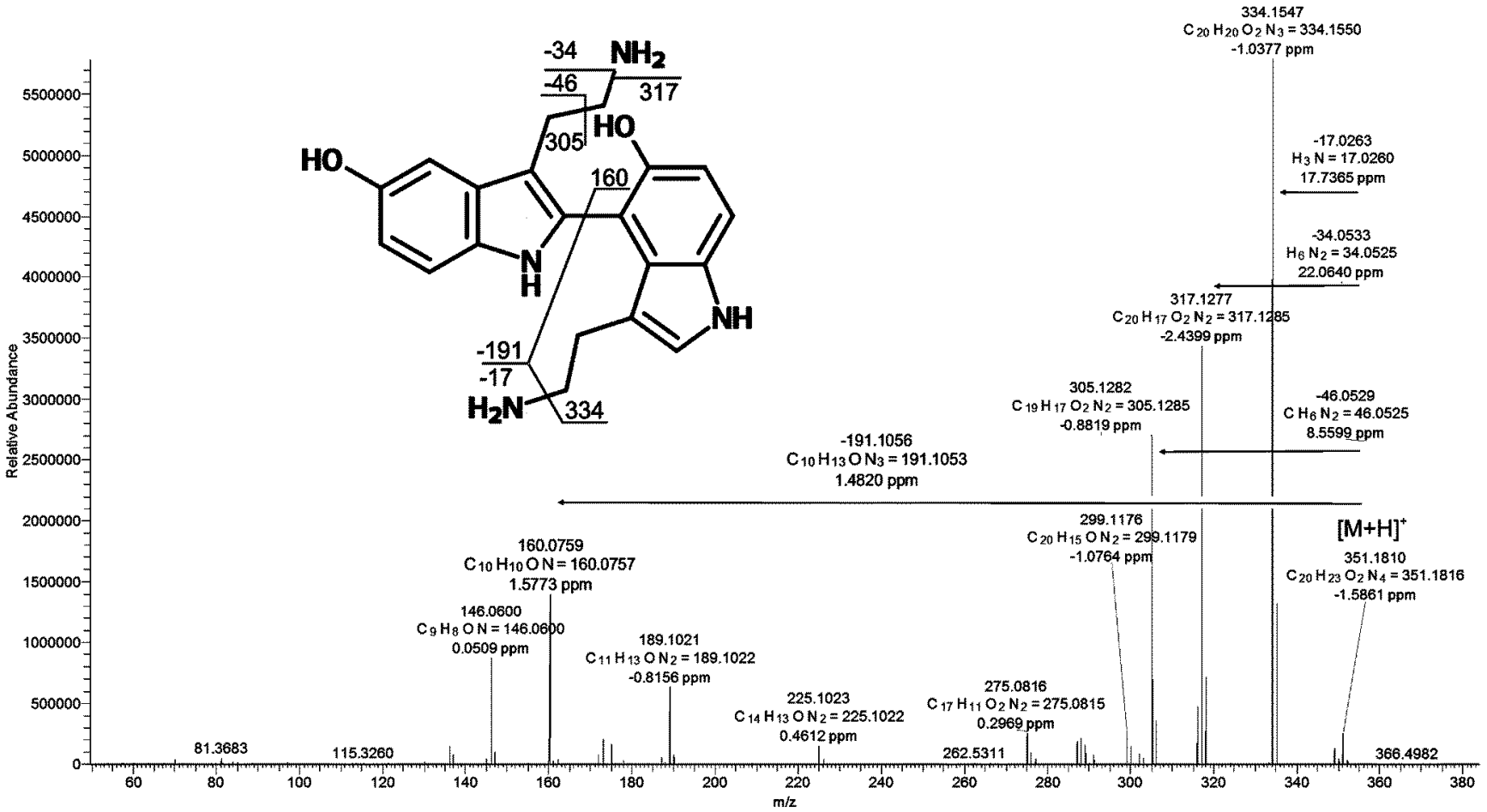

Supplementary figure 10: Mass spectra of 5,5′-dihydroxy-2,4′-bitryptamine in positive ionization with suggested structure and fragmentation mechanism.

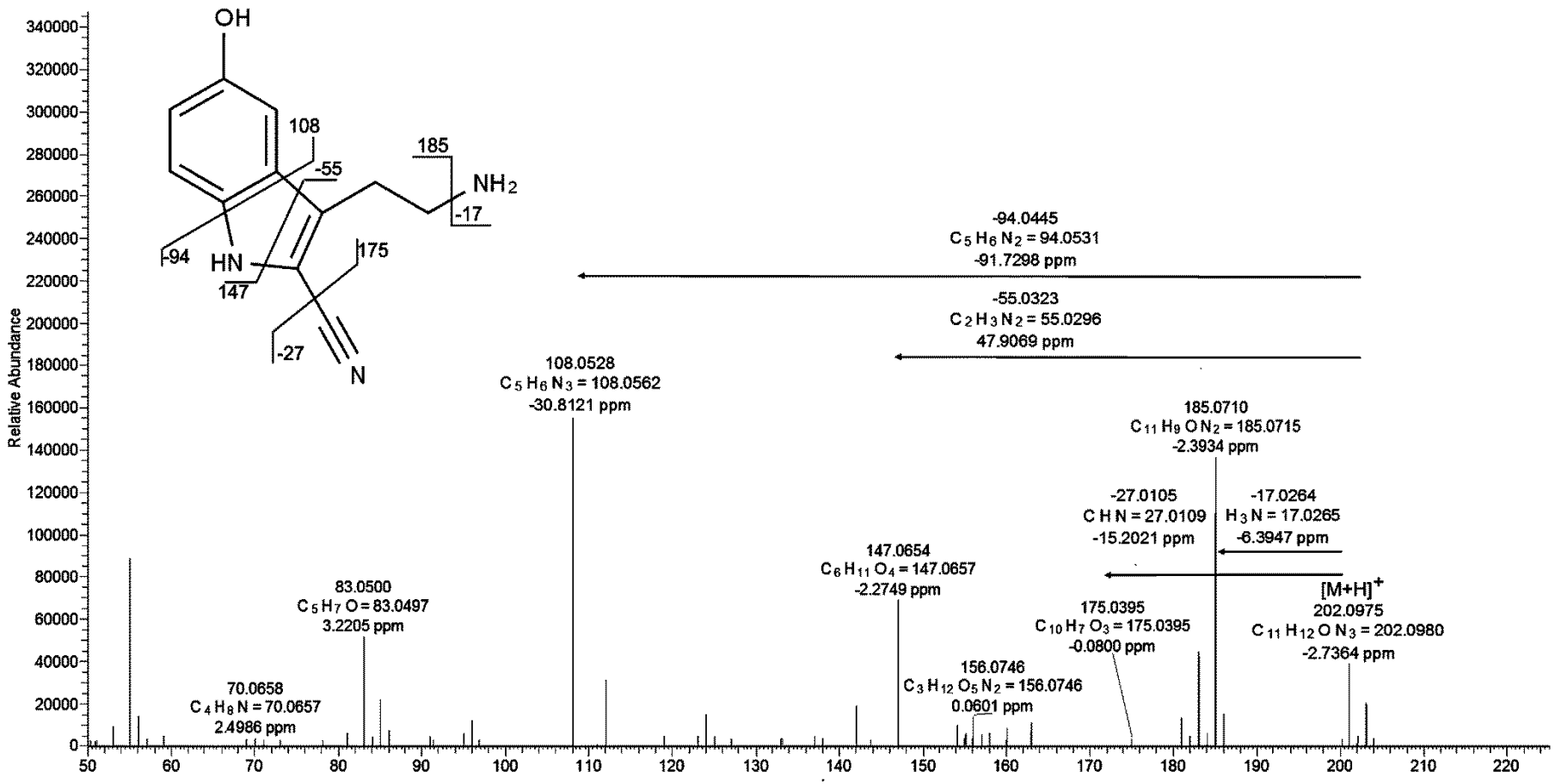

Supplementary figure 11: Mass spectra of 3-(2-aminoethyl)-5-hydroxy-1H-indole-2-carbonitrile (serotonin-2-carbonitrile) in positive ionization with suggested structure and fragmentation mechanism.

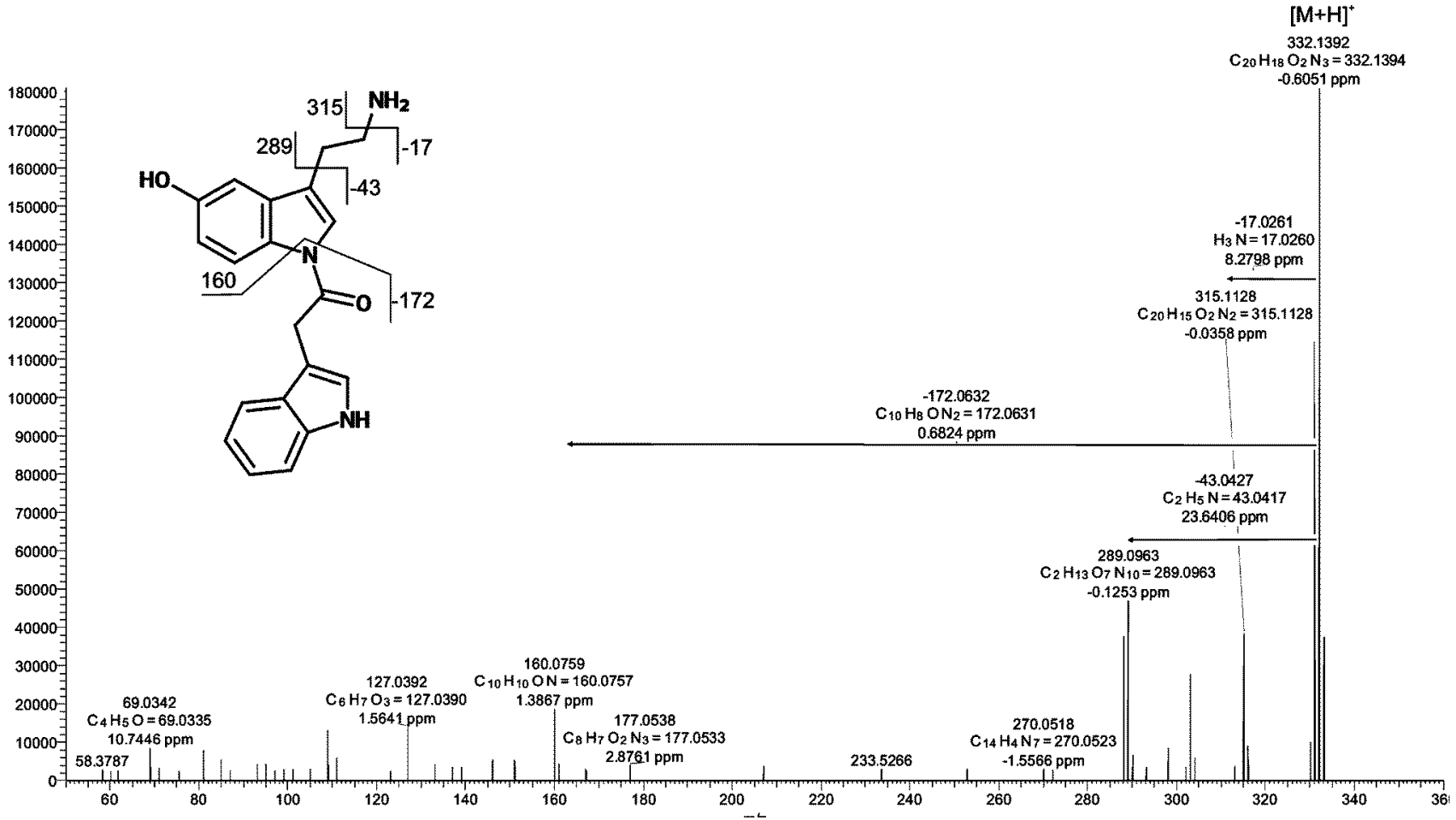

Supplementary figure 12: Mass spectra of serotonin–indolyl-3-acetic acid in positive ionization with suggested structure and fragmentation mechanism.

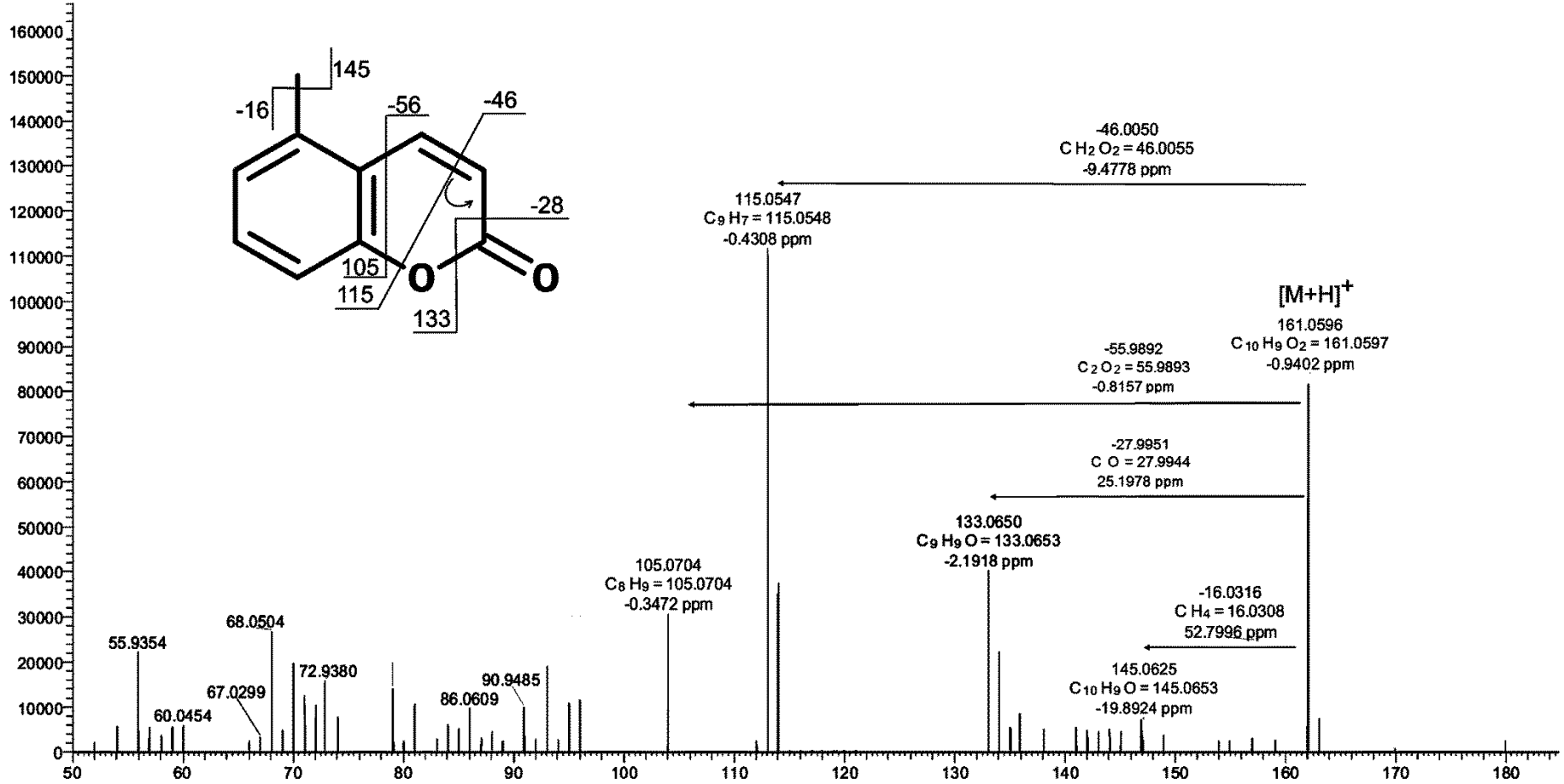

Supplementary figure 13: Mass spectra of 5-methylcoumarin in positive ionization with suggested structure and fragmentation mechanism.

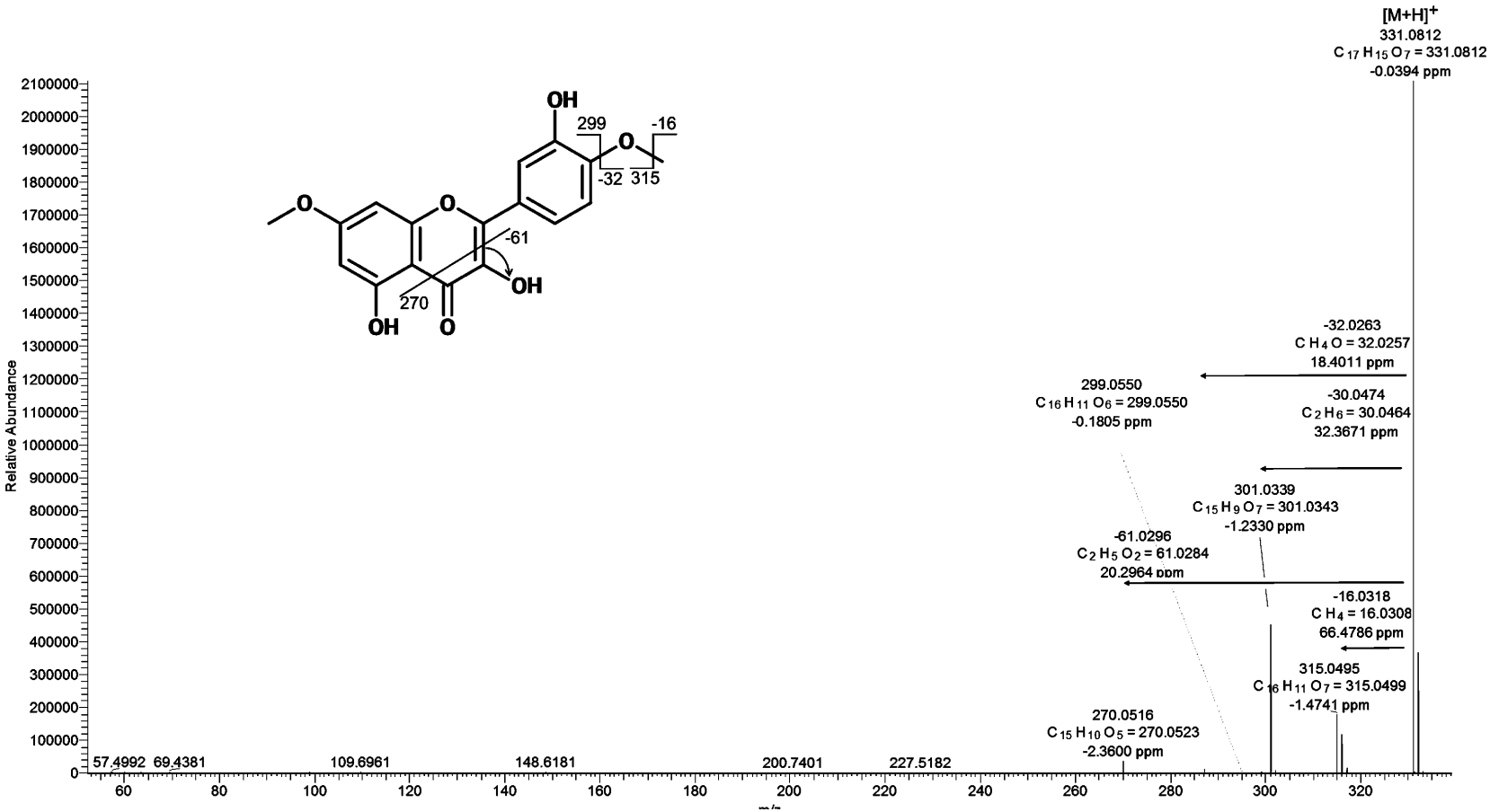

Supplementary figure 14: Mass spectra of di-*O*-methylquercetin in positive ionization with suggested structure and fragmentation mechanism.